Doctoral Thesis

Analysis of notched specimens made of traditionally and additively manufactured metals subject to multiaxial non-proportional low cycle fatigue

September 2019

Doctoral Program in Advanced Mechanical Engineering and Robotics

Graduate School of Science and Engineering
Ritsumeikan University

BRESSAN STEFANO

Doctoral Thesis Reviewed

by Ritsumeikan University

Analysis of notched specimens made of traditionally and additively manufactured metals subject to multiaxial non-proportional low cycle fatigue

（機械加工および積層造形で作製した切欠き材料の非比例多軸応力下における低サイクル疲労強度）

September 2019

2019 年 9 月

Doctoral Program in Advanced Mechanical Engineering and Robotics
Graduate School of Science and Engineering
Ritsumeikan University

立命館大学大学院理工学研究科
機械システム専攻博士課程後期課程

BRESSAN STEFANO

ブレッサン ステファノ

Supervisor: Professor ITOH Takamoto

研究指導教員：伊藤　隆基　教授

Contents

1. Introduction

1.1. Multiaxial low cycle fatigue of notched components

Components and structures in mechanical applications are subject to external static and dynamic loads. When dealing with static loadings, the definition of the material strength and the analysis of the stress distribution are sufficient for a reliable design. In case of dynamic loading, a different failure mechanism occurs, leading to the fracture of the component even in presence of loadings which in the case of static would be harmless to the structure. This phenomenon is known as fatigue, and the failure mechanism consists of microcracks originating from the surface, slip bands or grain interface which slowly propagate and, upon reaching a critical dimension, suddenly leading to the rupture of the components. It is estimated that more than 90% of all failures of metallic structures is due to fatigue. Fatigue can be broadly categorized in relation to the magnitude and direction of the applied loading. It is defined high cycle fatigue when the material rupture occurs after more than 10^5 cycles and it is characterized by material elastic deformation. Low cycle fatigue is defined by a repeated plastic deformation and occurs below 10^5 cycles. For what concern the loading direction, it is defined uniaxial fatigue when the loading is applied on one axis and multiaxial fatigue when the loadings are applied multiple directions. The investigation of low cycle fatigue finds its importance in situations when the materials undergoes a plastic deformation or when high strains provoked by thermal loading occur. Low cycle fatigue life estimation models require the definition of the cyclic stress-strain curves of the material. The definition of the cyclic stress-strain curves of a given material are generally demanding in terms of time and several times hard to find in the literature. To simplify the low cycle fatigue life evaluation, methods which only requires the data of a simple tensile test have been introduced. Firstly, Manson suggested the universal slope method [1]. The method proposed by Manson has been modified, and the Muralidharan-Manson method has been introduced [2] The uniform material law which was suggested by Bäumel and Seeger [3] and it has been applied to several experimental data, returning sound results. This method can be considered another type of universal slopes method. The advantage of this method compared with other models is that it requires only the tensile strength as input. The Bäumel-Seeger model can be applied for steels, aluminum and titanium alloys.

Different from the uniaxial fatigue loading condition, multiaxial fatigue is a more complex phenomenon and fatigue life predictions are far from being easy. In addition, non-proportional loading is defined as the condition characterized by the variation of the first principal stress direction over the cycle. As a consequence, the number of activated slip bands in the material increases, causing additional hardening and a reduction of fatigue life, as evidenced in several works [4-9]. Additional hardening is a property depending on the material and represent one of the causes of the lower fatigue life [10] (Fig. 1.1).

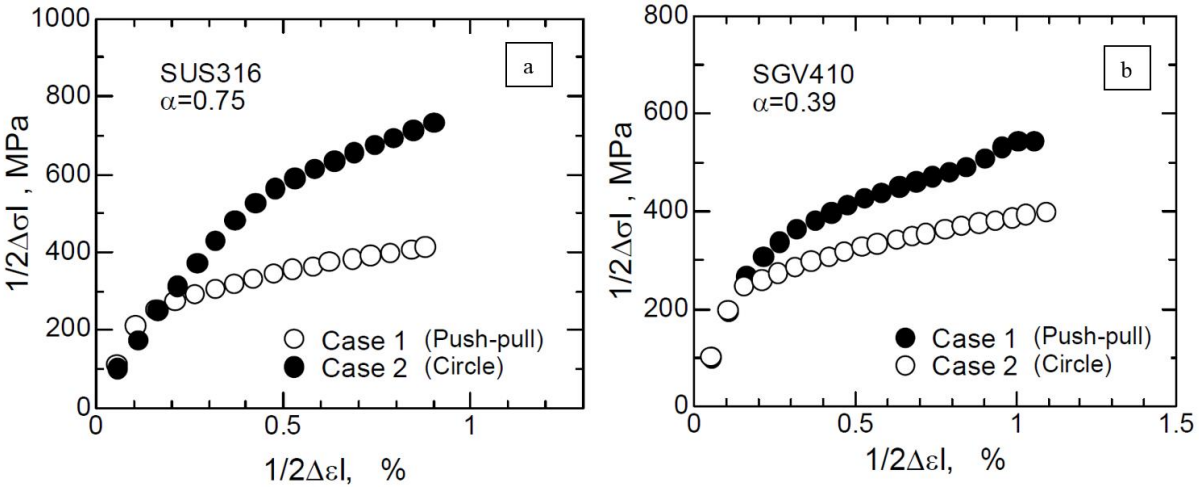

Fig. 1.1. Comparison of additional hardening occurring in stainless steel SUS316 (a) and in SGV410 (b) [10]

Although the complexity, several evaluation models which take into account of the multiaxiality of the loading have been developed in the past and recent years. The evaluation approaches can be broadly divided in three main categories. Stress based models [11-13] are based on a parameter obtainable from the applied stresses and they are commonly applied in the field of high cycle fatigue. Models based on strain are instead applied for in the field of low cycle fatigue, where significant plasticity may occur. The models developed by Brown-Miller [14], Fatemi-Socie [15] and Smith-Watson-Topper [16] are models are based on critical plane, a surface which experiences the highest level of damaging over the cycle. Brown-Miller proposed that both the cyclic shear and normal strain on the plane of maximum shear must be considered:

$$\frac{\Delta\gamma_{max}}{2} + S\Delta\varepsilon_n \tag{1.1}$$

$\Delta\gamma_{max}$ is the maximum shear strain range occurring on the critical plane, $\Delta\varepsilon_n$ is the strain amplitude acting on the normal direction to the critical plane and *S* a

factor quantifying the material sensitivity to axial loading. Fatemi–Socie model assumes that the main contribution to the fatigue damage is given by the maximum shear strain occurring on the critical plane, and a secondary damage is due to the maximum normal stress acting on such plane:

$$\frac{\Delta\gamma_{max}}{2}\left(1 + k\frac{\sigma_{n,max}}{\sigma_y}\right) \tag{1.2}$$

While the Brown-Miller and Fatemi-Socie critical plane assumes that the dominant failure mechanism is shear crack nucleation and growth, the Smith-Watson-Topper model was developed for materials which failure mechanism is due predominantly to tensile stress or strain:

$$\sigma_{n,max}\frac{\Delta\varepsilon_1}{2} \tag{1.3}$$

where $\sigma_{n,max}$ is the normal stress acting on the critical plane and $\Delta\varepsilon_1$ the first principal strain amplitude. Critical plane approaches are well known to estimate accurately the number of cycles to failure, although the detection of such plane might be time taking and the parameters associated with the model can be complex to obtain. An alternative model developed by Itoh and Sakane introduces several advantages one of which is the simplicity of application and the wide range of loading conditions for which the model can be applied [17,18]. Several materials and loading conditions have been tested with this model and the obtained results confirmed its reliability. Itoh-Sakane model is based on the strain. The applied first principal strain range is modified with the parameter α and f_{NP}:

$$\Delta\varepsilon_{NP} = \Delta\varepsilon_I(1 + \alpha f_{NP}) \tag{1.4}$$

The parameter α takes into account of the additional hardening, while the parameter f_{NP} takes into account of the severity of the loading.

Mechanical components feature notches and grooves due to the geometrical requirements in the design phase. Such geometrical discontinuities weaken the structure by provoking a local increasing of the stress. In case of static applications in the linear elastic field, the stress concentration factor K_t represents the ratio between the stress at the notch tip and the nominal applied stress. The value of stress concentration factor depends on the geometry of the component and it can be determined via analytical and empirical approaches [19]. However, when dealing with mechanical components undergoing fatigue and/or plastic deformation, such stress concentration factor cannot be considered

as an adequate parameter to estimate the reduction of fatigue life. Being plastic deformation a non-linear material behavior, both the stress concentration factor K_σ and strain concentration factor K_ε must be considered in order to define the stress/strain status at the notch tip. Pioneering works conducted by Neuber [20] and Glinka [21] developed approaches to estimate the stress and strain concentration factors. In the field of fatigue, the effect of the notch on the fatigue life is quantified with the notch fatigue factor K_f, defined as the ratio between the fatigue strength of the smooth specimen and fatigue strength of the notched specimens under the same experimental conditions and the same number of cycles [22]. K_f takes a value between 1 and K_t and depends on the material notch sensitivity q or a and can be calculated through several approaches. The higher the notch sensitivity, the closer is K_f to K_t. In the field of low cycle fatigue K_f can also be employed but the non-linear plastic behavior of the material affects the accuracy of fatigue life estimation. The multiaxiality of the loading introduces further complications and predicting the stress and strain status at the notch tip is far from being easy. For this reason, simpler models which takes into account of non-proportionality of the loading, the cyclic plasticity and the stress concentration are desirable.

In the literature, the number of works related to multiaxial low cycle fatigue of notched components are sparse. In a work conducted by Sakane et al. [23] notched specimens made by stainless steel SUS304 have been tested with multiaxial non-proportional loading, focusing on the analysis of the number of cycles to crack initiation, crack propagation and failure. Itoh *et al.* conducted several tests on notched specimens made by stainless steel SUS 316L [24] and proposed a model for notched components based on Itoh-Sakane model (Eq. 1.5):

$$\Delta\varepsilon_{NP} = K_t \Delta\varepsilon_I (1 + \alpha f_{NP}) \tag{1.5}$$

The model returned satisfying results despite the simplicity of application of the modified damage parameter. In the tests conducted in [24], the crack initiation site was detected in a shifted position from the notch tip as depicted in Fig. 1.2.

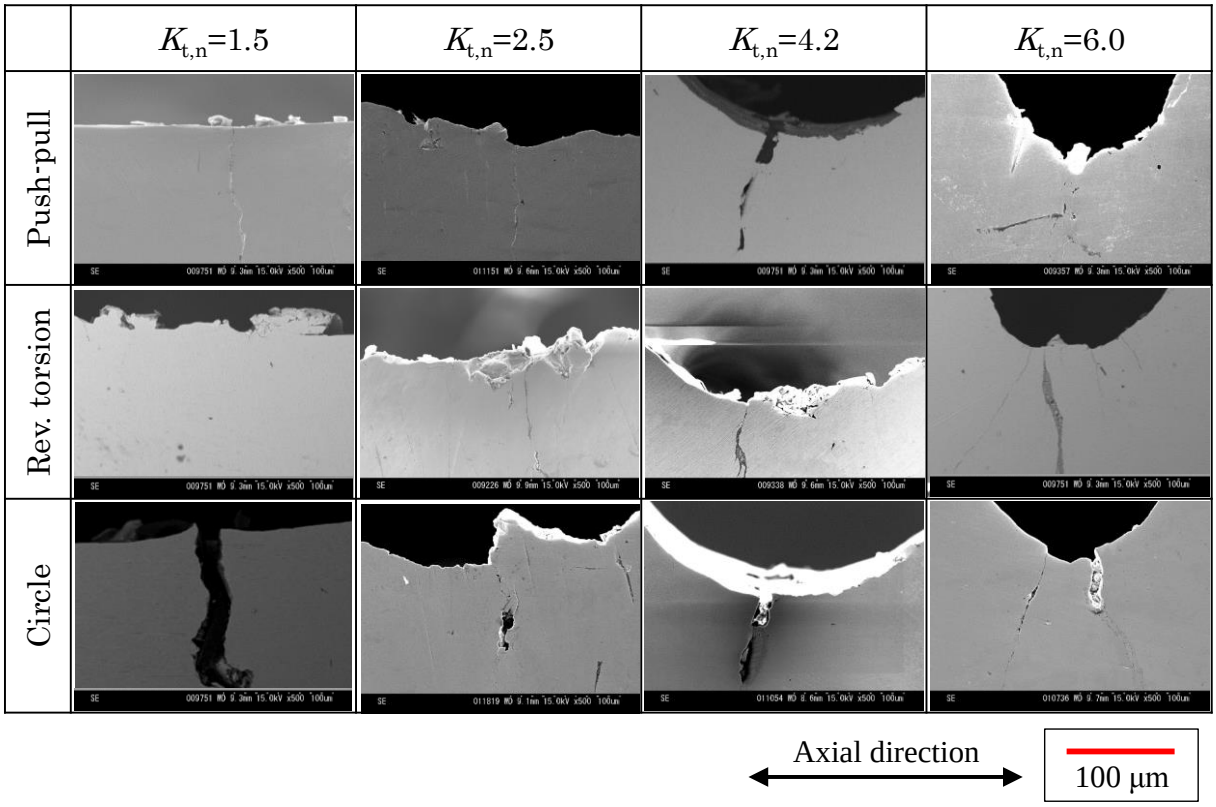

Fig. 1.2. Crack initiation site on the notch tip [25]

Such phenomenon has not been reported in the literature and further investigations to clarify the causes and the influence of the crack initiation site on the fatigue must be conducted. Furthermore, the model of Eq. 1.5 has been applied only for SUS 316L and additional verifications on materials with different cyclic plastic behavior such as aluminum or titanium must be conducted.

1.2. Additive manufacture

3D printing or additive manufacturing is a fabrication technique which allows to create components by the subsequent creation of layers. Additive manufacturing or AM [1,2] represents one of the most innovative fabrication technologies of the recent years and several techniques have been developed. The powder bed system is the most employed technique for the fabrication of additively manufactured components. A powder bed is created by raking powder across a work area. The powder is successively melted by means of an energy source such as laser or an electron beam until the fabrication process is complete. When the laser is used as source of energy the technique is referred as laser powder bed fusion (L-PBF). Electron beam can be also used as power source to

melt the powders. The powder can be also deposited directly through a nozzle on the platform allowing to create parts with a larger volume or repair damaged parts. The advantages of the AM are the high fabrication speed, the possibility to create components with a complicate shape and the relatively low cost. On the other hand, the components created with AM techniques features a fragile material structure, voids or lacks fusions and a rough surface [28-30]. Post process surface and heat treatments are performed to reduce the surface roughness and reduce the residual stresses [29]. The most employed metallic alloy with this fabrication technology is the Titanium alloy Ti-6Al-4V. Common applications of Ti-6Al-4V made by AM techniques are represented by aero engine turbine blades or medical prosthesis. To enhance the reliability of the design phase, the static and fatigue properties of AM material must be accurately estimated. The definition of mechanical properties of AM materials is complex because of the wide variety of material microstructures obtainable by the definition of several process parameters such as laser speed, thickness, layer thickness, etc. [31-34]. The basic mechanical properties obtainable through a monotonic axial test have been widely studied and reported in the literature [35-38]. In these studies, the AM material were characterized by a higher yield and ultimate strength stress accompanied by a lower ductility due to the martensitic structure and anisotropy compared to the wrought counterpart. Fatigue properties of AM materials have been also widely investigated, focusing on the uniaxial high cycle fatigue of Ti-6Al-4V created employing the L-PBF [39-44]. Although a direct comparison between the data is difficult due to the multitude of material structures and test conditions, the work by Li [45] gathered a consistent amount of data and drawn the following conclusions. Fatigue life of materials with coarse structure was shorter than those with a martensitic or fine grain structure. A fine structure can be obtained after annealing at a range of 600 °C –900 °C. An annealing heat treatment conducted at 1000°C might lead to a coarser structure, negatively influencing the fatigue resistance. The characteristics related to voids which affect fatigue life are morphology, position and density. Elliptical voids, superficial voids and areas with a high void density have a detrimental effect rather than circular, internal and isolated voids. The superficial roughness is the factor which exert the most influence of fatigue life among the material characteristics. Although there are several researches investigating AM Ti-6Al-4V high cycle fatigue, researches on multiaxial non-proportional low cycle fatigue are sparse. In [46], Sterling et. al analyzed samples made with the Laser Engineering Net Shaped (LENS) under uniaxial

high-cycle and lo-cycle fatigue. The influence of void size and distance of the void from the surface on fatigue life was discussed. Furthermore, a general softening behavior was detected when plastic deformation occurred. The wrought material has been tested under non-proportional low cycle fatigue in Ref. [47] and a reduction of approximately 1/10 in fatigue life due to non-proportional loading was observed. In a recent work conducted by Fatemi et al. [48-49] stress-controlled multiaxial fatigue tests were conducted on Ti-6Al-4V AM specimens built with the same layer orientation, discussing the influence of voids on fatigue life and successfully estimating fatigue life.

Although widely investigated, data regarding the influence of layer orientation and heat treatment on the uniaxial and non-proportional multiaxial low cycle fatigue are still sparse. Furthermore, data discussing the effect of stress concentration in addition to the aforementioned factors are not present in the literature. Therefore, it is necessary to conduct fatigue tests on smooth samples to verify the mechanical behavior under multiaxial loading and investigate the influence of notches under multiaxial low cycle fatigue conditions.

1.3. Content of the thesis

1.3.1 FEM investigation on the crack initiation site on notched components under uniaxial and non-proportional low cycle fatigue

A FEM (finite element method) analysis which simulates the tests of Ref. [24] has been conducted to clarify the causes of the crack initiation site position observed on the tested specimens made of SUS 316L. A hardening behavior similar to the one observed on the hardness maps obtained in [24] has been reproduced on the simulation environment, and the same loading condition of the experimental tests applied to the model. The stress-strain status in the vicinity of the notch tip has been analyzed and a correlation with the crack initiation position on the notch tip researched. Successively, a modified I-S based on the FEM analyses results has been proposed.

1.3.2 Notch sensitivity and crack initiation site influence on low cycle fatigue life evaluation of notched specimens under non-proportional loading

In this section, the I-S model has been modified accounting of the notch sensitivity of the material and crack initiation site. The modified I-S model for notched specimens of Ref. [24] has not been verified for materials with a low degree of additional hardening. Furthermore, the I-S model has been correlated with the USM, without considering alternative models which might further

improve the fatigue life evaluation under non-proportional loading conditions. Therefore, four notched specimens made of Al 6061 with the same notch geometry of the SUS 316L notched specimens have been tested with both uniaxial and multiaxial non-proportional loading. The crack initiation site on the notched surface have been observed and compared with the one observed in the specimens made by SUS 316L. The model has been further modified by correlating the Itoh-Sakane model with the Bäumel-Seeger model and by replacing the stress concentration factor referred to the net section K_t with the fatigue notch factor K_f which takes into account the notch sensitivity of the material.

1.3.3 Additive manufacturing: analysis of layer orientation and heat-treatment influence on low cycle uniaxial and multiaxial non-proportional fatigue life

The influence of layer orientation and heat-treatment on low cycle uniaxial and multiaxial non-proportional fatigue life of smooth specimens made of AM Ti-6Al-4V has been investigated in this section. Four types of specimens depending on the fabrication direction and the application of a stress-relief heat treatment have been tested. The analyses to characterize the material properties such as the material microstructure and the cyclic stress-strain curves have been conducted. Fatigue tests have been conducted and considerations regarding the influence of the specimen variety of fatigue life, plastic deformation and crack initiation site have been conducted.

1.3.4 Influence of layer orientation, heat-treatment and notch on low cycle uniaxial and multiaxial non-proportional fatigue life

Low cycle uniaxial and multiaxial non-proportional fatigue tests have been conducted on four varieties of notched specimens made by AM Ti-6Al-4V. The specimen varieties were obtained with the same machine and process parameters of the previously tested smooth specimens to ensure the same mechanical properties. The notch geometry and the applied strain amplitude was identical regardless of the specimen type. The discrepancy in terms of fatigue life among the specimens' types have been analyzed. An investigation on the fracture surface have been also conducted to analyze the crack initiation site. Final considerations in relation to the results obtained for traditionally manufactured materials are also reported in this section. In this section the results and analysis reported in the previous chapters are summarized and discussed. Ideas for future developments are also proposed.

References

[1] Manson, S.S. (1965). Fatigue – a complex subject – some simple approximations, Experimental Mechanics, 5(7), pp. 193-226. DOI: 10.1007/BF02321056.

[2] Muralidharan, U. and Manson, S.S. (1988). A modified universal slopes equation for estimation of fatigue characteristics of metals, Journal of Engineering Materials and Technology, 110(1), pp. 55-58. DOI: 10.1115/1.3226010.

[3] Bäumel Jr., A. and Seeger, T. (1990). Materials Data for Cyclic Loading, Elsevier Science Publishers, Amsterdam, (supplement 1).

[4] Kanazawa, K., Miller, K.J., Brown, M.W. (1979). Cyclic deformation of 1%Cr–Mo–V steel under out-of-phase loads, Fatigue and Fracture of Engineering Materials and Structures, 2(3), pp. 217-228.DOI:10.1111/j.1460-2695.1979.tb01357.x.

[5] McDowell, F.L. (1983). On the path dependence of transient hardening and softening to stable states under complex biaxial cyclic loading, in: Desai, Gallagher (Eds.), Proceedings of the International Conference on Constitutive Laws for Engineering Materials, pp. 125-135.

[6] Krempl, E. and Lu, H. (1983). Comparison of the stress response of an aluminum alloy tube to proportional and alternate axial and shear strain paths at room temperature, Mechanics of Materials, 2(3), pp. 183-192.

[7] Nitta, A., Ogata, T., Kuwabara, K. (1987). The effect of axial–torsional straining phase on elevated-temperature biaxial low-cycle fatigue life in SUS304 stainless steel, Journal of the Society of Materials Science, Japan, 36(403), pp. 376-382.

[8] Doong, S.H., Socie, D.F., Robertson, I.M. (1987), Dislocation substructures and nonproportional hardening, Transactions of the American Society of Mechanical Engineers – Journal of Engineering Materials and Technology, 112(4), pp. 456-465.

[9] Doong, S.H. and Socie, D.F. (1991). Constitutive modeling of metals under non-proportional cyclic loading Transactions of the American Society of Mechanical Engineers – Journal of Engineering Materials and Technology, 113(1), pp. 23-30.

[10] Itoh, T, and Yang, T. (2011). Material dependence of multiaxial low cycle fatigue lives under non-proportional loading, International Journal of Fatigue, 33(8), pp. 1025-1031.

[11] Gough, H.J. Pollard, H.V. (1935). The strength of metals under combined alternating stresses, Proceedings of the Institute of Mechanical Engineers, 131, pp. 3-103. DOI:10.1243/PIME_PROC_1935_131_008_02.

[12] Sines, G. (1955). Fatigue of materials under combined repeated stresses with superimposed static stresses, Tech. Note 3495, National Advisory Committee of Aeronautic, Washington DC.
[13] Findley, W.N. (1959). A theory for the effect of mean stress on fatigue of metals under combined torsion and axial loading or bending, Journal of Engineering for Industry, pp. 301-306.
[14] Brown, M.W. and Miller, K.J., (1978), A theory for fatigue under multiaxial stress-strain conditions, Proceedings of the Institute of Mechanical Engineers, 187, pp. 745-756. DOI: 10.1243/PIME_PROC_1973_187_069_02.
[15] Fatemi, A. and Socie, D.F. (1988). A critical plane approach to multiaxial fatigue including out-of-phase loading, Fatigue and Fracture of Engineering Materials and Structures, 11, pp. 149-166. DOI:10.1111/j.1460-2695.1988.tb01169.x.
[16] Smith, R.N., Watson, P., Topper, T.H. (1970). A stress-strain function for the fatigue of metals, Journal of Materials, 5(4), pp. 767-778.
[17] Itoh, T., Sakane, M., Ohnami., D.F., Socie, D.F. (1995). Nonproportional low cycle fatigue criterion for Type 304 stainless steel, Journal of Engineering Materials and Technology, 117(3), pp. 285-292. DOI: 10.1115/1.2804541.
[18] Itoh, T., Nakata, T., Sakane, M., Ohnami., M. (1999). Nonproportional low cycle fatigue of 6061 aluminum alloy under 14 strain paths, European Structural Integrity Society, 25, pp. 41-54. DOI: 10.1016/S1566-1369(99)80006-5.
[19] Pilkey, WD., Pilkey, DF., Peterson, RE. (2008). Peterson's stress concentration factors. 3rd ed. Hoboken, N.J. Wiley.
[20] Neuber, H. (1961). Theory of stress concentration for shear-strained prismatic bodies with arbitrary nonlinear stress-strain low, ASME Journal of Applied Mechanics, 28, pp. 544-550.
[21] Molski, K. and Glinka, G. (1981). A method of elastic-plastic stress and strain calculation at a notch root, Materials and Science Engineering, 50, pp. 93-100. DOI: 10.1016/0025-5416(81)90089-6.
[22] Peterson, R.E. (1959). Metal Fatigue, McGraw-Hill, New York, pp. 293-306.
[23] Sakane, M., Itoh, T., Susaki, T., Kawazoe, Y. (2004). T. Life prediction for notched components in nonproportional low cycle fatigue: experiment and FEM analysis, Pressure Vessel and Piping Codes and Standards, ASME. pp. 31- 38. DOI:10.1115/PVP2004-2670.
[24] Itoh, T., Chen, W., Yamamoto, R. Multiaxial low cycle fatigue life of notched specimen for Type 316L stainless steel under non-proportional loading, Journal of Solid Mechanics and Materials Engineering, 5, pp. 230-241.DOI:10.1299/jmmp.5.230.

[25] Gallo, P., Bressan, S., Morishita, T., Itoh, T., Berto, F. (2017). Analysis of multiaxial low cycle fatigue of notched specimens for type 316L stainless steel under non-proportional loading, Theoretical and Applied Fracture Mechanics, 89, pp. 79-89. DOI: 10.1016/j.tafmec.2017.01.009.

[26] Kruth, J-P., Leu, MC., Nakagawa, T. (1998) Progress in additive manufacturing and rapid prototyping. CIRP Ann, 47, pp.525–540. https://doi.org/10.1016/S0007-8506(07) 63240-5.

[27] Levy, GN., Schindel, R., Kruth, JP. (2003) Rapid manufacturing and rapid tooling with layer manufacturing (LM) technologies, state of the art and future perspectives. CIRP Ann, 52, pp. 589–609. https://doi.org/10.1016/S0007-8506(07)60206-6.

[28] Shiomi, M., Osakada, K., Nakamura, K., Yamashita, T., Abe, F. (2004). Residual stress within metallic model made by selective laser melting process. CIRP Ann, 53, pp. 195–198. https://doi.org/10.1016/S0007-8506(07)60677-5.

[29] Leuders, S., Thöne, M., Riemer, A., Niendorf, T., Tröster, T., Richard, HA., et al. (2013). On the mechanical behaviour of titanium alloy TiAl6V4 manufactured by selective laser melting: fatigue resistance and crack growth performance. International Journal of Fatigue, 2048, pp. 300–307. https://doi.org/10.1016/j.ijfatigue.2012.11.011.

[30] Baufeld, B., Brandl, E., van der Biest, O. (2011). Wire based additive layer manufacturing: comparison of microstructure and mechanical properties of Ti–6Al–4V components fabricated by laser-beam deposition and shaped metal deposition. Journal of Material Process Technology, 211, pp. 1146–1158. https://doi.org/10.1016/j.jmatprotec.2011.01.018.

[31] Wang, F., Williams, S., Colegrove, P., Antonysamy, AA. (2013). Microstructure and mechanical properties of wire and arc additive manufactured Ti-6Al-4V. Metallurgical and Materials Transactions, 44, pp. 968–977. https://doi.org/10.1007/s11661-012-1444-6.

[32] Zheng, B., Zhou, Y., Smugeresky, JE., Schoenung, JM., Lavernia, EJ. (2008). Thermal behavior and microstructural evolution during laser deposition with laser-engineered net shaping: Part I. Numerical calculations. Metallurgical and Materials Transactions, 2008;39:2228–36. https://doi.org/10.1007/s11661-008-9557-7.

[33] Vilaro, T., Colin, C., Bartout, JD. (2011). As-fabricated and heat-treated microstructures of the Ti-6Al-4V alloy processed by selective laser melting. Metallurgical and Material Transactions, 42, pp. 3190–3199. https://doi.org/10.1007/s11661-011-0731-y.

[34] Zheng, B., Zhou, Y., Smugeresky, JE., Schoenung, JM., Lavernia, EJ. Thermal behavior and microstructure evolution during laser deposition with laser-engineered net shaping: Part II. Experimental investigation and discussion. Metallurgical and Materials Transactions. https://doi.org/10.1007/s11661-008-9566-6.

[35] Koike, M., Greer, P., Owen, K., Lilly, G., Murr, LE., Gaytan, SM., et al. (2011) Evaluation of titanium alloys fabricated using rapid prototyping technologies—electron beam melting and laser beam melting. Materials (Basel), 4, 1776–1792. https://doi.org/10.3390/ma4101776.

[36] Fan, Z., Feng, H. (2018). Study on selective laser melting and heat treatment of Ti-6Al-4V alloy. Results in Physics, 10, pp. 660–664. https://doi.org/10.1016/j.rinp.2018.07.008.

[37] Tan, X., Kok, Y., Tan, YJ., Descoins, M., Mangelinck, D., Tor, SB., et al. (2015). Graded microstructure and mechanical properties of additive manufactured Ti–6Al–4V via electron beam melting. Acta Materialia, 97, pp. 1–16. https://doi.org/10.1016/j.actamat.2015.06.036.

[38] Liu, S., Shin, YC. (2019) Additive manufacturing of Ti6Al4V alloy: a review. Materials & Design, 164. https://doi.org/10.1016/j.matdes.2018.107552.

[39] Sterling, AJ., Torries, B., Shamsaei, N., Thompson, SM., Seely, DW. (2016), Fatigue behavior and failure mechanisms of direct laser deposited Ti–6Al–4V. Materials Science and Engineering: A, 655, pp. 100–112. https://doi.org/10.1016/j.msea.2015.12.026.

[40] Rekedal, K., Liu, D. Fatigue life of selective laser melted and hot isostatically pressed Ti-6Al-4V absent of surface machining. Proceedings of the 56th AIAA/ASCE/AHS/ASC Structures, Dynamics, and Materials Conference, Kissimmee, FL. 2015.

[41] Seifi, M., Dahar, M., Aman, R., Harrysson, O., Beuth, J., Lewandowski, JJ. (2015). Evaluation of orientation dependence of fracture toughness and fatigue crack propagation behavior of as-deposited ARCAM EBM Ti-6Al-4V. JOM, 67, pp. 597–607. https://doi.org/10.1007/s11837-015-1298-7.

[42] Wycisk, E., Solbach, A., Siddique, S., Herzog, D., Walther, F., Emmelmann, C. (2014). Effects of defects in laser additive manufactured Ti-6Al-4V on fatigue properties. Physics Procedia, 56, pp. 371–8. https://doi.org/10.1016/j.phpro.2014.08.120.

[43] Xu, W., Sun, S., Elambasseril, J., Liu, Q., Brandt, M., Qian, M. (2015) Ti-6Al-4V additively manufactured by selective laser melting with superior mechanical properties. JOM, 67, 668–673. https://doi.org/10.1007/s11837-015-1297-8.

[44] Liu, QC., Elambasseril, J., Sun, SJ., Leary, M., Brandt, M., Sharp, PK. (2014) The effect of manufacturing defects on the fatigue behaviour of Ti-6Al-4V specimens fabricated using selective laser melting. Advanced Materials Research, 891–892, pp.1519–1524. doi.org/10.4028/www.scientific.net/AMR.891-892.1519.

[45] Li, P., Warner, DH., Fatemi, A., Phan, N. (2016) Critical assessment of the fatigue performance of additively manufactured Ti–6Al–4V and

perspective for future research. International Journal of Fatigue, 85, pp. 130–43. https://doi.org/10.1016/j.ijfatigue.2015.12.003.

[46] Sterling, A., Shamsaei, N., Torries, B., Thompson, SM. (2015). Fatigue behaviour of additively manufactured Ti-6Al-4V. Procedia Engineering, 133, pp. 576–589. https://doi.org/10.1016/ j.proeng.2015.12.632.

[47] Wu, M., Itoh, T., Shimizu, Y., Nakamura, H., Takanashi, M. (2012). Low cycle fatigue life of Ti–6Al–4V alloy under non-proportional loading. International Journal of Fatigue, 44, pp. 14–20. https://doi.org/10.1016/j.ijfatigue.2012.06.006.

[48] Fatemi, A., Molaei, R., Sharifimehr, S., Shamsaei, N., Phan, N. (2017) Torsional fatigue behavior of wrought and additive manufactured Ti-6Al-4V by powder bed fusion including surface finish effect. International Journal of Fatigue, 99, pp. 187–201. https://doi.org/10.1016/j. ijfatigue.2017.03.002.

[49] Fatemi, A., Molaei, R., Sharifimehr, S., Phan, N., Shamsaei, N. (2017). Multiaxial fatigue behavior of wrought and additive manufactured Ti-6Al-4V including surface finish effect. International Journal of Fatigue, 100, pp. 347–366. https://doi.org/10.1016/j.ijfatigue.2017.03.044.

2. FEM investigation on the crack initiation site on notched components under uniaxial and non-proportional low cycle fatigue

2.1. Introduction

In this chapter a finite element method analysis has been conducted in order to analyze the stress-strain distribution on the notched surface of samples subject to non-proportional loading. The modeling has been conducted based on the experimental tests on notched components made of stainless steel SUS 316L of Ref. [1]. The causes of the crack initiation site shifted from the notch tip found in Ref. [1] have been investigated and discussed based on the results of the simulation. The results of the simulation have been also employed to modify the I-S model and improve fatigue life evaluation. A detailed overview of the Itoh-Sakane model is also presented in this chapter.

2.2. Experimental tests

2.2.1 Specimens shape and material

Experimental fatigue tests have been conducted on notched specimens made by stainless steel SUS 316L with four different stress concentration factors referred to the net section $K_{t,n}$ [1]. The specimens shape is reported in Fig. 2.1 (a-b). The chemical composition of the material is reported in Table 2.1.

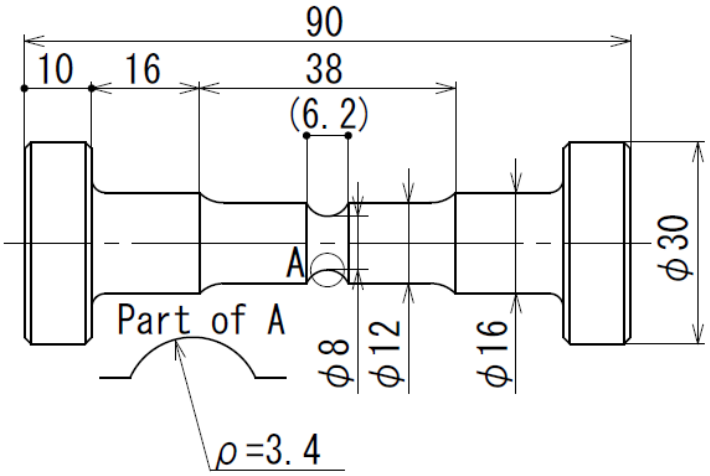

Fig. 2.1. (a) Notched specimen with $K_{t,n}$=1.5 (dimensions in mm) [1]

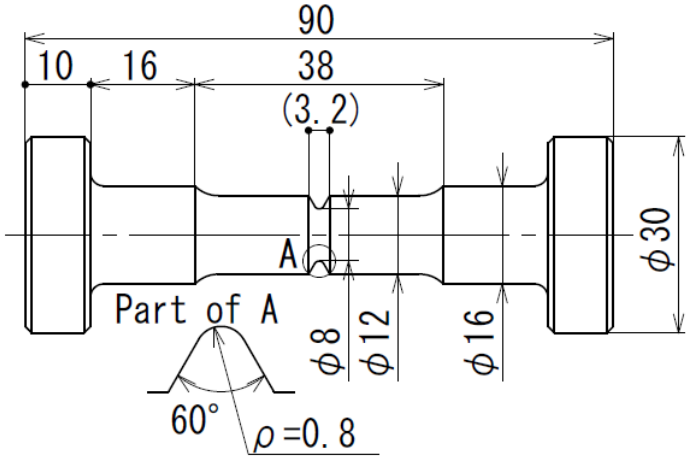

Fig.2.1. (b) Notched specimen with $K_{t,n}$=2.5 (dimensions in mm)[1]

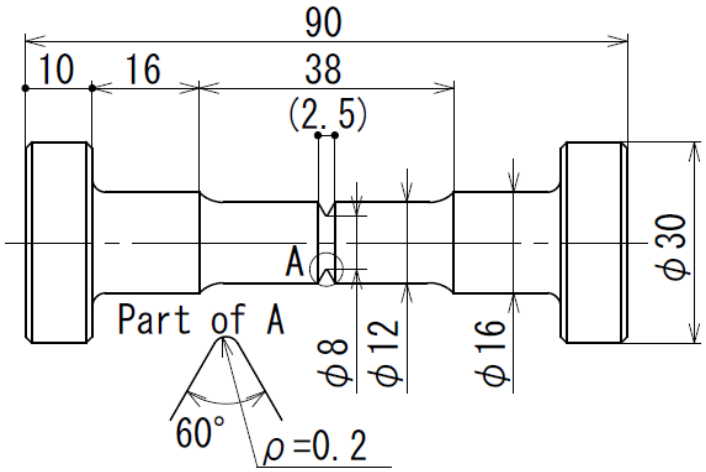

Fig. 2.1. (c) Notched specimen with $K_{t,n}$=4.2 (dimensions in mm) [1]

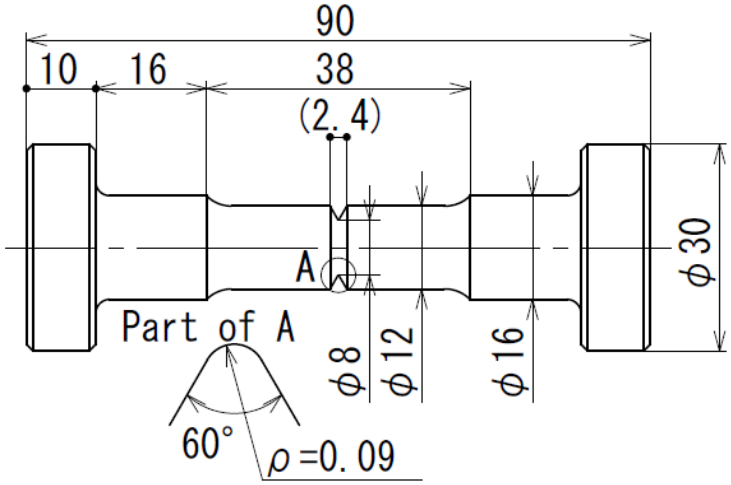

Fig. 2.1. (d) Notched specimen with $K_{t,n}$= 6.0 (dimensions in mm) [1]

Table 2.1 Chemical composition of SUS 316L

C (%)	Si (%)	Mn (%)	P (%)	S (%)	Ni (%)	Cr (%)	Mo (%)
0.07	0.75	1.5	0.03	0.015	12.00	17.00	2.5

2.2.2 Experimental apparatus

The employed testing machine is a hydraulic than can apply both axial stress and torsional stress. The low cycle fatigue tests are conducted under strain control by means of an extensometer attached to the specimens. A schematic representation of the testing machine is represented in Fig. 2.2.

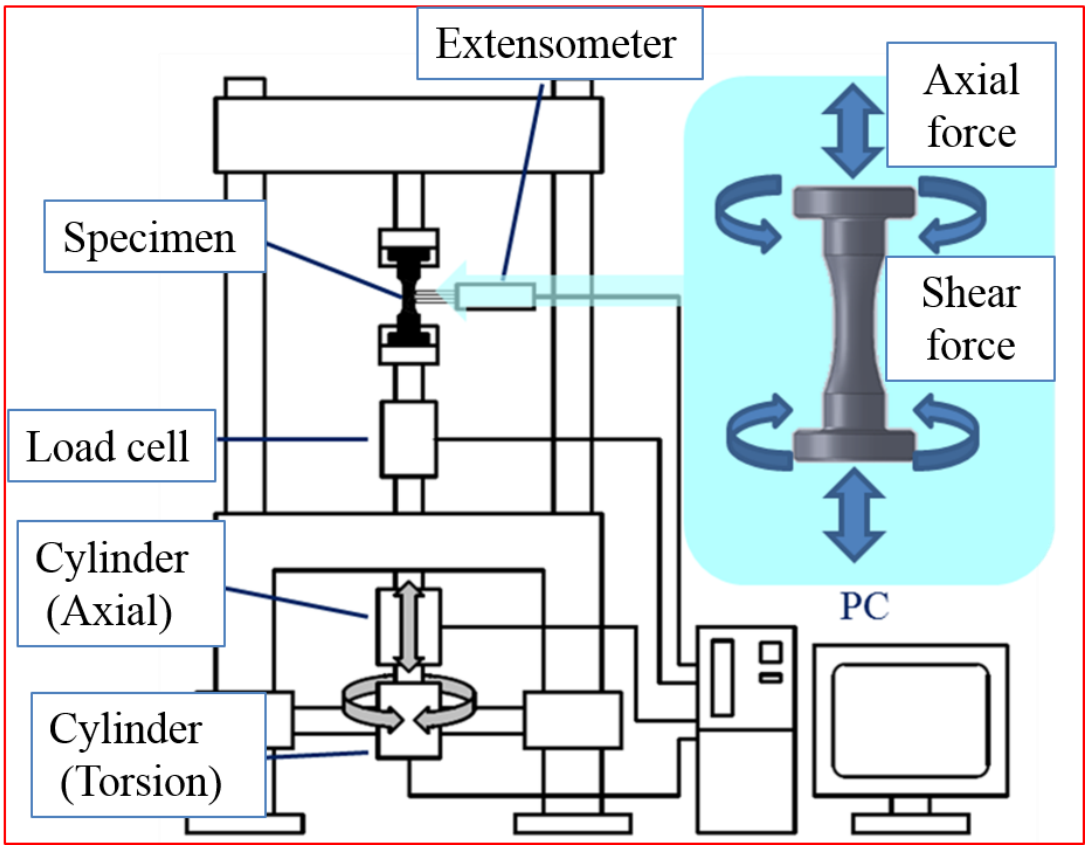

Fig. 2.2. Servo-hydraulic testing machine schematic representation

2.2.3 Test conditions

The specimens have been tested with a push-pull loading (PP), a reverse-torsion loading (RT) and a 90 degree out of phase push-pull and reverse torsion loading denominated circle (OP). In the circle strain path, the von Mises' equivalent strain range does not change although the direction of the first

principal strain range rotates within the cycle. The strain paths are represented in Fig. 2.3.

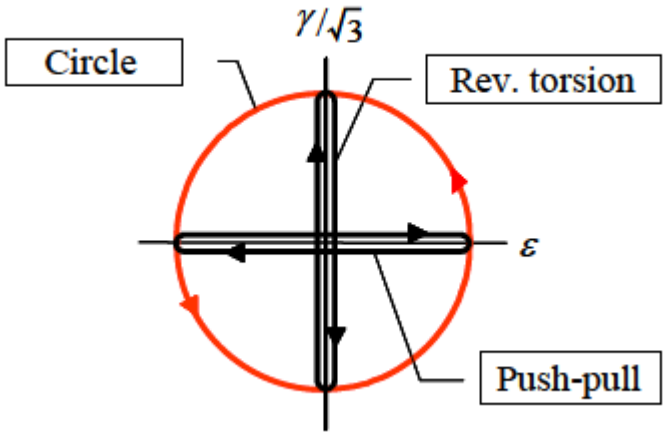

Fig. 2.3. Applied strain paths: push-pull (PP), reverse torsion (RT) and Circle (OP) [1]

2.2.4 Stress-strain cyclic curves

As mentioned in the introduction, the material stress-strain cyclic curves are a fundamental indicator of the material cyclic plastic behavior occurring in case of low cycle fatigue. Furthermore, it provides valuable information regarding additional hardening phenomena typical of non-proportional multiaxial loading. In order to obtain the stress-strain cyclic curves, the incremental step method has been employed. An equivalent strain range $\Delta\varepsilon_{eq}$ varying from 0.1% and increased by 0.1% every 10 cycles is applied to a smooth specimen. The stress-strain at the 10th cycle of each applied strain range represents a dot of the final cyclic stress-strain curve. The results for SUS 316L are reported in Fig. 2.4. The cyclic curve associated with OP is higher than the one of PP due to the additional hardening effect.

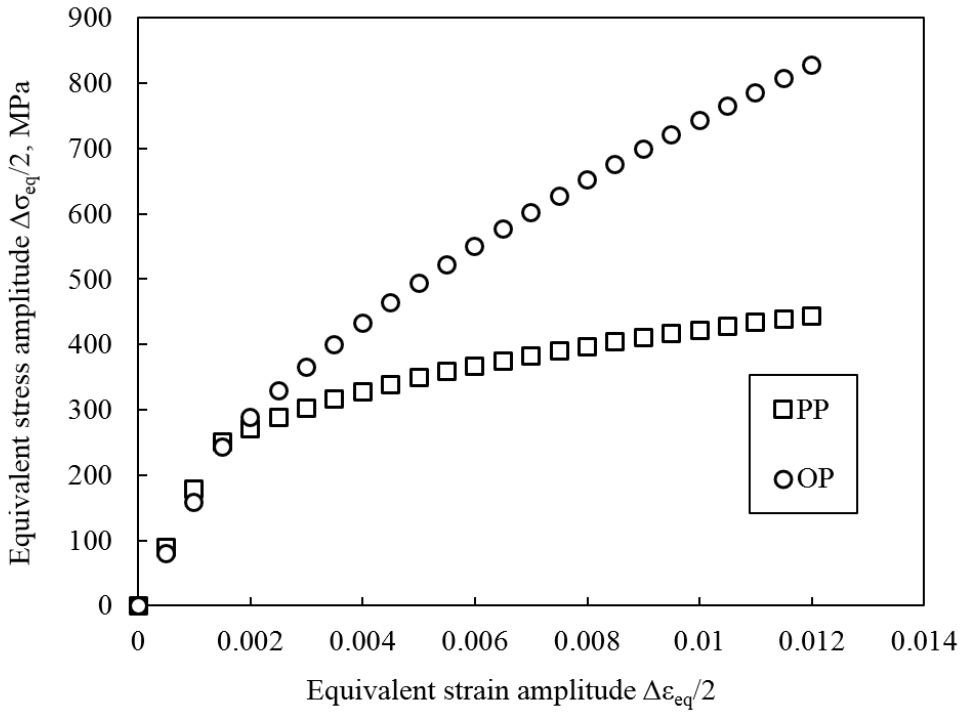

Fig. 2.4. Cyclic stress-strain curves of SUS 316L under PP and OP [2]

2.2.5 Hardening of the notched area

Although Fig. 2.4 is representative of the hardening behavior of the material for both uniaxial and multiaxial non-proportional loading, it does not consider the effect of stress or strain concentration. In order to obtain an estimation of the hardening behavior in the vicinity of the notch tip, interrupted tests at 0.3 N_f have been conducted. The specimens have been cut along the section and the Vickers hardness measured every 0.3mm along 5 directions as represented in Fig. 2.5. The influence of the strain path on hardness have been verified by plotting the measured values of HV for each notch geometry along the direction 0°. The results are represented in Fig. 2.6 and Fig. 2.7. The maximum value of hardness for PP in $K_{t,n}$=2.5, 4.2 and 6 is approximately the same. The value of hardness for $K_{t,n}$=1.5 is an intermediate level between those of $K_{t,n}$=1 and $K_{t,n}$=1.5-6. The maximum value of hardness in case of PP is approximately 300HV and it stabilizes at 200HV at a distance of 0.5mm from the notch tip. In case of OP, a direct correlation between the maximum hardness at the notch tip and the value of stress concentration factor has been observed. the maximum level of hardness has been recorded for $K_{t,n}$ = 6.0 and it is equal to 370HV. In conclusion, the value of hardness is not only depending on the strain path but also on the value of stress concentration factor. In order to visualize the hardness distribution around the notch tip hardness maps have been created. The hardness

maps provide an indication of the material hardening and therefore the material plastic deformation in the vicinity of the notch in case of push-pull and circle loading. Some example of hardness maps is reported in Fig. 2.8.

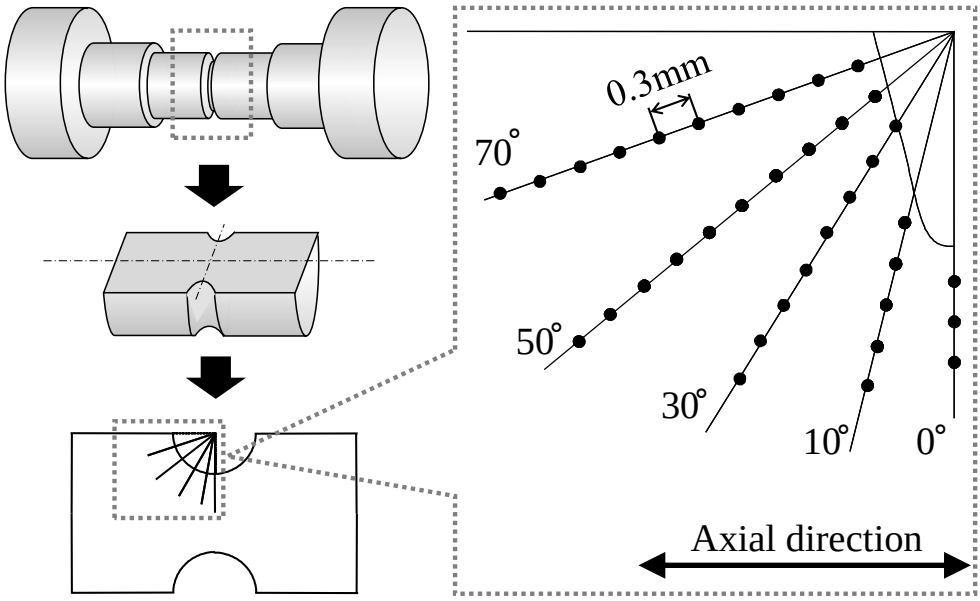

Fig. 2.5. Spot for HV analysis on the cut surface [2]

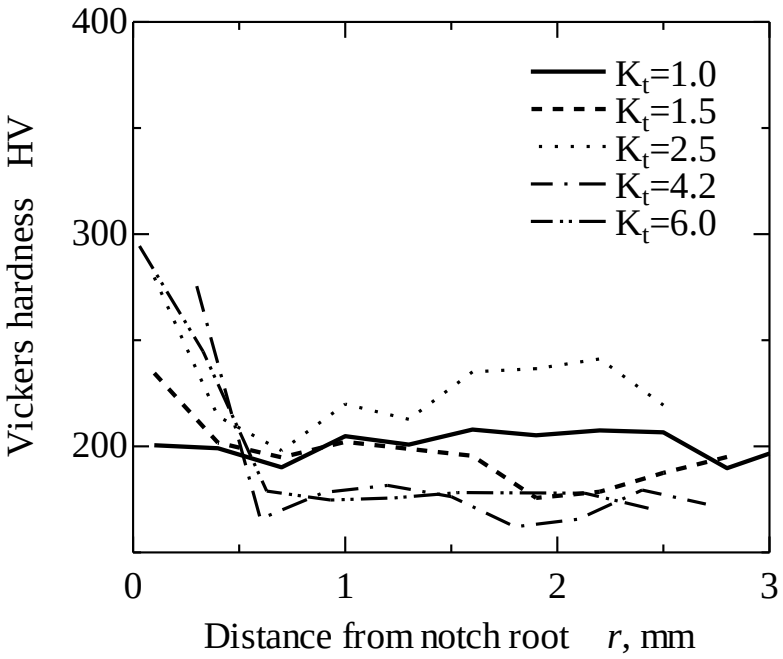

Fig. 2.6. Hardness for PP tests along 0° direction [1]

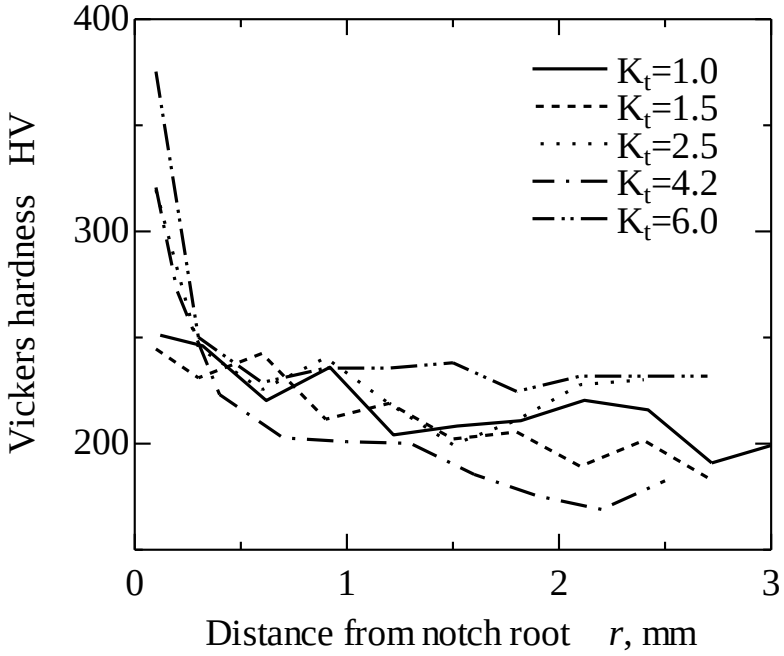

Fig. 2.7. Hardness for OP tests along 0 degrees direction [1]

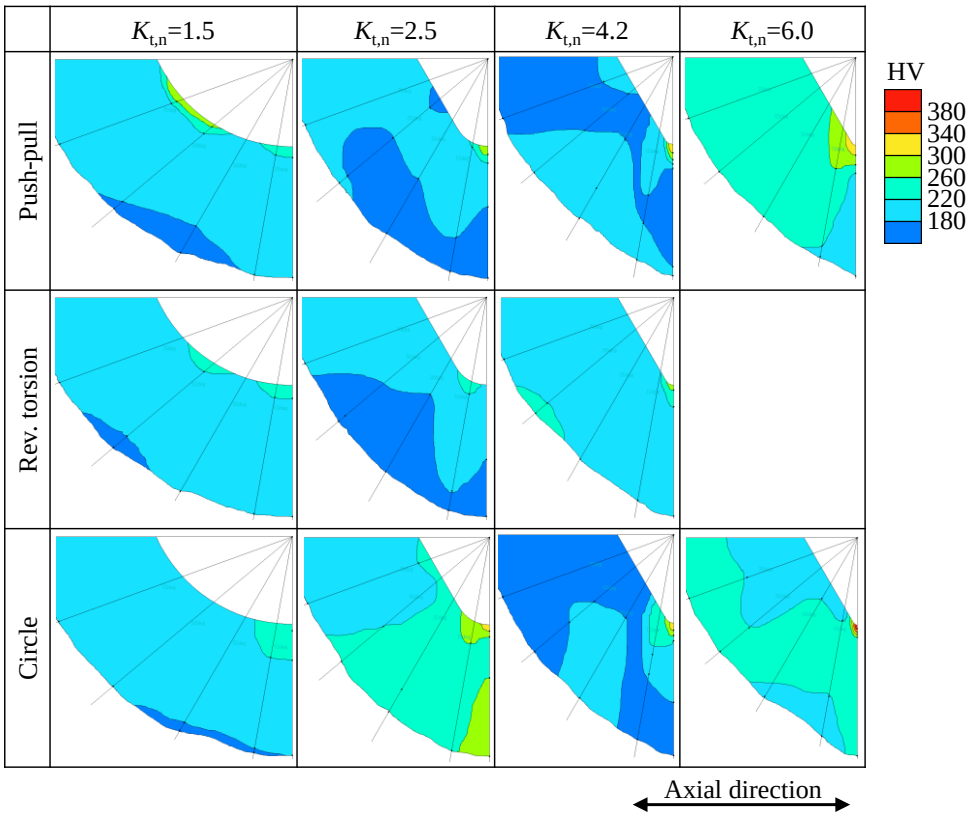

Fig. 2.8. Hardness maps for several $K_{t,n}$ and strain paths.[2]

2.2.6 Test results

The fatigue tests results summarized in Table 2.2. The tests interrupted when the stress becomes the 3/4 of the maximum stress recorded in the test. The number of cycles to failure are indicated with N_f.

Table 2.2 Fatigue tests results of notched specimens made of SUS 316L [1]

Strain Path	$K_{t,n}$	$\Delta\sigma$ at 1/2 N_f (MPa)	$\Delta\tau$ at 1/2 N_f (MPa)	N_f (Cycles)
Push-Pull	1	680	-	6909
	1.5	800	-	2237
	2.5	800	-	871
	4.2	810	-	571
	6	830	-	418
Circle	1	780	1050	2082
	1.5	850	1030	2248
	2.5	880	1080	475
	4.2	900	1140	212
	6	850	930	156
Reverse Torsion	1	-	600	Run Out
	1.5	-	720	54809
	2.5	-	910	4806
	4.2	-	890	3094
	6	-	850	2243

In case of push-pull, N_f decrease is proportional to the increasing of $K_{t,n}$. In case of $K_{t,n}$=6.0, N_f becomes approximately 6% of that in $K_{t,n}$=1.0. However, in circle, N_f at $K_{t,n}$= 1.5 is slightly higher than the one of smooth specimen. Except for $K_{t,n}$, N_f decreases with increasing $K_{t,n}$ in the range $K_{t,n}$=2.5-6.0 also for circle. The levels of maximum axial stress for circle are slightly higher than the ones recorded for PP due to additional hardening. Fatigue life of the specimens subject to circle are lower than the ones subject to push-pull except for $K_{t,n}$= 1.5.

2.3. Itoh-Sakane model

The Itoh-Sakane (I-S) model has been originally introduced for smooth specimen as an alternative to the critical plane models to asses fatigue life for proportional and non-proportional loadings [3-4]. The model is strain based and considers two factors which take into account the non-proportionality of the

loading: non-proportional factor $f_{NP,}$ which express the severity of non-proportional loading and material constant α, which is related to the material additional hardening due to non-proportional loading. These parameters are employed to modify the first principal strain range and the non-proportional strain range $\Delta\varepsilon_{NP}$ is defined as follows:

$$\Delta\varepsilon_{NP} = (1 + \alpha f_{NP})\Delta\varepsilon_1 \tag{2.1}$$

The factor f_{NP} depends on the rotation of the first principal stress over the cycle and depends exclusively on the strain path [5]. An example of values of f_{NP} can be observed in Fig. 2.9.

Type	1	2	3	4	5	6
Loading path	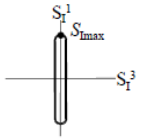	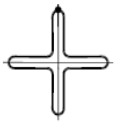	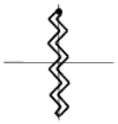		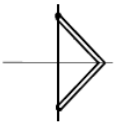	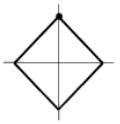
f_{NP}	0	0.39	0.10	0.20	0.79	0.79
f'_{NP}	0	0.49	0.12	0.24	0.71	0.71
Type	7	8	9	10	11	12
Loading path	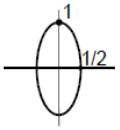	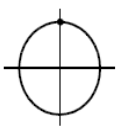	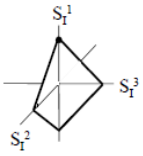			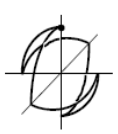
f_{NP}	0.53	1.06	-	-	-	-
f'_{NP}	0.5	1	0.71	0.98	0.49	1.78

Fig 2.9. Values of f_{NP} for several loading paths [5]

The non-proportional intensity factor f_{NP} assumes the value of 1 for circle and it has a considerable detrimental effect on fatigue life. The factor α depends on the material and quantifies the magnitude of additional hardening due to the non-proportionality of the loading. This factor can be obtained in two methods. The first one is the ratio between the stress of the stress-strain cyclic curve obtained for circle loading and push-pull loading:

$$\alpha = \frac{\Delta\sigma eq/2_{Circle}}{\Delta\sigma eq/2_{Push-Pull}} \tag{2.2}$$

A representation of Eq. 2.2 on the cyclic curves of the material is depicted in Fig. 2.10. Another method for the definition of α is the ratio between the number of

cycles to failure in case for non-proportional loading and the number of cycles to failure in case of uniaxial loading for the same strain range.

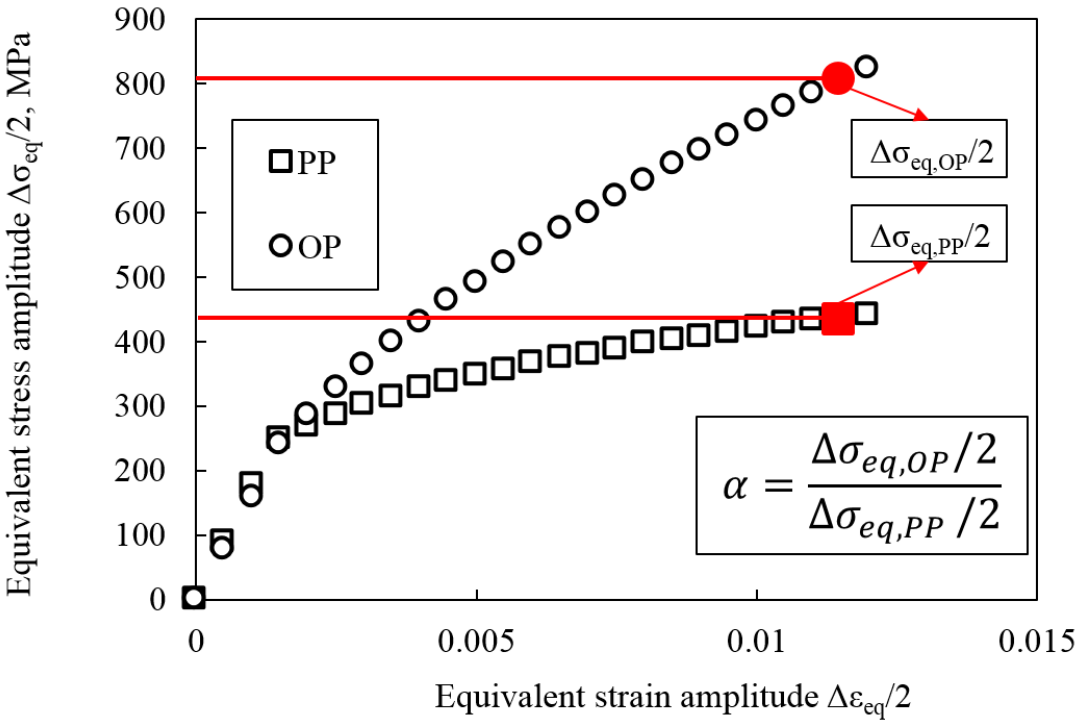

Fig. 2.10. Additional hardening parameter α parameter defined as ratio between $\Delta\sigma_{eq}$ of the PP and OP stress-strain cyclic curves

Itoh *et al.* proposed a modified I-S model for fatigue life evaluation of fatigue life of notched specimens under non-proportional loading [1]. The non-proportional strain range $\Delta\varepsilon_{NP}$ is multiplied by $K_{t,n}$. In presence of plastic deformation, the strain concentration factor K_ε should be considered. However, in order to simplify the fatigue life evaluation the model assumes that $K_{t,n} \approx K_\varepsilon$. The final model is:

$$K_{t,n}\Delta\varepsilon_{NP} = K_{t,n}(1 + \alpha f_{NP})\Delta\varepsilon_1 \quad (2.3)$$

The application of the model returns satisfying results in a factor of 2 scatter band [1]. Non-proportional strain range can be well correlated with N_f also for notched specimens despite the simplifying assumption that $K_{t,n} \approx K_\varepsilon$.

2.4. Finite element method model

2.4.1 Modeling concept

The application of I-S model relies on the knowledge of local parameters that can be evaluated through different ways: on the basis of liner elastic behavior

neglecting the plastic contribution; through a finite element analysis in order to take into account the plastic effects and hardening occurring at the notch tip. The objective of the proposed FEM methodology employing the software ANSYS is to replicate the hardening behavior observed in Fig. 2.8 and conduct a simulation to verify the stress-strain distribution in the vicinity of the notch tip in order to: find a correlation between the stress-strain status and the crack initiation position on the notch tip and improve the IS model based on the results. In detail, the notch tip has been divided in different hardening areas such as the ones observed in Fig. 2.8, and a cyclic curve has been assigned to each area representing a different hardening level. The PP and OP cyclic stress-strain curves of Fig. 2.4 represent the minimum and maximum hardening respectively. For this reason, the PP stress-strain cyclic curve has been assigned to the material close to the axis of symmetry, while the OP stress-strain cyclic curve has been assigned to the outer surface of the notch tip. This choice has been made based on the hardness maps of Fig. 2.8 which show a decrease of the hardness moving away from the notch tip. Furthermore, the choice is justified by the shear stress distribution on the specimens (Fig. 2.11). The shear stress assumes the maximum value on the notch tip and gradually decreases until the axis, where only the axial stress induced by the axial loading is present. The portion of material between the axis and the notch tip has been modeled with intermediate curves obtained through best fitting procedures [2,6]. In detail, as limit conditions, circle curve was related to 100% of shear stress while PP to 0%. The procedures followed for the determination of the intermediate cyclic curves is presented exhaustively in the next section. Thanks to this modeling technique, the cyclic hardening behavior has been intrinsically taken into account, and a static axial loading corresponding to the maximum axial nominal stress range recorded in experimental tests has been applied. As a result, values and positions of local strain and stresses have been obtained.

2.4.2 Intermediate curves evaluation

In order to evaluate the intermediate hardening behavior through best fitting, the equations describing the PP and OP have been obtained. The following material power law constitutive equation has been employed to describe the non-linear relationship between the stress and plastic strain:

$$\Delta\sigma = K'\Delta\varepsilon^{n'} \tag{2.4}$$

The parameters *K*' and *n*', have been obtained through best fitting procedures of the PP and OP curves. The intermediate curves have been defined based on the percentage of shear stress R_τ. OP stress-strain cyclic curve represents the 100% of shear stress while PP stress-strain cyclic curve represents 0% of shear stress. In order to evaluate *K*' and *n*' variation between OP and PP, few curves have been obtained by imposing a certain percentage of stress for each value of strain given by experimental curves, in order to obtain a curve corresponding to a certain percentage of shear stress.

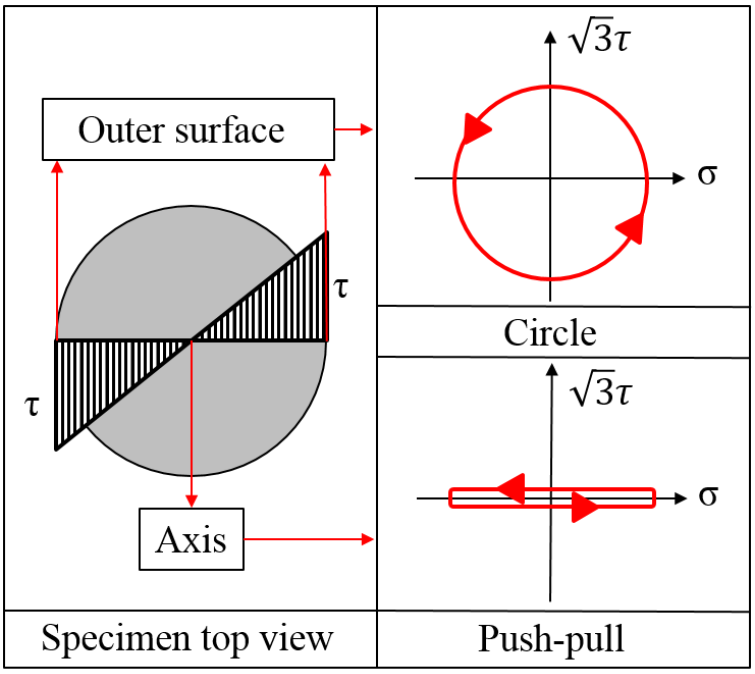

Fig. 2.11. Shear stress distribution and effectiveness of circle loading

The selected values of R_τ values were 20, 40, 60 and 80%. A further another regression with the same constitutive equation of Eq. 2.4 has been conducted in order to obtain *K*' and *n*' for such curves. Finally, the equation describing the variation of *K'* and *n'* in function of R_τ has been obtained (Fig. 2.12 and Fig. 2.13). The intermediate curves to describe the material hardening behavior between the notch tip and the axis could be obtained with the equations reported in Figs. 2.12 and 2.13. A representation of the intermediate curves based on the percentage of shear stress between PP and OP is visualized in Fig. 2.14. For the proposed simulation, 100 intermediate curves have been selected to simulate the decrease of hardening between the tip and the axis.

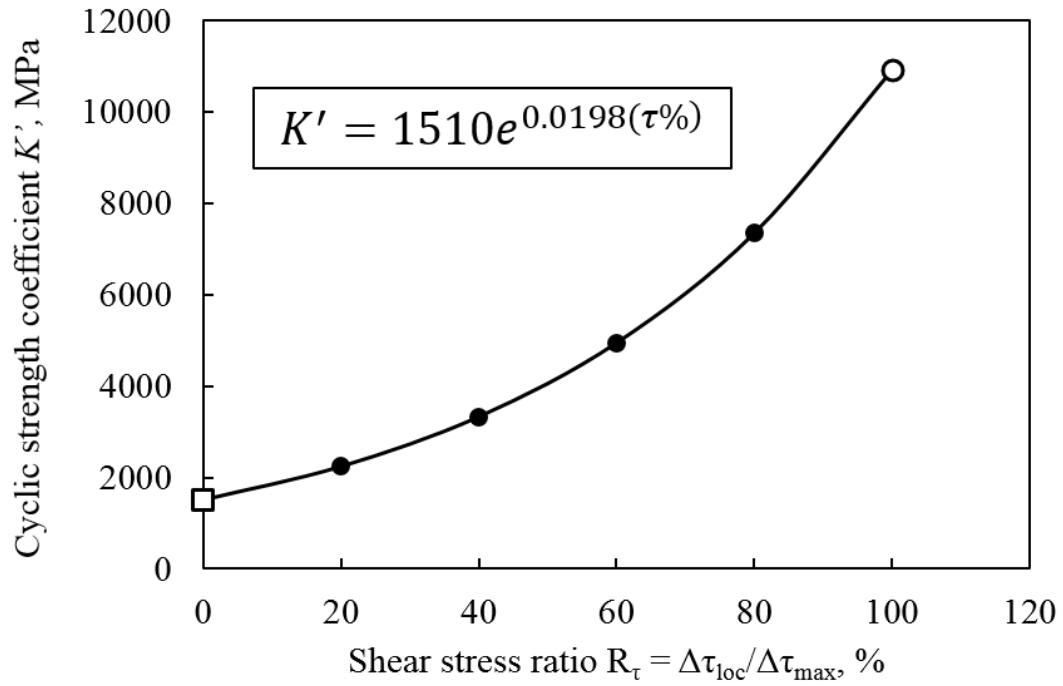

Fig. 2.12. K' variation between Push-Pull and Circle curves.

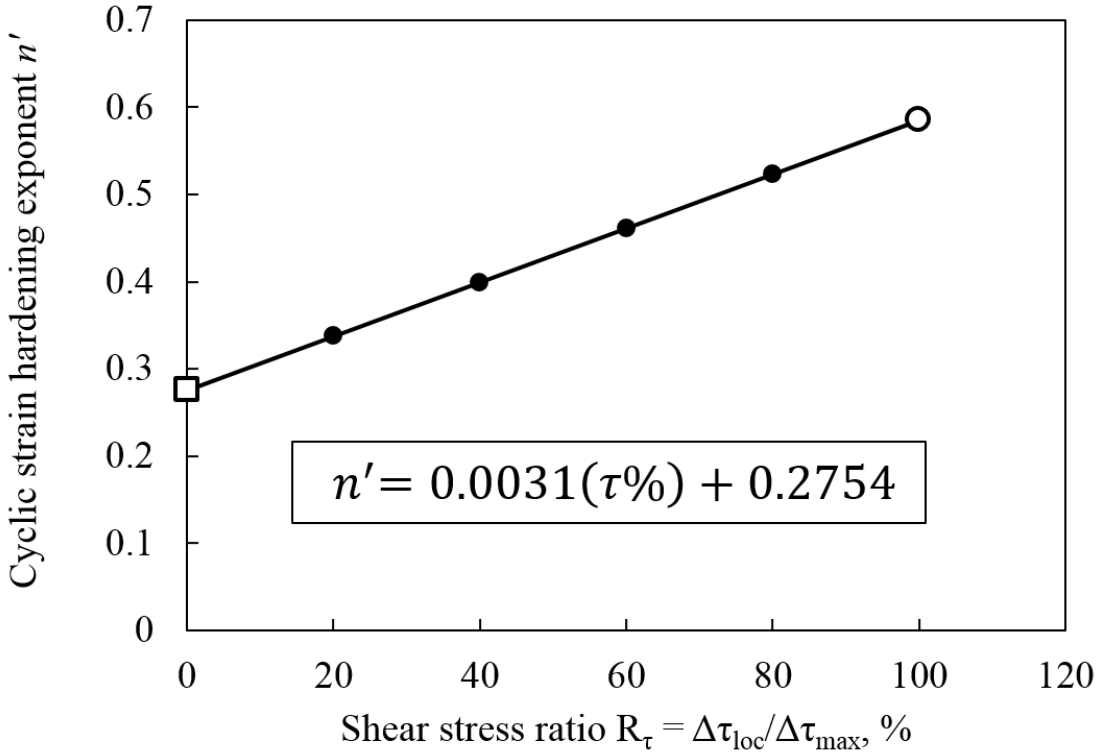

Fig. 2.13. n' variation between Push-Pull and Circle curves

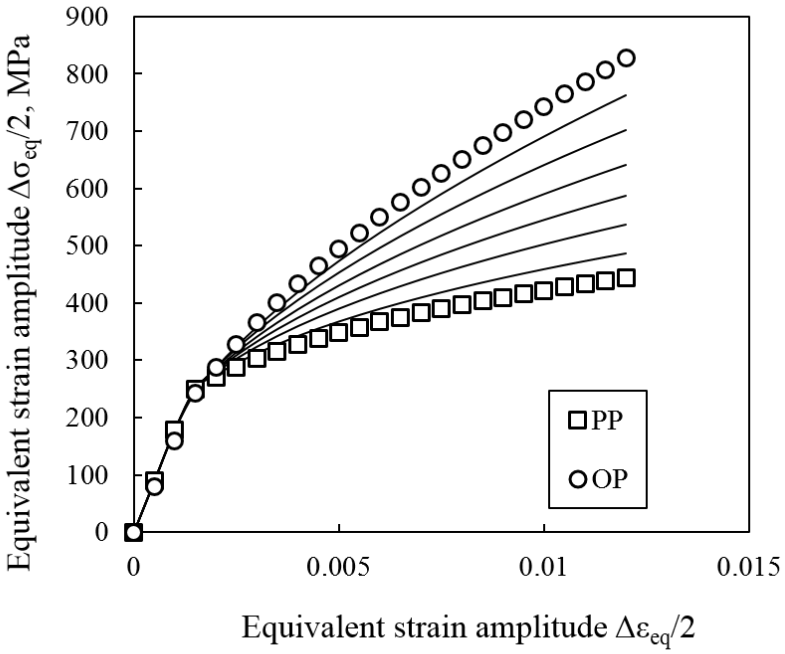

Fig. 2.14 Example of curves obtainable with the equations of K' and n'

2.4.3 Areas size and shape

In order to simplify the modeling process, the shape of the area with the same level of hardening has been assumed circular. The division of the areas with different value of hardening has been made based on the variation of the shear stress, which depends on the value of $K_{t,n}$. The variation of shear stress is represented in Fig. 2.15.

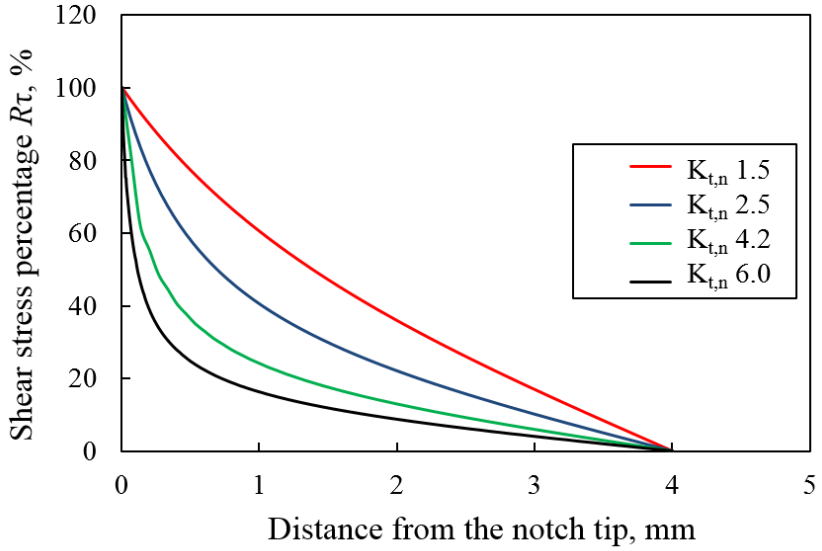

Fig. 2.15. Shear stress variation for different $K_{t,n}$ in percentage values

The areas have been modeled following the shear stress percentage variation showed on Fig. 2.15. A new circular area has been modeled for each 1% of shear stress percentage variation. The FEM software employed was ANSYS 14.5. The specimen has been created as a 2D plate to simplify the modeling process. Although the analysis has been conducted in a 2D environment, an element which takes in account of the axial symmetry of the component have been employed to model the specimen. A hundred material curves have been defined in the program, each of which has been assigned to a different area. Each material is constituted by two components: a linear behavior corresponding to the elastic trait and a non-linear behavior which describes the plastic trait. A free mesh has been generated after the creation of the areas. A fine mesh has been defined in the vicinity of the notch tip to detect the sudden variations of the stress and strain. The size of the smallest created element was approximately 7µm for $K_{t,n}$ =1.5 and 0.25µm for $K_{t,n}$=6.0. Each area has been meshed with a different material, representing a different hardening curve. The area at the notch tip has been meshed with the OP stress-strain cyclic curve, and the intermediate curve representing a lower hardening level has been employed to mesh the subsequent areas. The process has been repeated until reaching the PP stress-strain cyclic curve, representing the lower level of hardening. The final result was a new simplified hardness map that has been tested by applying the same axial stress recorded in the test and the results has been acquired based on this model. The final model is represented in Fig. 2.16.

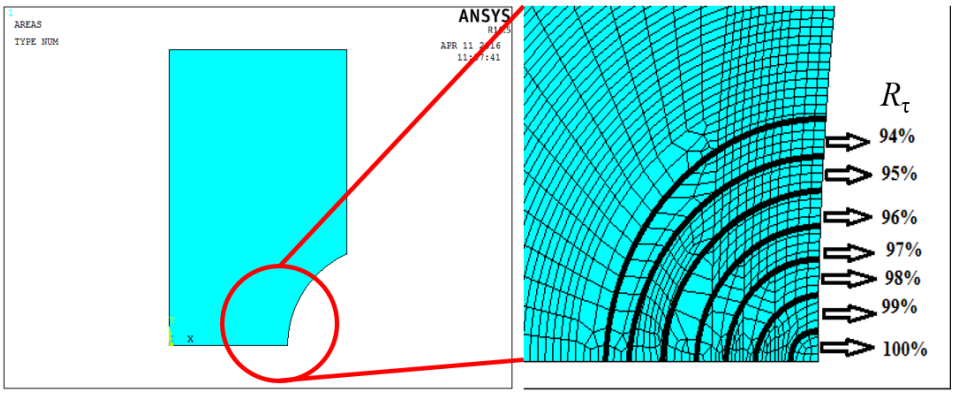

Fig 2.16. Meshed area in the vicinity of the notch tip. Each percentage indicates a different hardening level.

2.5. Results and discussion

2.5.1 Analysis of stress-strain distribution

Local parameters of tangential strain ε_θ and von Mises' stress have been obtained through the finite element simulations. The contour plots show that the local maximum strain is not at the tip and the maximum equivalent stress is always at the tip (Fig. 2.17 and Fig. 2.18).

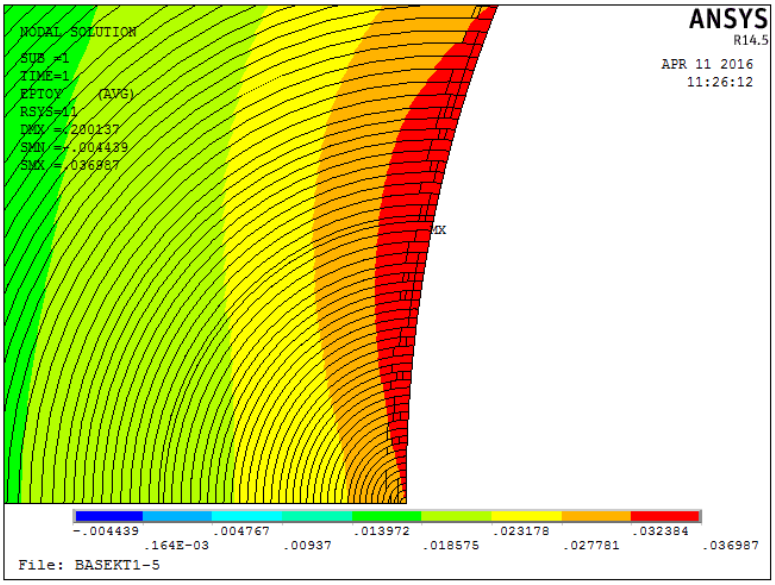

Fig. 2.17 Contour plot ε_θ $K_{t,n}$ =1.5

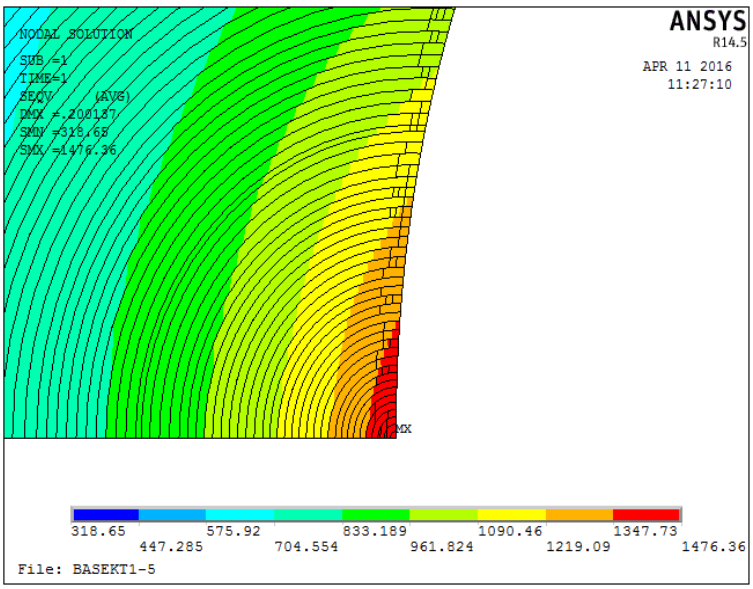

Fig 2.18 Contour plot stress $K_{t,n}$ = 1.5

This is due to the different hardness which occurs in the specimen as the result of an LCF test. The position of the maximum ε_θ is the result of a combination of stress and hardening curve. The higher $K_{t,n}$ the lower is the distance between the notch tip and the position of the maximum tangential strain ε_θ. The maximum local strain was located away from the notch tip in each analyzed geometry. The value of the distance in mm and degrees is reported in Table 2.3.

Table 2.3 Location of the maximum tangential strain ε_θ from the notch tip in mm and degrees

$K_{t,n}$ ()	ρ (mm)	2α (°)	r_0 (mm)	θ (°)
1.5	3.4	48.64	1.44	29.3
2.5	0.8	60	0.32	37.4
4.2	0.2	60	0.08	53.4
6.0	0.09	60	0.036	57.6

The higher is $K_{t,n}$, the lower is the distance of the maximum strain ε_θ from the notch tip. This is probably due to the combination of variation of the stress along the notched surface and the hardness distribution on the notch tip. The point of maximum strain has been assumed to coincide with the crack initiation site position of the notched surface.

2.5.2 Modification of I-S model

In order to take into account of the results obtained to modify and improve the I-S model of Eq. 2.3 the following procedure has been proposed. The stress concentration factor evaluated on the net section $K_{t,n}$ has been replaced with a stress concentration factor that takes into account of the point of maximum strain and, by assumption, with the crack initiation site. A new stress concentration factor denominated here K_t' has been evaluated as the ratio of the stress in the point of the notched surface where the ε_θ assumes the maximum value. The stress in such point is referred as σ'_{loc}, while the stress at the notch tip is σ_{max}:

$$K_{t,n} = \frac{\sigma_{loc}}{\sigma_n} \tag{2.5}$$

$$K'_t = \frac{\sigma'_{loc}}{\sigma_n} \tag{2.6}$$

The values of K_t' are reported in Table 2.4. A schematic representation of the evaluation of K_t' in relation to the crack initiation site is reported in Fig. 2.28. The values of K_t' are lower than $K_{t,n}$ since $\sigma'_{loc} < \sigma_{max.}$ This modification has been made under the assumption that the crack initiation site coincides with the maximum strain position and that the number of cycle to crack initiation represent a consistent portion of the total fatigue life. The modified model is reported in Eq. 2.12.

$$K'_t \Delta\varepsilon_{NP} = K'_t(1 + \alpha f_{NP})\Delta\varepsilon_1 \tag{2.7}$$

The results of the application of the model of Eq 2.11 have been compared with the ones obtained by using Eq. 2.3 and are visualized in Fig. 2.20.

Table 2.4 $K_{t,n}$ and K'_t values

$K_{t,n}$ ()	K'_t ()
1.5	1.2
2.5	1.8
4.2	2.8
6	3.4

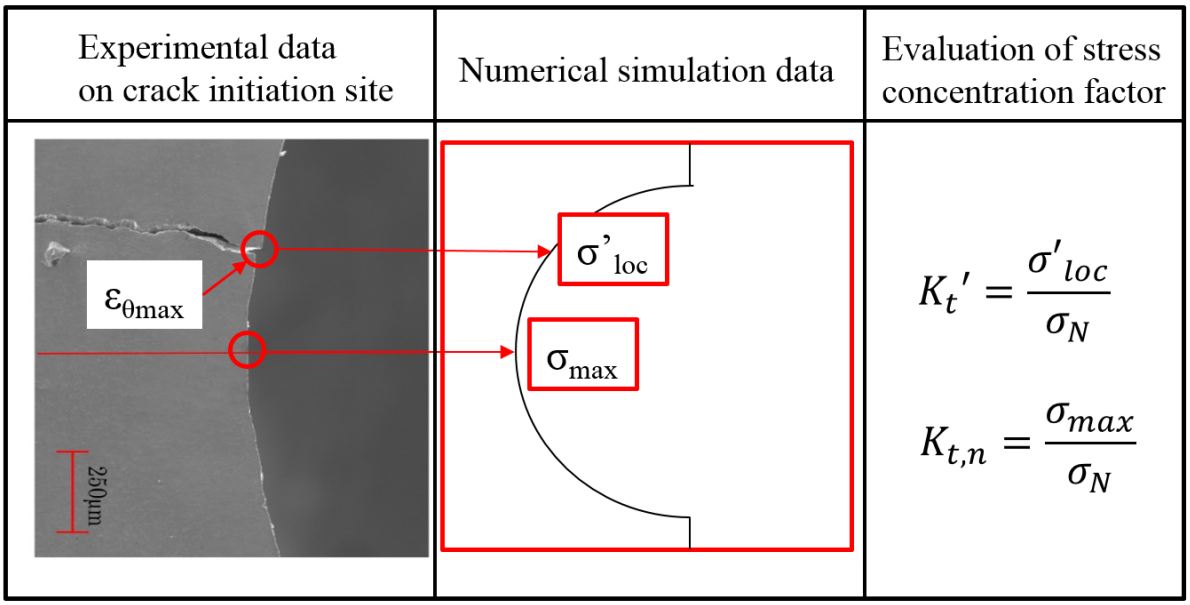

Fig. 2.19. Procedure for the evaluation of K'_t

Fatigue life evaluation conducted considering the modified proposed model of Eq. 2.12 is slightly improved. Fatigue life evaluated with Eq. 2.12 are synthesized in a factor of band 1.6 compared to the factor of 2 band of Eq. 2.3

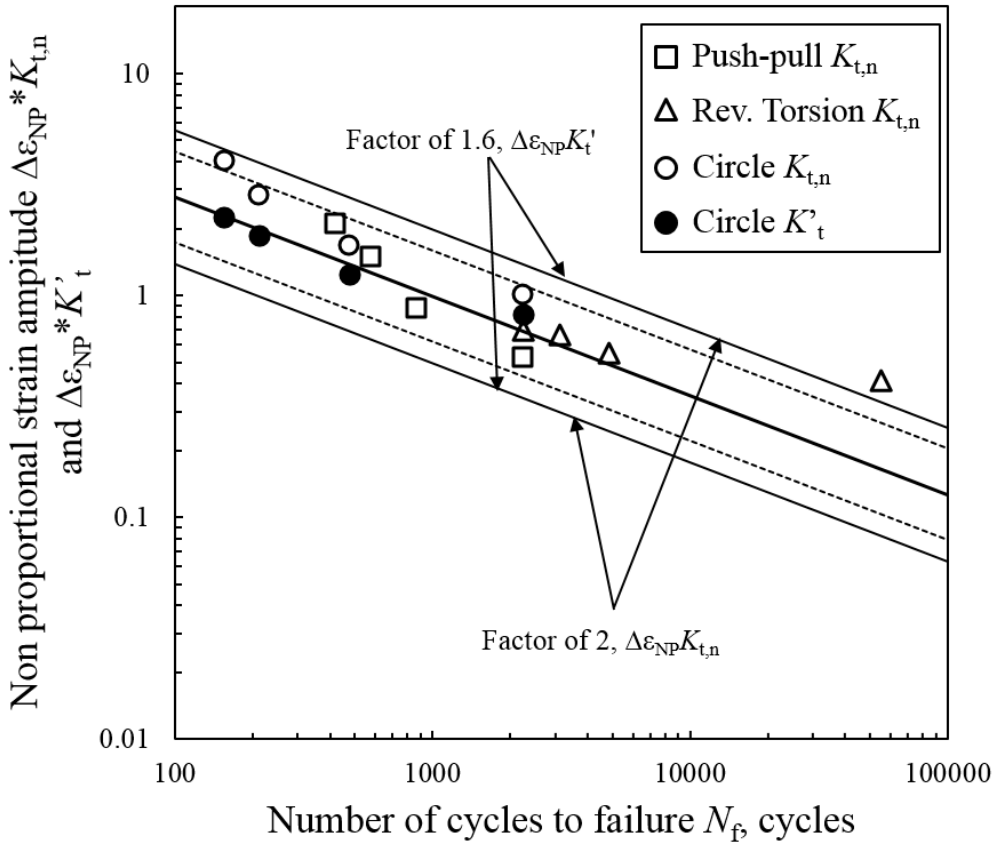

Fig. 2.20. Comparison between $\Delta\varepsilon_{np}K_{t,n}$ and $\Delta\varepsilon_{np}K'_t$

2.6. Discussion

The simulation demonstrated that the additional hardening occurring on materials such as the one tested might originate anomalous strain distributions around the notch tip. The combination of stress concentration intensity and additional hardening is the cause of the strain distribution observed. Even under simplifying assumptions, the FEM modeling reproduced the hardening maps and therefore the real behavior of the material. However, in order to further validate such assumptions, materials with a diametrically oppose plastic behavior must be analyzed. Furthermore, the theory that the crack initiation site coincide with the location of the maximum strain ε_θ must be verified by measuring accurately the distance of the crack initiation site from the notch tip on the specimens. Although the model modified with K_t' has been applied to every geometry, the application on the specimens with higher $K_{t,n}$ such as 4.2 and 6.0 might be unnecessary given due to the low contribution to the fatigue life by the crack

initiation process [7]. The modified model could improve the results by considering the real behavior of the material under non-proportional loading.

2.7. Conclusions

FEM simulations have been conducted to verify the stress-strain field on the vicinity of the notch tip of SUS 316L notched specimens subject to uniaxial and multiaxial non-proportional loading. The results of the simulations have been employed to modify the I-S for life evaluation and improve the results. The conclusions can be summarized as follows:

1. The maximum tangential strain ε_θ is not located at the notch tip but it is shifted by a magnitude which is dependent on the stress concentration effect intensity. The higher the $K_{t,n}$ the lower the distance of the maximum tangential strain.

2. The I-S model modified with a new stress concentration factor K_t' which takes into account the crack initiation site returns more satisfying results than the original I-S model.

3. The model provides a sound interpretation of the hardening behavior of the material under non-proportional loading. The model can be employed by knowing the stress-strain cyclic curves and can be easily used as opposed to model requiring the application of complicated hardening rules.

References

[1] Itoh, T., Chen, W., Yamamoto, R. Multiaxial low cycle fatigue life of notched specimen for Type 316L stainless steel under non-proportional loading, Journal of Solid Mechanics and Materials Engineering, 5, pp. 230-241.DOI:10.1299/jmmp.5.230.

[2] Gallo, P., Bressan, S., Morishita, T., Itoh, T., Berto, F. (2017). Analysis of multiaxial low cycle fatigue of notched specimens for type 316L stainless steel under non-proportional loading, Theoretical and Applied Fracture Mechanics, 89, pp. 79-89. DOI: 10.1016/j.tafmec.2017.01.009.

[3] Itoh, T., Sakane, M., Ohnami., D.F., Socie, D.F. (1995). Nonproportional low cycle fatigue criterion for Type 304 stainless steel, Journal of Engineering Materials and Technology, 117(3), pp. 285-292. DOI: 10.1115/1.2804541.

[4] Itoh, T., Nakata, T., Sakane, M., Ohnami., M. (1999). Nonproportional low cycle fatigue of 6061 aluminum alloy under 14 strain paths, European Structural Integrity Society, 25, pp. 41-54. DOI: 10.1016/S1566-1369(99)80006-5.

[5] Morishita, T. and Itoh, T. (2016). Evaluation of multiaxial low cycle fatigue life for Type 316L stainless steel notched specimen under non-proportional loading, Theoretical and Applied Fracture Mechanics, 84, pp. 98-105. DOI:10.1016/j.tafmec.2016.02.007.

[6] Bressan, S., Gallo, P., Morishita, T., Itoh, T. And Berto., F. (2017). Numerical analysis of multiaxial low cycle fatigue of notched specimens made by stainless steel 316 L under non-proportional loading, Proceedings of the 14th International Conference on Fracture, June 18-23, Rhodes, Greece.

[7] Sakane, M., Itoh, T., Susaki, T., Kawazoe, Y. (2004). T. Life prediction for notched components in nonproportional low cycle fatigue: experiment and FEM analysis, Pressure Vessel and Piping Codes and Standards, ASME. pp. 31- 38. DOI:10.1115/PVP2004-2670.

3. Notch sensitivity and crack initiation site influence on low cycle fatigue life evaluation of notched specimens under non-proportional loading

3.1. Introduction

In this chapter, a further modification of the I-S model based on the crack initiation site on the notch surface and the notch sensitivity of the material is proposed. A new series of tests have been conducted on notched specimens made of aluminum alloy Al 6061. The crack initiation site has been analyzed both for the previous tests conducted on SUS 316L and Al 6061. The I-S model has been modified and improved by considering the crack initiation position, the notch sensitivity and by correlating the parameter with the Bäumel-Seeger model for the evaluation of low cycle fatigue life.

3.2. Experimental procedure

3.2.1 Material properties

The material static properties and chemical composition of the austenitic stainless steel SUS 316L (316LSS) and aluminum alloy Al 6061 (6061Al) are listed in Table 3.1, Table 3.2 and Table 3.3 respectively

Table 3.1 Static mechanical properties of the materials [1]

Material (-)	$\sigma_{Y0.2}$ (MPa)	E (GPa)	ε_U (%)	σ_U (MPa)
6061Al	143	72	23	311
316LSS	356	178	55	518

Table 3.2 Chemical composition of 6061Al

Si (%)	Fe (%)	Cu (%)	Mn (%)	Mg (%)	Cr (%)	Zn (%)	Ti (%)
0.14	0.23	0.03	0.7	4.3	0.1	0.01	0.02

Table 3.3 Chemical composition of 316LSS

C (%)	Si (%)	Mn (%)	P (%)	S (%)	Ni (%)	Cr (%)	Mo (%)
0.07	0.75	1.5	0.03	0.015	12.00	17.00	2.5

The yield stress $\sigma_{Y0.2}$, ultimate tensile stress σ_U, ultimate tensile strain ε_U and Young modulus *E* of the 316LSS are higher than 6061Al. Although the static properties provide the basic information about the material strength, the cyclic plastic stress-strain curves are fundamental to understand the low cycle fatigue resistance. The plastic cyclic stress-strain curves have been obtained for both uniaxial push-pull strain path (PP) and a non-proportional 90 degrees out of phase axial and torsional strain path, called circle (OP). The paths are the same to the ones employed to test the notched specimens of 316LSS which results are presented in Chapter 2. Cyclic stress-strain curves of uniaxial and non-proportional loading have been obtained by a step-up test. Strain increment at each step was set at $\Delta\varepsilon_{eq}/2=0.05\%$ every 10 cycles from $\Delta\varepsilon_{eq}/2=0\%$ to $\Delta\varepsilon_{eq}/2=1.0\%$. The dots constituting the curves shown in Fig. 3.1 represent the stress and strain amplitude values at the 10^{th} cycle of each step, assuming that the cyclic behavior of both 316LSS and 6061Al is stabilized.

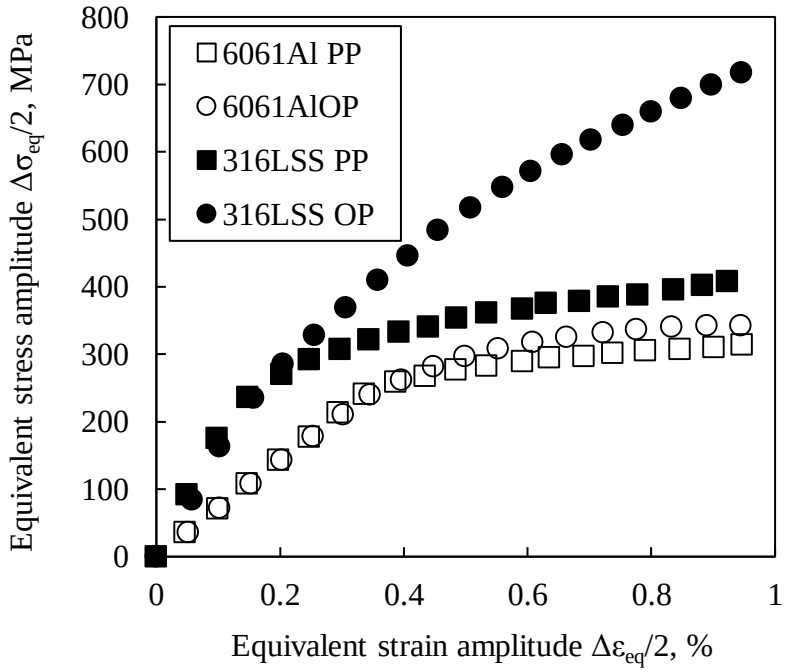

Fig. 3.1. Cyclic curves of 6061Al and 316LSS [1]

The additional hardening effect due the non-proportionality of the strain path in case of 316LSS is considerably higher than the additional hardening behavior of 6061Al. In fact, in case of 6061Al the plastic trait of the PP and OP cyclic stress-strain curves coincide. The elastic traits are not influenced by the strain path type.

Another mechanical property which definition is necessary when dealing with notched components is the notch sensitivity. Notch sensitivity is a material characteristic indicating the sensitivity of the material towards stress concentration effects when subject to cyclic loading. Several models for the definition of the fatigue stress concentration factor K_f which takes into account of the notch sensitivity have been developed. have been develop over the years. The model developed by Kuhn and Hardraht [2] assumes that fatigue failure occurs if the average stress over a length A from the notch root is equal to the fatigue limit of the smooth specimen. The model has been modified by Neuber assuming that the length A it's a constant depending on the ultimate tensile strength of the material σ_U [3]. The final equation proposed by Neuber is as follows:

$$K_f = 1 + \frac{(K_{t,n}-1)}{1+\sqrt{\frac{\rho}{r}}} \qquad (3.1)$$

Where ρ is the material notch sensitivity and r is the notch root radius. The higher the value of notch sensitivity ρ the closer is the value of K_f to the one of $K_{t,n}$. In case of 6061Al ρ = 0.5 and for 316LSS ρ = 0.9.

3.2.2 Specimens and test conditions

Circumferentially notched cylindrical specimens machined from round bars have been employed for the experimental tests. The specimens feature four different values of stress concentration factors referred to the net section $K_{t,n}$: 1.5, 2.5, 4.2 and 6.0 (Fig. 3.2).

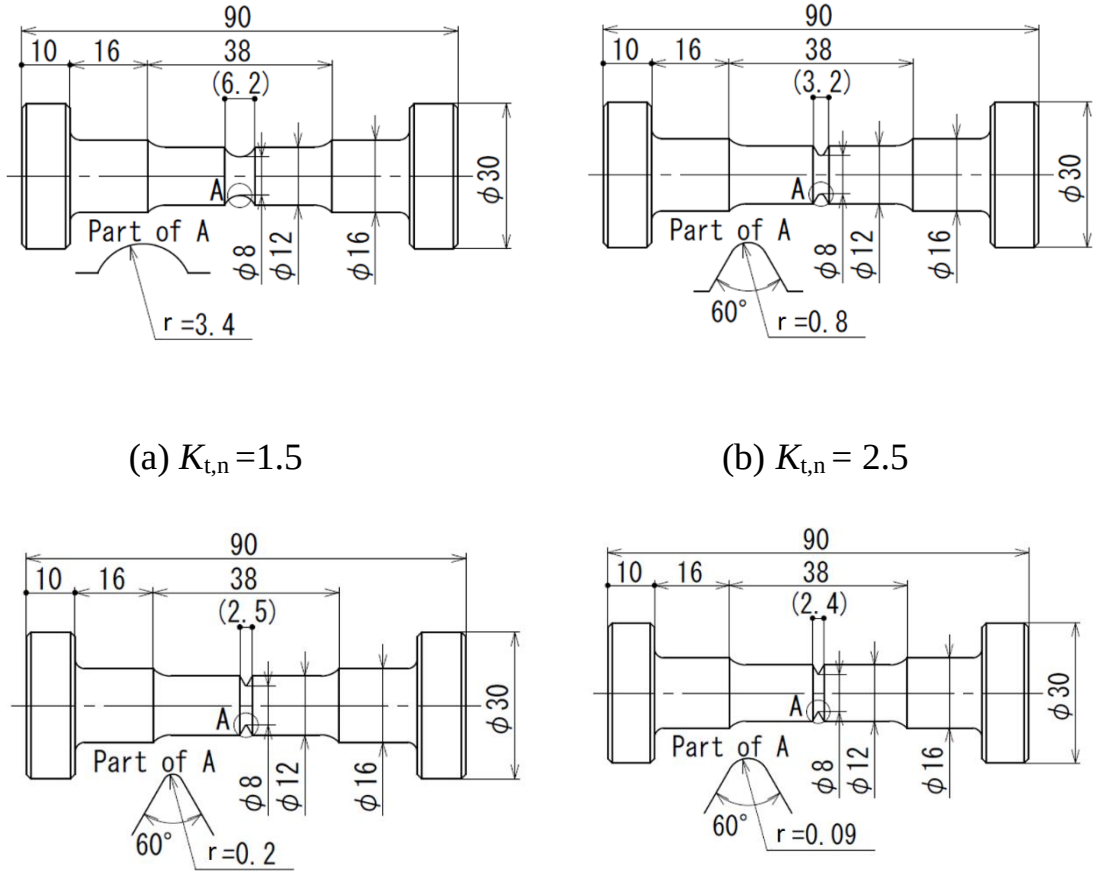

Fig. 3.2. Tested notched specimens (mm) [1]

Strain controlled tests have been carried under a strain range $\Delta\varepsilon_{eq}/2$=0.25% for 6061Al and $\Delta\varepsilon_{eq}/2$=0.35% for 316LSS. A servo hydraulic testing machine which can perform tensile and torsion tests has been employed for the tests. The strain has been measured by means of an extensometer with a gage length of 12 mm.

3.3. Experimental procedure

3.3.1 Fatigue life

The number of cycles to failure N_f for each specimen is listed in Table 3.4. The fatigue life is defined as the cycle where the equivalent stress amplitude $\Delta\sigma_{eq}$ becomes the 3/4 of the maximum equivalent stress in a cycle to avoid the complete propagation of the crack and therefore rupture of the specimen.

Table 3.4 Fatigue test results [1]

Loading paths	$K_{t,n}$	6061Al		316LSS	
		$\Delta\varepsilon_{eq}/2$ (%)	N_f (Cycles)	$\Delta\varepsilon_{eq}/2$ (%)	N_f (Cycles)
PP	1	0.25	44500	0.35	6089
	1.5		3848		2237
	2.5		1267		871
	4.2		788		571
	6		730		418
OP	1	0.25	6500	0.35	2082
	1.5		1020		2248
	2.5		298		475
	4.2		207		212
	6		205		156

Non-proportional loading causes a reduction of fatigue life for both steel and aluminum. The reduction of fatigue life due to the non-proportionality of the loading is approximately 75%. The stress concentration effects due to the notch has also influence on N_f. The trend of fatigue life reduction caused by stress concentration effects depends on the material. In case of 6061Al, the discrepancy between the fatigue life of specimens with $K_{t,n}$=4.2 and 6.0 is small for both non-proportional and proportional loading. The fatigue life of 316LSS is instead sensibly reduced also for high values of $K_{t,n}$ because of the high notch sensitivity compared to aluminum. An anomalous test result in case of 316LSS $K_{t,n}$ = 1.5 was observed. For this combination of material and geometry, the non-proportionality of the loading did not have influence on the fatigue life.

3.3.2 Crack analysis

Crack initiation site was found to be shifted from the notch tip in 316LSS notched specimens analyzed in a previous study. Through the sophisticated FEM model introduced in chapter 2, the shift in the crack initiation position cause was found in the strain gradient around the notch tip. Additional hardening process due to the application of a non-proportional loading path has been detected as the cause of those strain gradients. The maximum value of the distance from the notch tip was found for low values of $K_{t,n}$. Considering crack initiation site through a new stress concentration factor improved the results of fatigue life evaluation. In this case the crack initiation site was analyzed also for 6061Al and the results of the observations are reported in Fig. 3.3 and Fig. 3.4

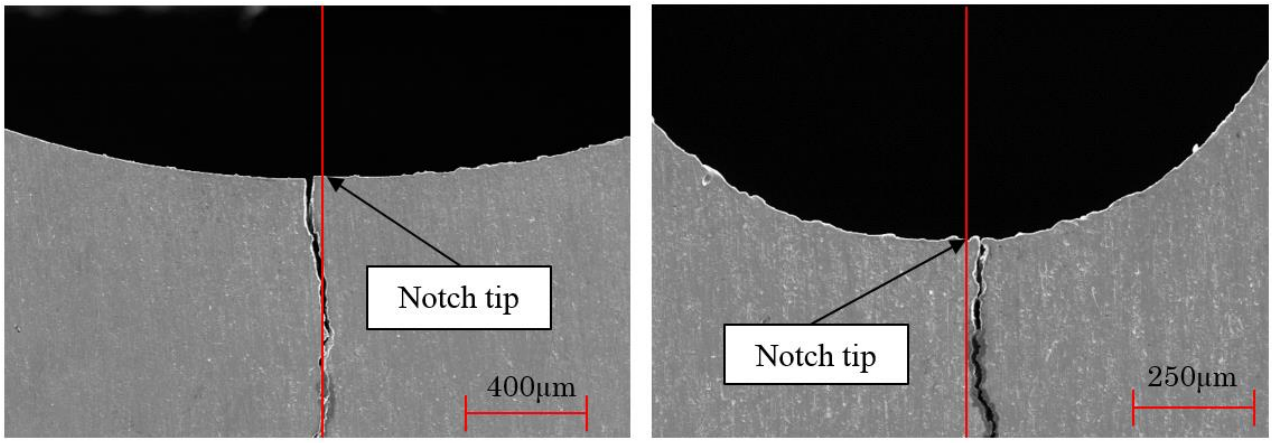

(a) $K_{t,n}$ =1.5 (b) $K_{t,n}$ = 2.5

Fig. 3.3. Crack initiation site on the notch surface for 6061Al [1]

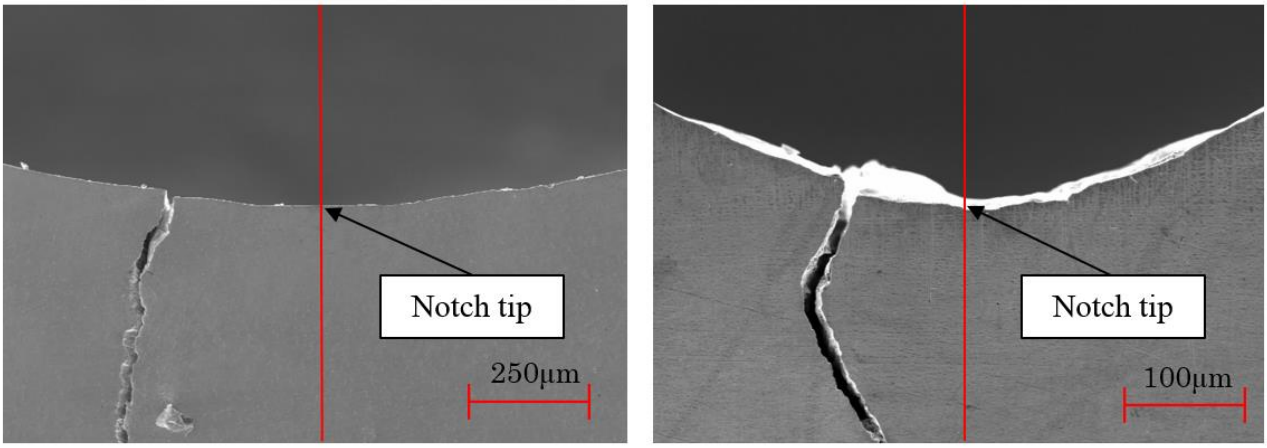

(a) $K_{t,n}$ =1.5 (b) $K_{t,n}$ = 2.5

Fig. 3.4. Crack initiation site on the notch surface for 316LSS [1]

The crack initiation site was located on the notch tip on the notched specimens made by 6061Al. The result confirmed that the crack initiation site position is not shifted for those material which level of additional hardening is low, as hypothesized in the previous chapter. For what concerns the specimens with $K_{t,n}$=4.2 and 6.0, the investigation of the crack initiation site has been avoided both for 6061Al and 316LSS as fatigue life can be attributed mostly to crack propagation in case of high stress concentration effects at the notch tip [4].

3.4. Itoh-Sakane parameter and Bäumel-Seeger model

The presented models for life evaluation are based on the Itoh-Sakane (I-S) model already introduced in the Chapter 1 and Chapter 2 [5,6]:

$$\Delta\varepsilon_{\mathrm{NP}} = \Delta\varepsilon_{\mathrm{eq}}(1 + \alpha f_{\mathrm{NP}}) \tag{3.2}$$

The method consists in a modification of the equivalent applied strain range. Additional hardening and severity of non-proportional loading path are included through the parameters α and f_{NP}, respectively. The value of α for 316SSL is 0.9, evaluated as the ratio of the stress amplitude of the stress-strain cyclic curve in case of circle with the one in case of push-pull. The reduction of fatigue life due to non-proportional loading in 6061Al is not attributed to additional hardening effects [7]. Therefore, the material constant for the evaluation of the reduction of fatigue life α* replaces the additional hardening parameter α in the evaluation of $\Delta\varepsilon_{\mathrm{NP}}$ in case of 6061Al:

$$\Delta\varepsilon_{\mathrm{NP}} = \Delta\varepsilon_{\mathrm{eq}}(1 + \alpha^{*} f_{\mathrm{NP}}) \tag{3.3}$$

Where α* is defined as the ratio of N_{f} in OP with N_{f} in PP at the same applied $\Delta\varepsilon_{\mathrm{eq}}$. The parameter α* can be also accurately evaluated considering an equation correlating the stress σ_{U} and Yield stress $\sigma_{\mathrm{Y0.02}}$ [7]:

$$\alpha^{*} = \frac{(\sigma_U - \sigma_Y)}{\sigma_B} \tag{3.4}$$

In the case of 6061Al α*=0.5 [7]. I-S model requires in input the principal (or equivalent in case of circle) strain range, f_{NP} and α, resulting in a parameter simple to obtain compared to the models currently available.

Originally, the model has been correlated with the Universal Slope Method (USM) developed by Manson-Coffin [8] in order to be able to estimate the fatigue life in the design phase. The USM model can be utilized by knowing the static mechanical properties of the material and it is therefore simple to apply.

However, several models which employ the static mechanical properties have been developed and two additional models are considered in this research. In particular, Muralidharan-Manson (M-M) [9] and Bäumel-Seeger (B-S) [10] have been considered. The models are presented in the equations below:
Universal Slope Method (USM):

$$\Delta\varepsilon = A(N_\mathrm{f})^{-0.12} + B(N_\mathrm{f})^{-0.6} \tag{3.5}$$

Muralidharan-Manson (M-M):

$$\Delta\varepsilon = 1.17\left(\frac{\sigma_\mathrm{U}}{E}\right)^{0.832}(N_\mathrm{f})^{-0.09} + 0.0266{\varepsilon_\mathrm{U}}^{0.155}\left(\frac{\sigma_\mathrm{U}}{E}\right)^{-0.56}(N_\mathrm{f})^{-0.56} \tag{3.6}$$

Bäumel-Seeger (B-S) for aluminum alloy

$$\frac{\Delta\varepsilon}{2} = 1.67\frac{\sigma_\mathrm{U}}{E}(2N_\mathrm{f})^{-0.095} + 0.35(2N_\mathrm{f})^{-0.69} \tag{3.7}$$

Bäumel-Seeger (B-S) for steel alloys:

$$\frac{\Delta\varepsilon}{2} = 1.50\frac{\sigma_\mathrm{U}}{E}(2N_\mathrm{f})^{-0.087} + 0.59\psi(2N_\mathrm{f})^{-0.58} \tag{3.8}$$

where,

$$\psi = 1 \quad if \quad \frac{\sigma_U}{E} \tag{3.9}$$

$$\psi = 1.375 - 125\frac{\sigma_\mathrm{U}}{E} \quad \text{if} \quad \frac{\sigma_\mathrm{U}}{E} < 0.003 \tag{3.10}$$

The most suitable model to associate with the I-S model have been research by correlating the USM, M-M and B-S with the fatigue life of smooth specimens made by 316LSS and 6061Al subject to uniaxial and multiaxial non-proportional low cycle fatigue tests. The result of the correlation with USM, M-M and B-S for both 6061Al and 316LSS have been represented in Fig. 3.5 and Fig. 3.6. In case of 6061Al I-S model associated with B-S model returns the most accurate results. In case of 316LSS a significant discrepancy between the models was not observed. Therefore, I-S model has been associated with B-S model. The model for 6061Al is:

$$\frac{\Delta\varepsilon_\mathrm{NP}}{2} = 1.67\frac{\sigma_U}{\mathrm{E}}(2N_\mathrm{f})^{-0.095} + 0.35(2N_\mathrm{f})^{-0.69} \tag{3.11}$$

The model for 316LSS is:

$$\frac{\Delta\varepsilon_\mathrm{NP}}{2} = 1.50\frac{\sigma_U}{\mathrm{E}}(2N_\mathrm{f})^{-0.087} + 0.59(2N_\mathrm{f})^{-0.58} \tag{3.12}$$

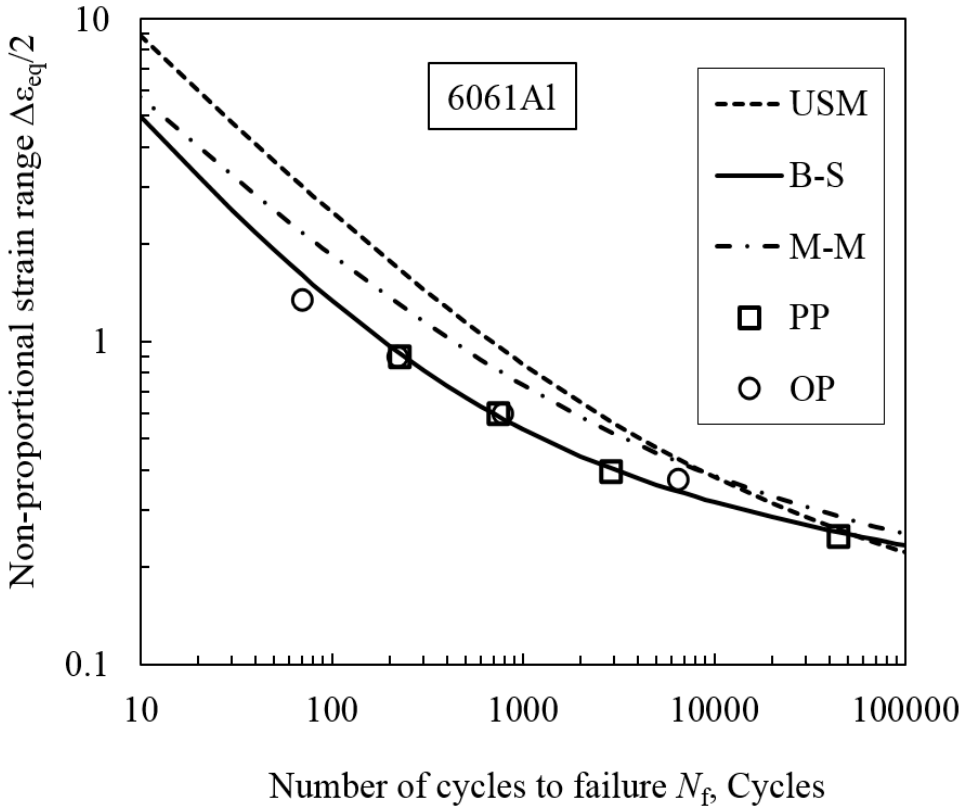

Fig. 3.5. Fatigue life correlation for 6061Al smooth specimens subject to PP and OP loading with I-S model and USM, B-S and M-M models [1]

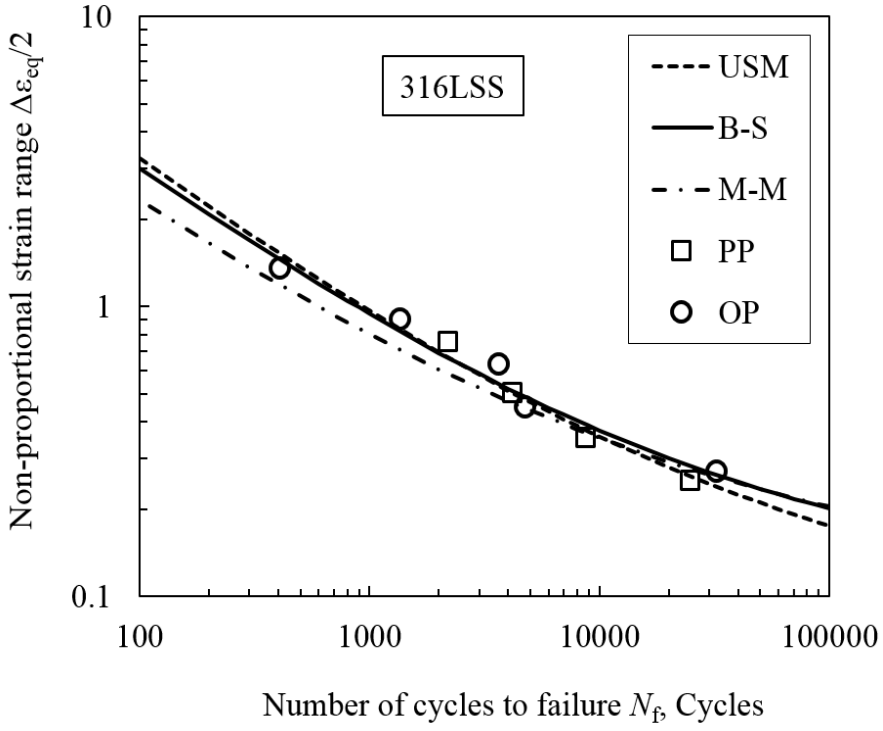

Fig. 3.6. Fatigue life correlation for 316LSS smooth specimens subject to PP and OP loading with I-S model and USM, B-S and M-M models [1]

3.5. Fatigue life evaluation

In this chapter, the fatigue life of notched specimens has been correlated with the I-S model associated with the BS model. The I-S model for the evaluation of fatigue life under non-proportional loading of notched specimens is here reported:

$$K_{t,n}\Delta\varepsilon_{NP} = K_{t,n}\Delta\varepsilon_{eq}(1 + \alpha f_{NP}) \tag{3.13}$$

The model of Eq. 3.13 has been already employed to evaluate fatigue life of 316SSL notched specimens in chapter 2. According to Eq. (3.13), the left term of Eq. (3.11) and (3.12) were multiplied by $K_{t,n}$ resulting in Eq. (3.14) for 6061Al and (3.15) for 316LSS.

$$\frac{K_{t,n}\Delta\varepsilon_{NP}}{2} = 1.67\frac{\sigma_U}{E}(2N_f)^{-0.095} + 0.35(2N_f)^{-0.69} \tag{3.14}$$

$$\frac{K_{t,n}\Delta\varepsilon_{NP}}{2} = 1.50\frac{\sigma_U}{E}(2N_f)^{-0.087} + 0.59(2N_f)^{-0.58} \tag{3.15}$$

Eq 3.14 and 3.15 have been employed to correlate fatigue life Table 3.2) and the results are represented in Fig. 3.7 and Fig. 3.8.The stress concentration factor evaluated in the elastic field $K_{t,n}$ was replaced by the fatigue notch factor K_f (Eq. 3.1) to take into account the notch sensitivity of the material. The equations of the model are:

$$\frac{K_f\Delta\varepsilon_{NP}}{2} = 1.67\frac{\sigma_U}{E}(2N_f)^{-0.095} + 0.35(2N_f)^{-0.69} \tag{3.16}$$

$$\frac{K_f\Delta\varepsilon_{NP}}{2} = 1.50\frac{\sigma_U}{E}(2N_f)^{-0.087} + 0.59(2N_f)^{-0.58} \tag{3.17}$$

The results of the application of K_f on I-S model are shown in Fig. 3.9 and Fig. 3.10.

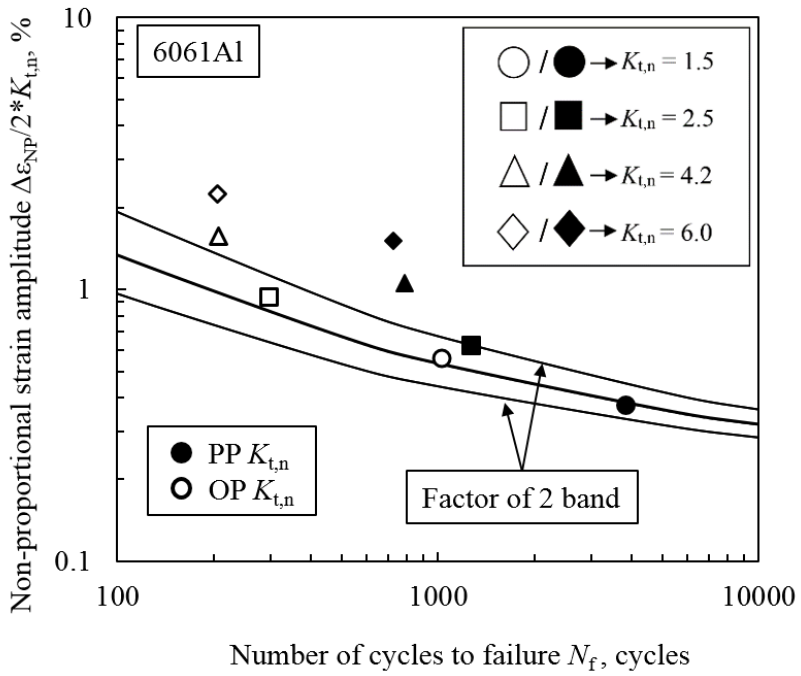

Fig. 3.7. Life evaluation of 6061Al employing I-S model associated with B-S model modified with $K_{t,n}$ [1]

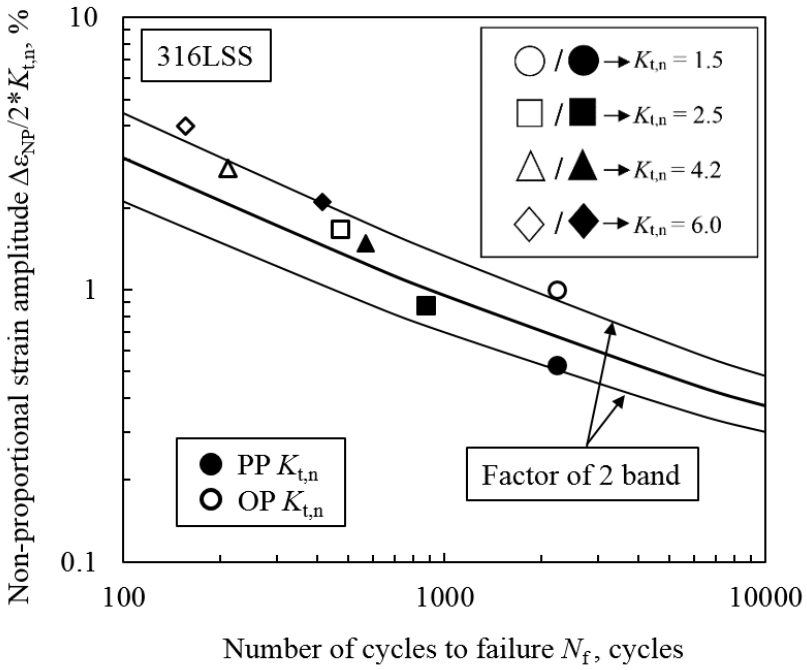

Fig. 3.8 Life evaluation of 316LSS employing I-S model associated with B-S model modified with K_f [1]

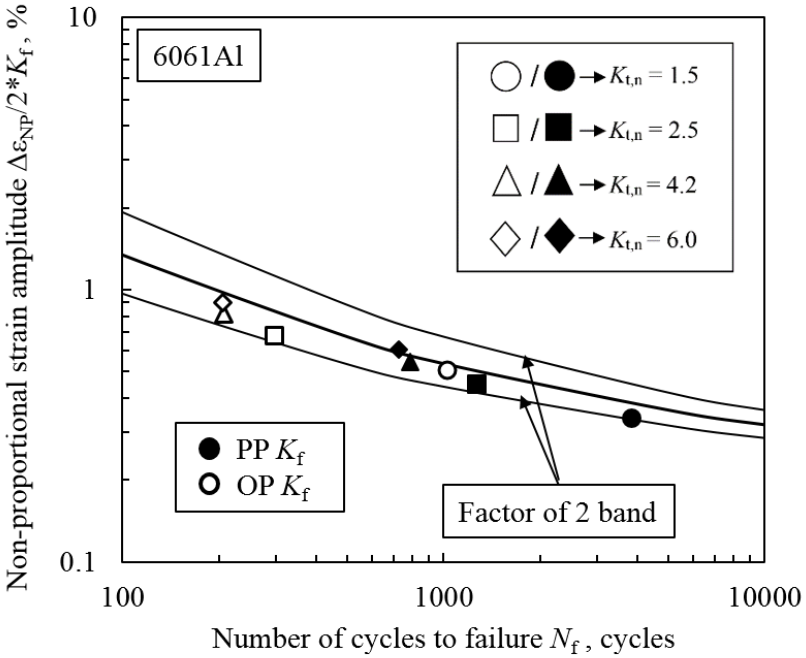

Fig. 3.9 Life evaluation of 6061Al employing I-S model associated with B-S model modified with K_f [1]

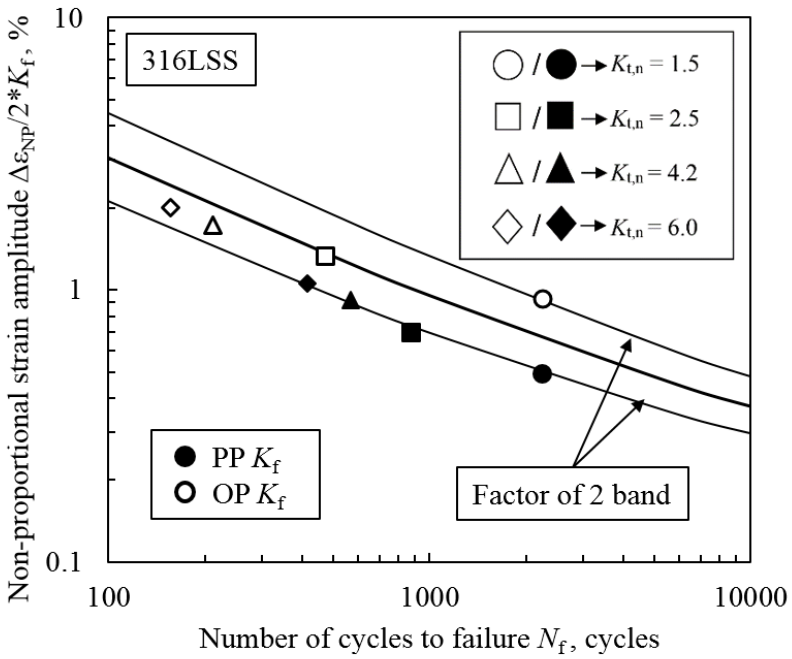

Fig. 3.10 Life evaluation of 316LSS employing I-S model associated with B-S model modified with K_f [1]

Fatigue life evaluation is improved with the model of Eq. 3.16 and 3.17, as the data lies in a factor of 2 band. Results related to aluminum specimens with high values of $K_{t,n}$ sensibly improves. The data related to PP and 316LSS are slightly overestimated. In case of non-proportional loading the data are well synthetized in the factor of 2 band for both 316LSS and 6061Al. A further modification of Eq. 3.16 and Eq 3.17 has been conducted by taking into account of the crack initiation site. The crack initiation site has been observed shifted in specimens with low stress concentration factor and material with high additional hardening. The influence of crack initiation on fatigue life is remarkable in cases where the $K_{t,n}$ has moderated values [7]. Therefore, the model has been modified and applied only in case of 316LSS and $K_{t,n}$ = 1.5 and 2.5. In order to take into account of the crack initiation site, a FEM analysis has been conducted on the considered specimens. The stress concentration factor K'_t has been taken into account and its definition is here reported:

$$K'_{\mathrm{t}} = \frac{\sigma'_{\mathrm{loc}}}{\sigma_{\mathrm{N}}} \tag{3.18}$$

In this case, notch sensitivity has been also accounted and a new notch fatigue factor called K'_f has been calculated:

$$K'_{\mathrm{f}} = 1 + \frac{(K'_{\mathrm{t}} - 1)}{1 + \sqrt{\frac{\rho}{r}}} \tag{3.19}$$

Then, fatigue life has been calculated by replacing the new fatigue notch factor of Eq. 3.19 on Eq. 3.17. The results of fatigue life evaluation are shown in Fig. 3.11.

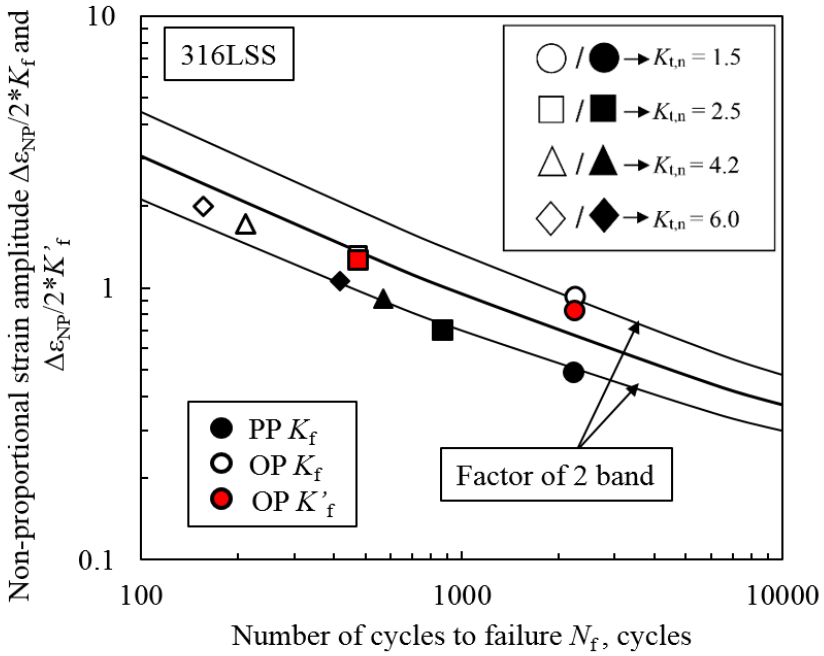

Fig. 3.11. Life evaluation of 316LSS employing I-S model modified with K'_f [1]

The application of the model accounting of crack initiation site and notch sensitivity slightly improves the results.

3.6. Discussion

The crack initiation position and the notch sensitivity influence on fatigue life evaluation are discussed. The modification of I-S by replacing $K_{t,n}$ with K_f sensibly improves the fatigue life evaluation. The application of K_f is particularly advantageous for material with a low notch sensitivity. Although the fatigue notch factor K_f has been traditionally applied for high cycle fatigue and uniaxial loading, the results of Fig. 3.9 and 3.10 evidence that the application of K_f for low cycle fatigue and non-proportional loading is efficient when integrated with the I-S model. Although with a lower improvement, materials with higher notch sensitivity such as 316LSS benefits from the application of K_f instead of $K_{t,n.}$ In this chapter the I-S model has been further modified to evaluate the number of cycles to failure by associating I-S model with the B-S model to take into account the different cyclic plastic behavior of titanium and aluminum compared to steel. The final equations of the I-S model modified with BS model and K_f are the following:

$$\frac{K_f \Delta\varepsilon_{NP}}{2} = 1.67 \frac{\sigma_U}{E} (2N_f)^{-0.095} + 0.35(2N_f)^{-0.69} \quad (3.20)$$

$$\frac{K_f' \Delta\varepsilon_{NP}}{2} = 1.50 \frac{\sigma_U}{E} (2N_f)^{-0.087} + 0.59(2N_f)^{-0.58} \quad (3.21)$$

Where Eq 3.20 is for steel and Eq 3.21 for aluminum and titanium alloys. The models of Eq. 3.20 and Eq. 3.21 only requires static mechanical properties of the materials. Despite the complicated phenomena involved such as the multiaxiality of the load and the stress concentration, the model returns accurate results.

A further discussion is needed for what concerns the crack initiation position. The crack initiation site position dependence on the additional hardening and stress concentration effects have been confirmed: the crack initiation site on materials with no additional hardening effects is always located in the immediate vicinity of the notch tip. Therefore, the hypothesis to explain mechanism in Chapter 2 have been verified. However, giving the results of Fig. 3.11, the field where the consideration of such phenomenon leads to considerable benefits is limited. Further tests on notched specimens with high additional hardening and notch concentration factors lower than $K_{t,n} = 1.5$ must be conducted to confirm the advantages of the consideration of the crack initiation site on fatigue life evaluation.

3.7. Conclusions

Notched specimens made by 316LSS and aluminum 6061Al were tested with proportional and non-proportional low cycle fatigue. The notch sensitivity and crack initiation position have been considered to modify the I-S model for fatigue life evaluation. The conclusions can be summarized as follows:

1. The crack initiation position dependence on additional hardening and notch geometry has been verified. The crack initiation site on material with low additional hardening is located at the notch tip.
2. The notch fatigue factor K_f can be applied in the I-S model and improves the accuracy of fatigue life evaluation. Fatigue notch factor K_f could be efficiently applied also for low cycle multiaxial fatigue.
3. I-S model modified with B-S model requires only the static mechanical properties of the material and returned good results for aluminum and steel alloys.

4. Crack initiation position was considered to improve the results for 316LSS and low $K_{t,n.}$

References

[1] Bressan, S., Ogawa, F., Itoh, T., Berto, F. (2019) Influence of notch sensitivity and crack initiation site on low cycle fatigue life of notched components under multiaxial non-proportional loading, Frattura ed Integrità Strutturale, 47, pp. 126-140.DOI:10.1299/jmmp.5.230.

[2] Kuhn, P. and Hardraht, H.F. (1952). An engineering method for estimating the notch-size effect in fatigue tests on steel, NACA TN2805, Langley aeronautical laboratory, Washington.

[3] Neuber, H. (1961). Theory of stress concentration for shear-strained prismatic bodies with arbitrary nonlinear stress-strain low, ASME Journal of Applied Mechanics, 28, pp. 544-550.

[4] Sakane, M., Itoh, T., Susaki, T., Kawazoe, Y. (2004). T. Life prediction for notched components in nonproportional low cycle fatigue: experiment and FEM analysis, Pressure Vessel and Piping Codes and Standards, ASME. pp. 31- 38. DOI:10.1115/PVP2004-2670.

[5] Itoh, T., Sakane, M., Ohnami., D.F., Socie, D.F. (1995). Nonproportional low cycle fatigue criterion for Type 304 stainless steel, Journal of Engineering Materials and Technology, 117(3), pp. 285-292. DOI: 10.1115/1.2804541.

[6] Itoh, T., Nakata, T., Sakane, M., Ohnami., M. (1999). Nonproportional low cycle fatigue of 6061 aluminum alloy under 14 strain paths, European Structural Integrity Society, 25, pp. 41-54. DOI: 10.1016/S1566-1369(99)80006-5.

[7] Itoh, T, and Yang, T. (2011). Material dependence of multiaxial low cycle fatigue lives under non-proportional loading, International Journal of Fatigue, 33(8), pp. 1025-1031.

[8] Manson, S.S. (1965). Fatigue – a complex subject – some simple approximations, Experimental Mechanics, 5(7), pp. 193-226. DOI: 10.1007/BF02321056.

[9] Muralidharan, U. and Manson, S.S. (1988). A modified universal slopes equation for estimation of fatigue characteristics of metals, Journal of Engineering Materials and Technology, 110(1), pp. 55-58. DOI: 10.1115/1.3226010.

[10] Bäumel Jr., A. and Seeger, T. (1990). Materials Data for Cyclic Loading, Elsevier Science Publishers, Amsterdam, (supplement 1).

4. Additive manufacturing: analysis of layer orientation and heat-treatment influence on low cycle uniaxial and multiaxial non-proportional fatigue life

4.1. Introduction

In this chapter the plastic cyclic behavior of additively manufactured Ti-6Al-4V under uniaxial and non-proportional multiaxial low cycle fatigue is investigated. The data regarding the plastic behavior of additively manufactured metallic alloys are sparse compared to the metallic materials manufactured with the traditional techniques such as the ones analyzed in chapter 2 and 3 [1]. Therefore, in order to discuss the low cycle fatigue behavior of notched specimens made by AM Ti-6Al-4V the understanding of the plastic behavior under uniaxial and multiaxial low cycle fatigue is necessary. In this chapter the influence of layer orientation, stress-relief heat treatments, and defects on low cycle strain-controlled multiaxial fatigue and plastic behavior has been investigated. The variety of specimens depends on the layer orientation and the presence of stress-relief heat treatment. Microstructure, cyclic stress-strain curves, low cycle uniaxial and non-proportional multiaxial low cycle fatigue, hardening and softening curves, hysteresis loops and fracture surface have been investigated to characterize the low cycle plastic behavior of the material.

4.2. Material and Specimens

4.2.1 Fabrication process

The specimens have been created with the laser powder bed fusion technique (L-PBF). The machine EOSINT M 290 400W, produced by EOS DMLS™ has been employed. The L-PBF technique consists in creating thin layers of the material by melting powder on a moving platform. After the creation of the first layer, the building platform lowers at a distance corresponding to the layer thickness. The process repeats itself until the creation of the component. A schematic representation of the fabrication process is reported in Fig. 4.1.

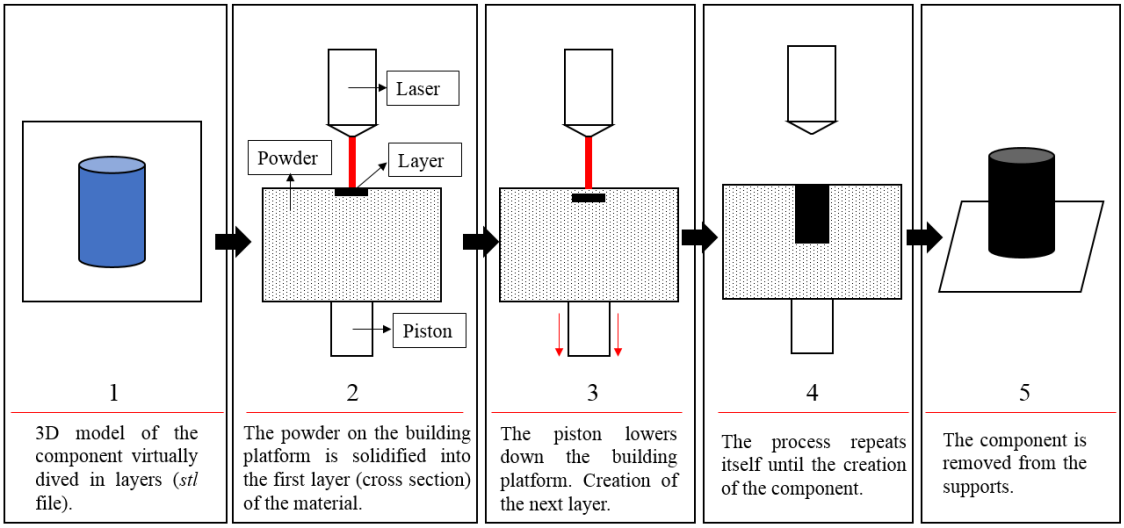

Fig. 4.1. Schematic representation of the L-PBF process [2]

As L-PBF technique employs powder of the metallic alloy, the definition of the particle size is fundamental. The particle size analysis conducted with a diffraction technique is reported in Table 4.1 and the chemical composition of the powder before the process and the material after the process are reported in Table 4.2.

Table 4.1 Particle size analysis [2]

Particle size analysis (-)	Specification (μm)	Results (μm)
D10	23.5-27.4	25.5
D50	34.5-38.4	37.5
D90	48.5-51.4	50.3

Table 4.2 Powder element content [2]

Stage -	Al (%)	V (%)	O (%)	N (%)	H (%)	Fe (%)	C (%)	Y (%)
Before process	6.35	4.23	0.120	0.003	0.003	0.140	0.008	<0.001
After process	6.15	4.25	0.15	0.03	0.002	0.2	0.01	<0.001

The fabrication process has been conducted with the parameters indicated in Table 4.3.

Table 4.3 Process parameters

Layer thickness (t)	Volume rate (L_v)	Scanning path	Hatching space (h)	Laser speed (L_s)	Laser power (L_P)
(μ)	(mm3/s)	(-)	(mm)	(mm/s)	(W)
60	9	stripes	0.12	1250	340

4.2.2 Specimens' types

Four specimen types have been considered for the tests. The specimen variety depended on the layer orientation and the application of a stress-relief heat treatment. The layer orientation has been defined horizontal (H) when plane defined by the layer was parallel to the specimen axis. The layer orientation has been defined vertical (V) when the plane defined by the layer was perpendicular to the specimen's axis. A stress-relief heat treatment conducted in argon atmosphere for 4h at 800°C has been also applied to part of the specimens. The heat treatment is applied to decrease the residual stresses occurring in the fabrication process, and therefore avoid undesired post-process deformations of the components. The specimen types were: HT, HNT, VT, VNT. The varieties are represented in Fig. 4.2. The static mechanical properties of each specimen type have been obtained by means of a uniaxial static tensile test. The results of the static tests are reported in Table 4.4.

Table 4.4 Static mechanical properties of the specimens [2]

Specimen type	E	σ_U	$\sigma_{Y0.2}$	ε_f
-	(GPa)	(MPa)	(MPa)	(%)
HT	116	1050	860	14
HNT	110	1230	1060	10
VT	114	1060	860	15
VNT	110	1200	1070	11
Wrought	118	1017	947	19

The not heat-treated components exhibited superior mechanical properties in terms of ultimate tensile stress (σ_U) and yield stress (0.2% proof stress, $\sigma_{Y0.2}$). On the other hand, the heat-treated components possess a superior ductility and a higher value of Young's modulus. The layer orientation does not provoke significant variations of the aforementioned material properties.

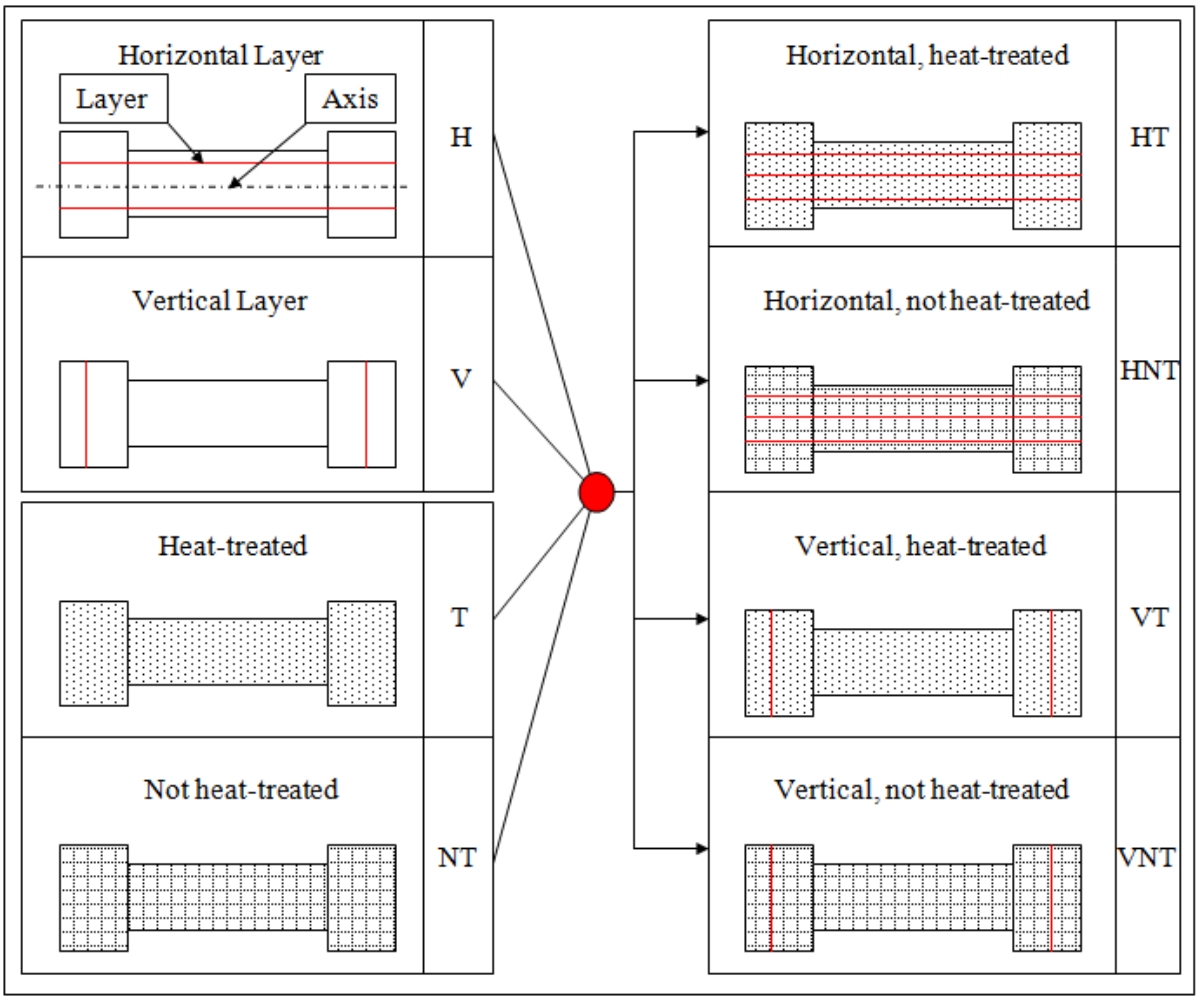

Fig. 4.2. Schematic representation of the tested specimens

After the additive manufacturing process the specimens have been machined to obtain hollow cylindrical specimens. The hollow cylinder shape allows to obtain a shear stress distribution which can be assumed as uniform. The surface has been further polished with a sandpaper #2000 on the internal surface and with an alumina powder solution (particle size 1 μm) on the external surface. The shape of the AM specimen and machined specimens are depicted in Fig. 4.3

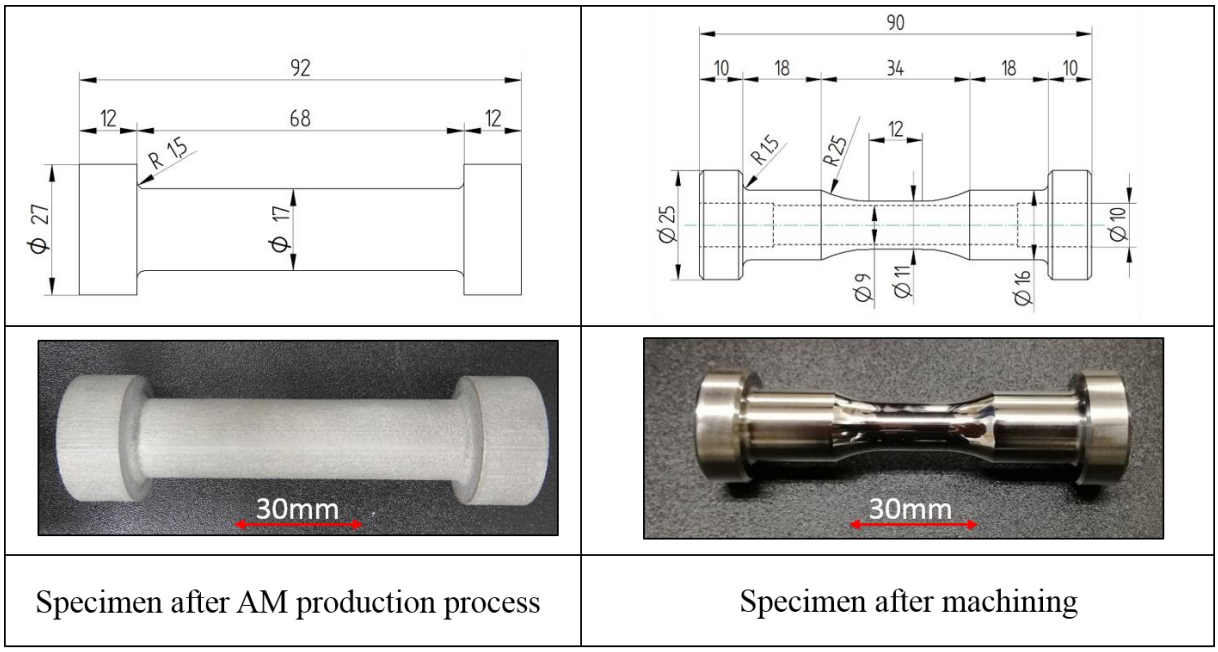

Fig. 4.3. Specimens after AM process and after machining

4.2.3 Microstructure analysis

The microstructure of the specimens has been analyzed to observe the orientation of the grains, grain morphology, presence of voids or defects. The surface has been polished and etched. The material microstructure has been observed from different observation directions. The results of the observations are depicted in Fig. 4.4, 4.5 and 4.6

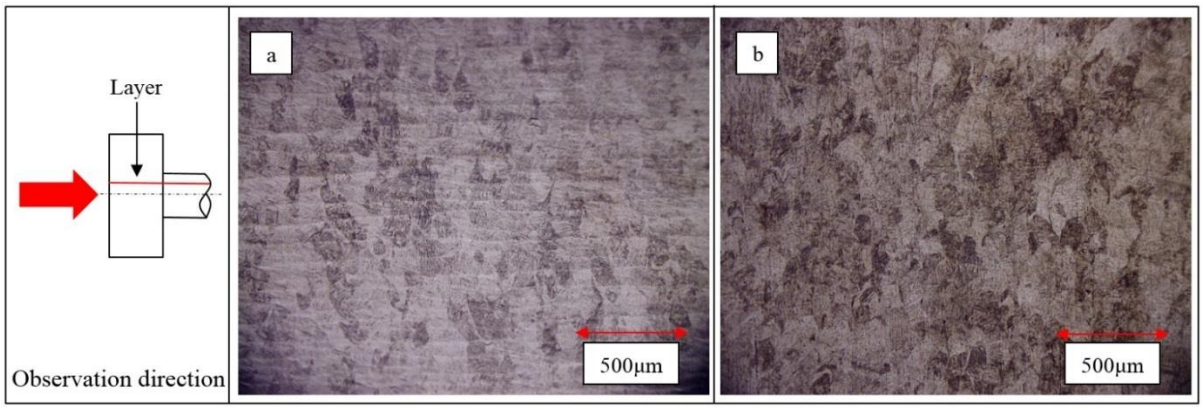

Fig. 4.4. Results of microstructure observation of (a) HT and (b) HNT specimens [2]

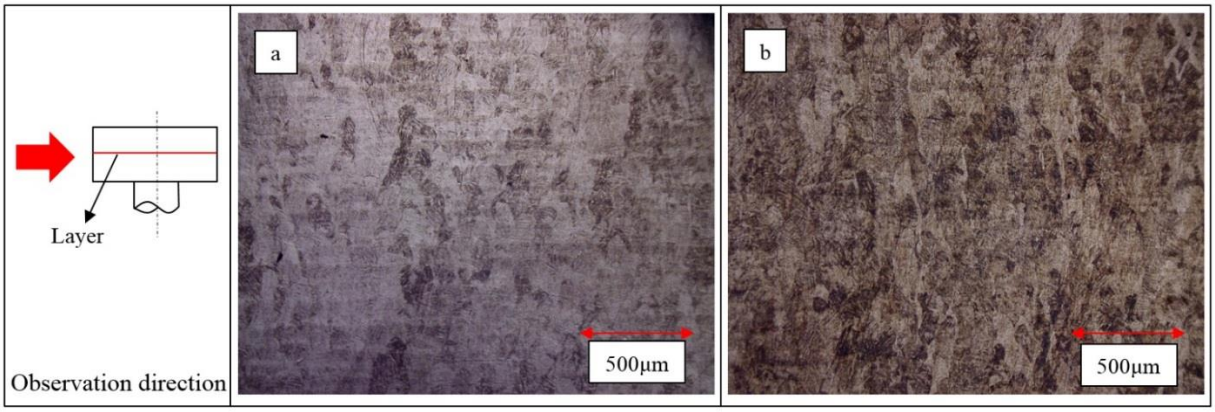

Fig. 4.5. Microstructure of (a) VT and (b) VNT specimens, observation direction parallel to the layer [2]

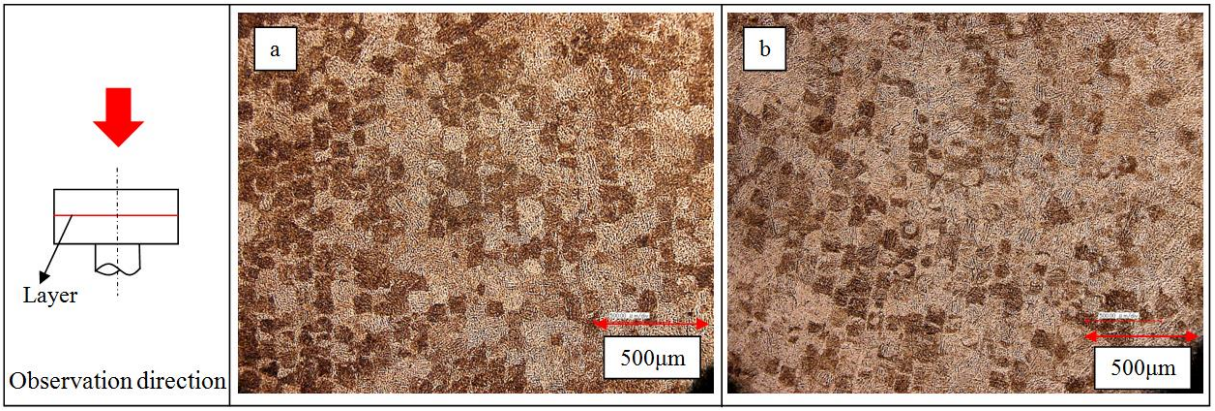

Fig. 4.6. Microstructure of (a) VT and (b) VNT specimens, observation direction perpendicular to the layer

The grain morphology is martensitic as already observed in several past works. The martensitic structure is due to the high cooling rates typical of the AM fabrication process. By consequence, it can be concluded that the stress-relief heat treatment has no influence on the material microstructure, such as grain coarsening. The dark and light areas are probably the boundaries of the prior β grains originated from the phase transformation α-β occurring in the fabrication process. The prior β grains shape is columnar. Giving the epitaxial grain growth in the plane defined by the layer, the axis of the columnar grain is perpendicular to the layer. In fact, based on the direction observation, the side (Fig. 4.5) and the circular base area (Fig. 4.6) of a hypothetical ideal cylindrical grain is visible. The dimension of the grains was averagely 500µm in height, similarly with the ones observed in [4]. A small number of voids have been observed in each specimen regardless of the specimen variety. In fact, the stress-relief heat treatment has no effect on void size, and different heat-treatments are necessary

to reduce the void number such as the hot isostatic pressure (HIP). Voids with an average dimension of 20 μm and with a spherical shape were detected. Dark bands could be observed for the not heat-treated components when the observation direction was parallel to the layer orientation (Fig. 4.4a and Fig. 4.5 a). Such dark bands are believed to be an intermetallic phase $TiAl_3$ as reported in [4]. In order to observe the acicular grain distribution, an electron backscatter diffusion analysis (EBSD) has been conducted on the specimen surface and the results are represented in Fig. 4.6. The EBSD observation has been conducted on the surface of the HT specimens, and the observation direction is the same of Fig. 4.4.

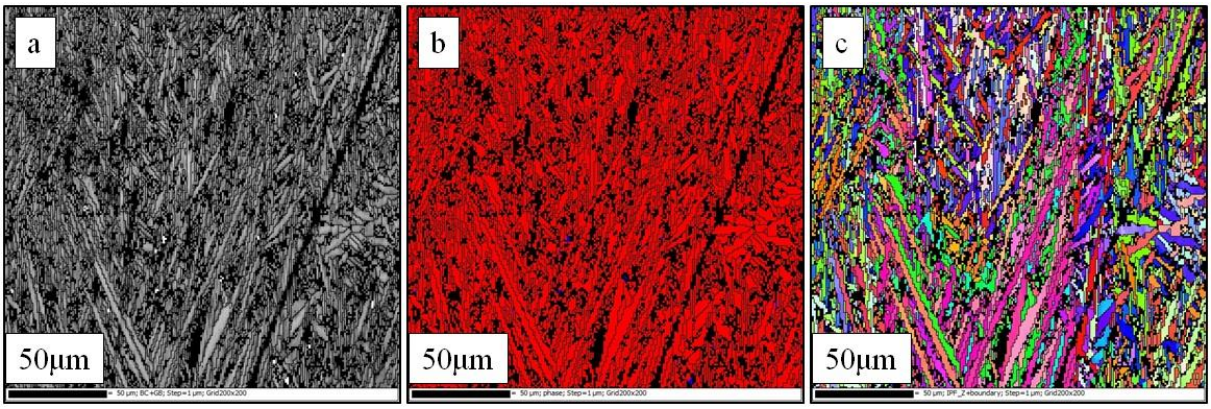

Fig. 4.6. EBSD analysis results: grain shape and distribution (a), distribution of the α phase (in red) (b), grain orientation (c)

As expected, the structure is acicular, and the grain dimension is averagely 30μm in length (Fig. 4.6 a). The hexagonal alpha phase constitutes almost the totality of the material structure, although a small percentage of beta cubic phase, typical of the Ti-6Al-4V alloy (Fig. 4.6 b). The grain distribution seems not following a determined pattern (Fig. 4.6 c).

4.3. Experimental procedure

4.3.1 Cyclic stress–strain plastic curves

The cyclic stress-strain curves have been obtained for each specimen type. The same machine, test procedure and strain path employed to obtain the cyclic stress-strain plastic curves of the 316LSS and 6061Al have been employed also in this case. The stress-strain cyclic curves for each specimen typology are reported in Fig. 4.7

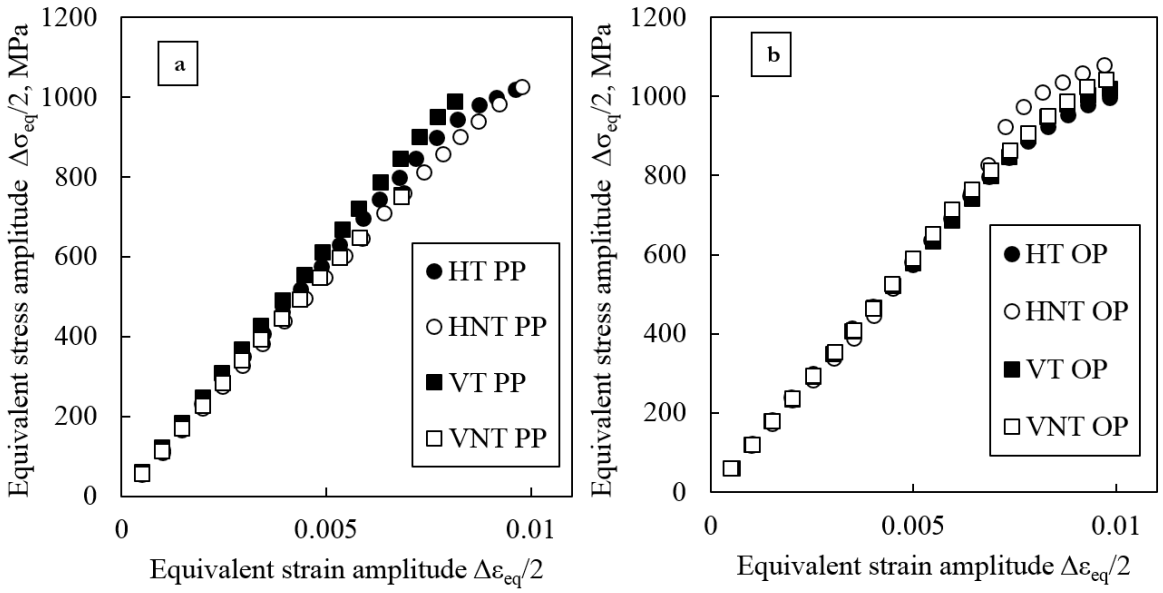

Fig. 4.7. Cyclic stress–strain curves obtained with an incremental step method for a PP (a) and (b) OP strain path [2]

At first glance it seems that the cyclic plastic behavior is similar regardless of the specimen variety. In case of push-pull, the Young modulus E of the heat-treated specimens appears to be higher than the not heat-treated specimens, similarly as reported in the static uniaxial tests (Table 4.3). The same could not be found in case of the out-of-phase strain path, where the Young modulus is not influenced by layer orientation or heat treatment. The plastic trait is similar for each specimen type and no remarkable difference can be observed. Furthermore, no additional hardening behavior occurred in case of OP. Such behavior is typical of the titanium alloys and the same result was observed in works dealing with traditionally manufactured titanium [5,6].

4.3.2 Fatigue tests

Strain controlled low cycle fatigue tests with uniaxial (PP) and out-of-phase (OP) strain paths have been conducted on each specimen by applying an equivalent strain range of $\Delta\varepsilon_{eq}$ = 1.8%, in order to provoke a deformation in the plastic field. PP is a push-pull test while OP is a combination of push-pull and reverse torsion loading paths with a 90° phase difference. The fatigue life (N_f) corresponds to the number of cycles at which the maximum stress is 3/4 of the maximum stress recorded. The results are represented in Table 4.5.

Table 4.5 Fatigue test results: fatigue life (N_f), maximum stress range recorded at $N = 0$ ($\Delta\sigma_{eq,max}/2$), stress range recorded at $N_f/2$ ($\Delta\sigma_{eq,av}/2$), shear stress range recorded at $N_f/2$ ($\Delta\tau/2$), plastic strain range at $N_f/2$ ($\Delta\varepsilon_p$) [2]

Loading path	Specimen Type	N_f	$\Delta\sigma_{eq,max}/2$	$\Delta\sigma_{eq,av}/2$	$\Delta\tau/2$	$\Delta\varepsilon_p$
-	-	cycles	MPa	MPa	MPa	%
PP	HT	1426	976	864	-	0.46
	HNT	1623	980	940	-	0.16
	VT	1268	1058	926	-	0.32
	VNT	1795	1033	970	-	0.17
OP	HT	300	970	937	579	0.61
	HNT	412	986	898	569	0.5
	VT	374	1004	954	542	0.71
	VNT	464	976	912	568	0.5

Although the not heat-treated component exhibits a longer fatigue life than the heat-treated components, the fatigue strength can be considered comparable for each specimen due to the data scatter typical of fatigue. Fatigue life of the AM components can be considered comparable to the wrought specimens tested in Ref. [5,6]. The layer orientation has no influence on the fatigue life. The failure reduction due to the non-proportionality of the loading is comparable to the one observed for wrought specimens. Although fatigue life itself does not provide information regarding the cyclic plastic behavior, several data which can be extrapolated from the tests are useful for the understanding of the cyclic plastic behavior.

4.3.3 Hardening/softening curves

The hardening and softening curves are obtained by plotting the variation of the maximum stress amplitude $\Delta\sigma_{eq,max}/2$ over the cycles. The hardening and softening curves reported in Fig. 4.8 and Fig. 4.9 were examined to investigate the material cyclic plastic behavior during the tests.

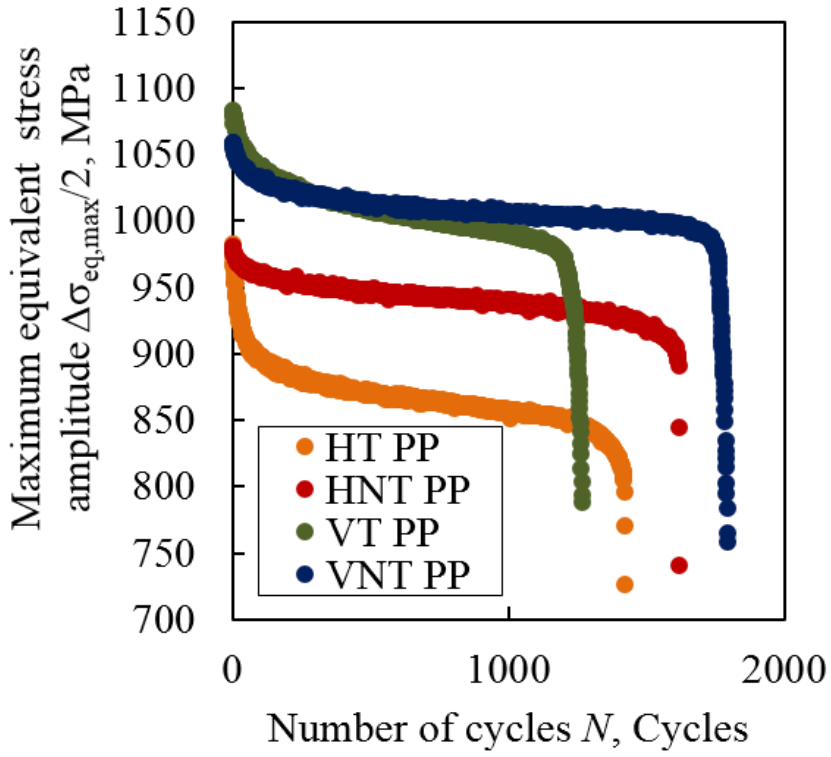

Fig. 4.8. Specimen hardening and softening curves obtained for (a) PP and (b) OP (b) strain paths [2]

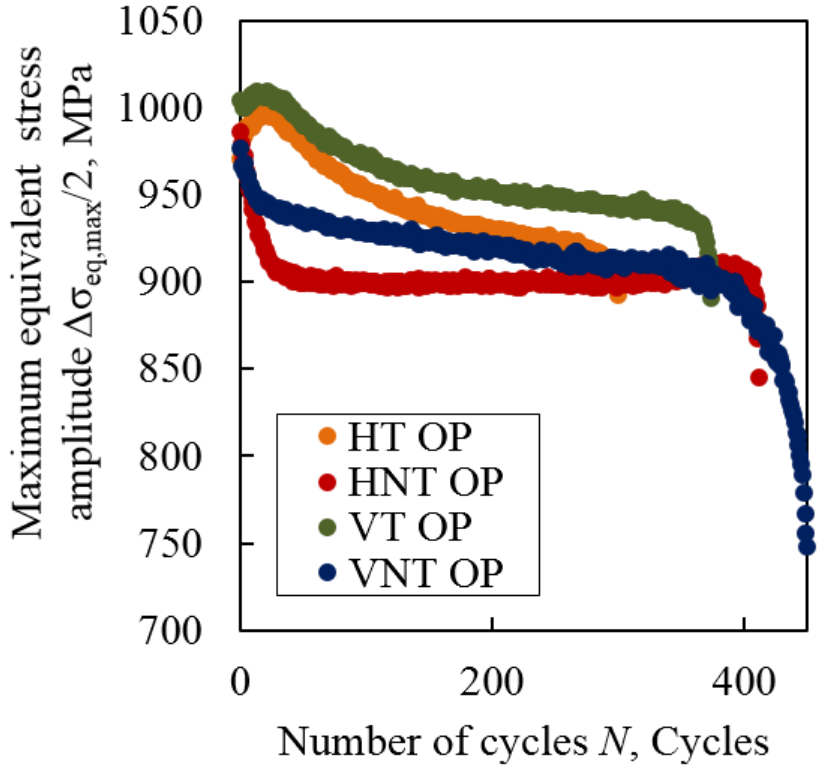

Fig. 4.9. Specimen hardening and softening curves obtained for (a) PP and (b) OP (b) strain paths [2]

The specimens showed a similar trend in case of PP. The trend consists in a rapid initial softening, followed by a constant softening upon reaching a rapid stress decreasing representing the final crack propagation leading to failure. The rapid initial softening was not observed in the wrought titanium alloys [5,6] nor in level of softening detected in the initial phase has not been observed in wrought titanium alloys [5,6] nor in torsional tests conducted on 3D printed titanium [7]; the possible causes for this will be discussed in the section dedicated to the crack observation and in the discussion session. In case of OP, the material behavior depended on the specimen variety. HT and VT were characterized by an initial additional hardening, which is anomalous for this type of alloy. The softening behavior of VNOP was comparable to the one observed in the PP tests. In HNTOP, the level of stress stabilized after the initial softening and did not change until failure. The magnitude of softening depended on the heat treatment for PP tests and the layering for OP tests. Information regarding the final crack propagation velocity can be also be obtained from the final trait of the hardening and softening curves. In case of uniaxial loading the last a more sudden crack propagation can be seen for specimen with vertical layer orientation. After the final crack propagation when the stress suddenly decreases, the number of recorded data point is less in case of V specimens, indicating that the crack propagates faster than the H samples.

4.3.4 Hysteresis loops

Additional information regarding the plastic deformation of the material during the test could be deduced by hysteresis loops which has been generated and reported in Figs. 4.10, 4.11, 4.12 and 4.13. The area of the hysteresis loops associated with the heat-treated samples is clearly greater than the one of the not heat-treated components for both PP and OP strain path. Therefore, the heat-treated components absorb more energy than the not heat-treated counterpart. The higher residual stresses in the NT samples might be the cause of this discrepancy. The higher absorbed energy might be also the cause of the lower fatigue life of the heat-treated components.

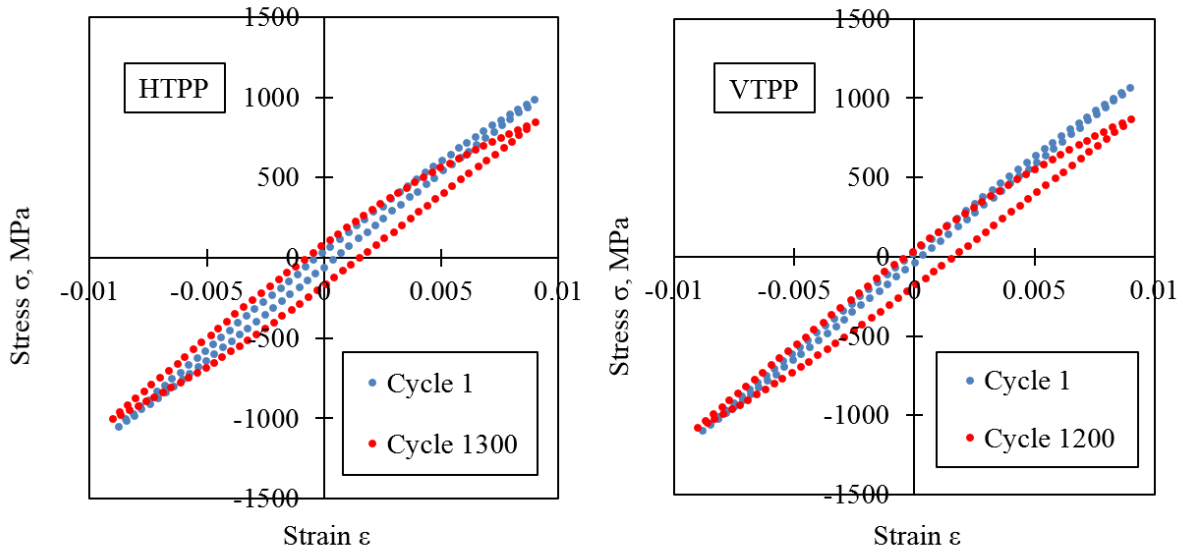

Fig. 4.10. Hysteresis loops obtained for HTPP and VTPP

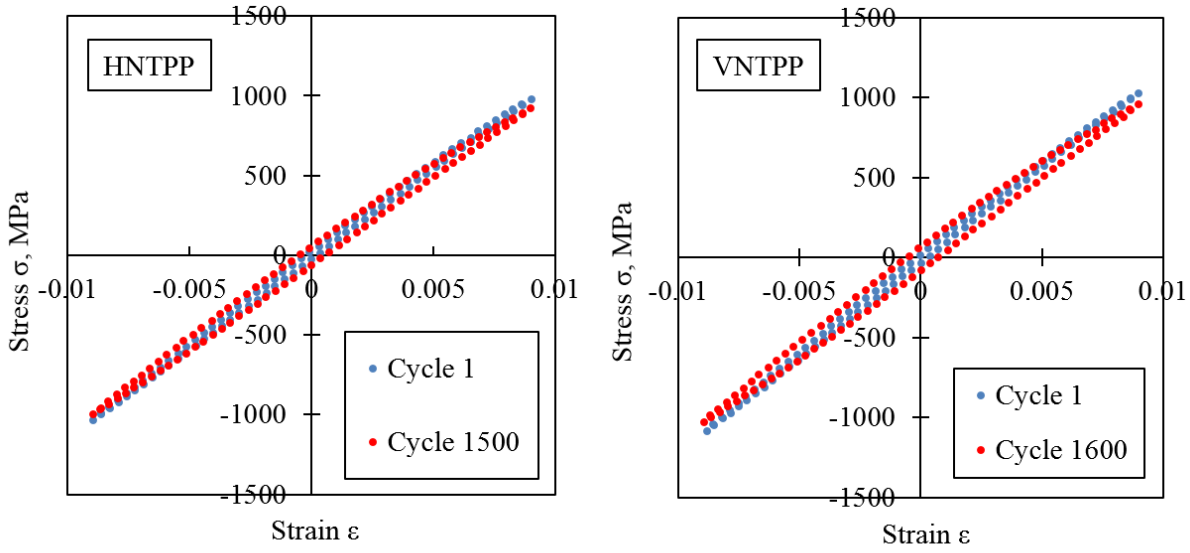

Fig. 4.11. Hysteresis loops obtained for HNTPP and VNTPP

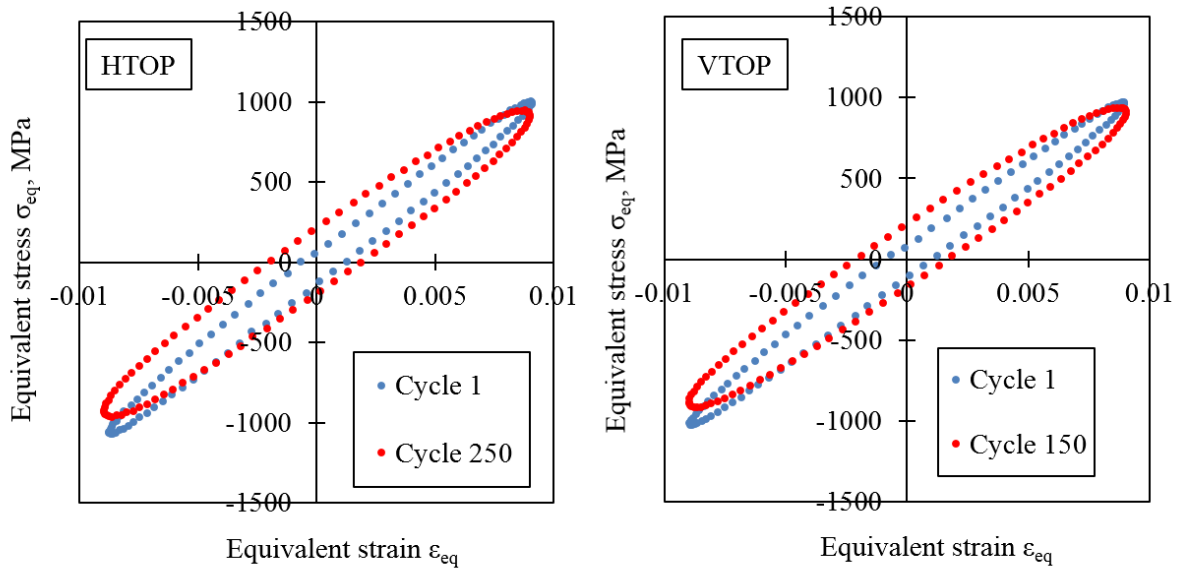

Fig. 4.12. Hysteresis loops obtained for HTOP and VTOP

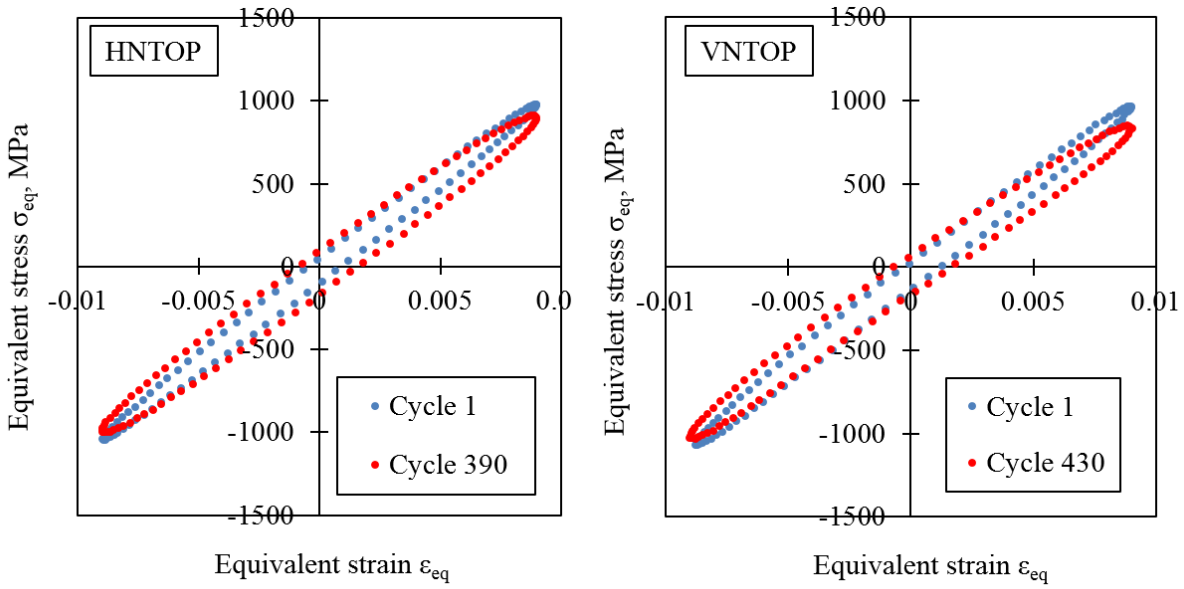

Fig, 4.13. Hysteresis loops obtained for HNTPP and VNTPP

4.4. Crack analyses

4.4.1 Superficial cracks

An optical microscope observation has been conducted on the specimens' surface in the vicinity of the main crack. Although the tests have been interrupted before the complete crack propagation in case of PP, in case of OP the tests interruption condition were such as the crack completely propagated and lead to the complete rupture of the specimens. The superficial cracks are represented in Fig. 4.11 and Fig. 4.12.

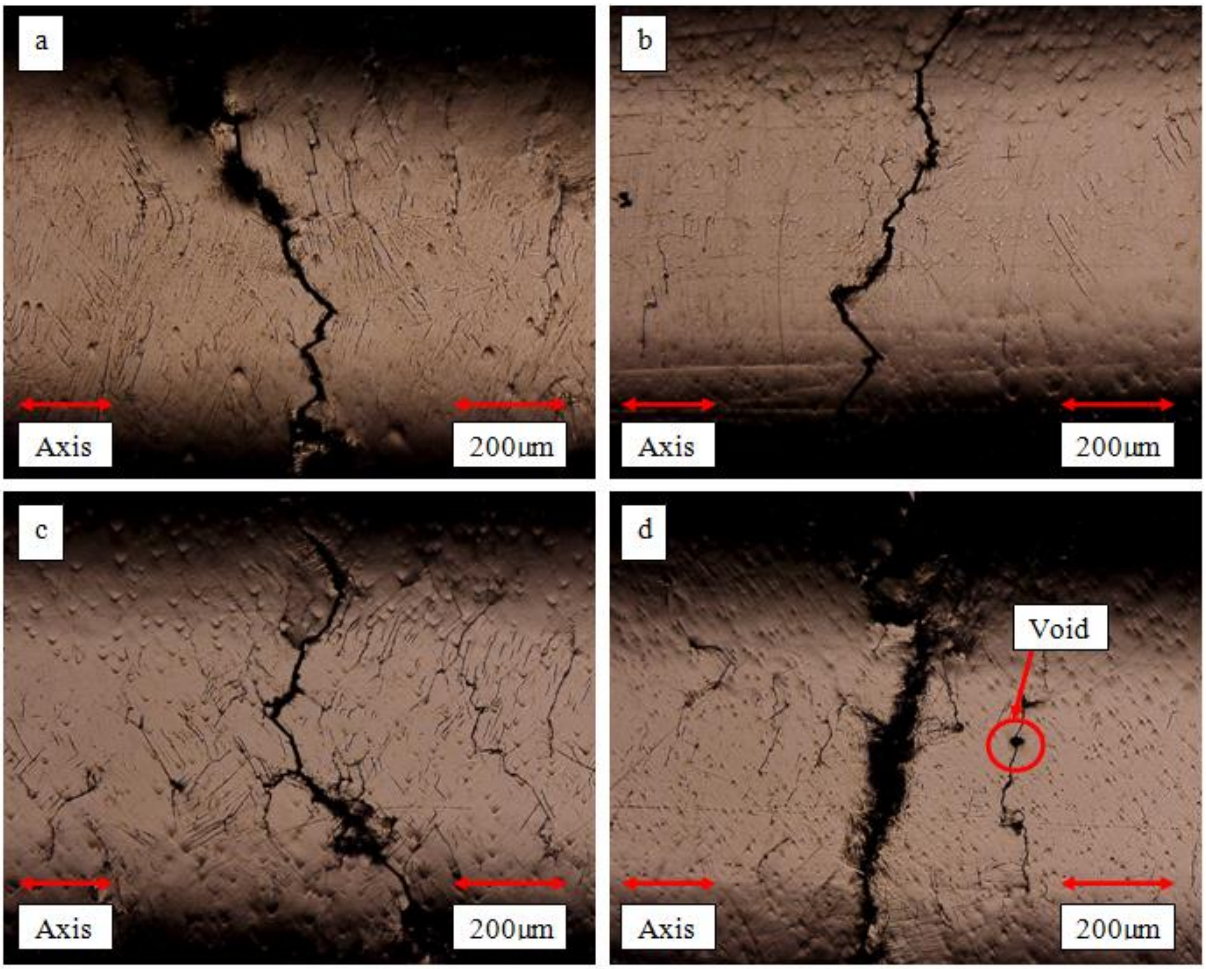

Fig. 4.14. Pictures of the main crack on (a) HTPP, (b) HNTPP, (c) VTPP and (d) VNTPP.

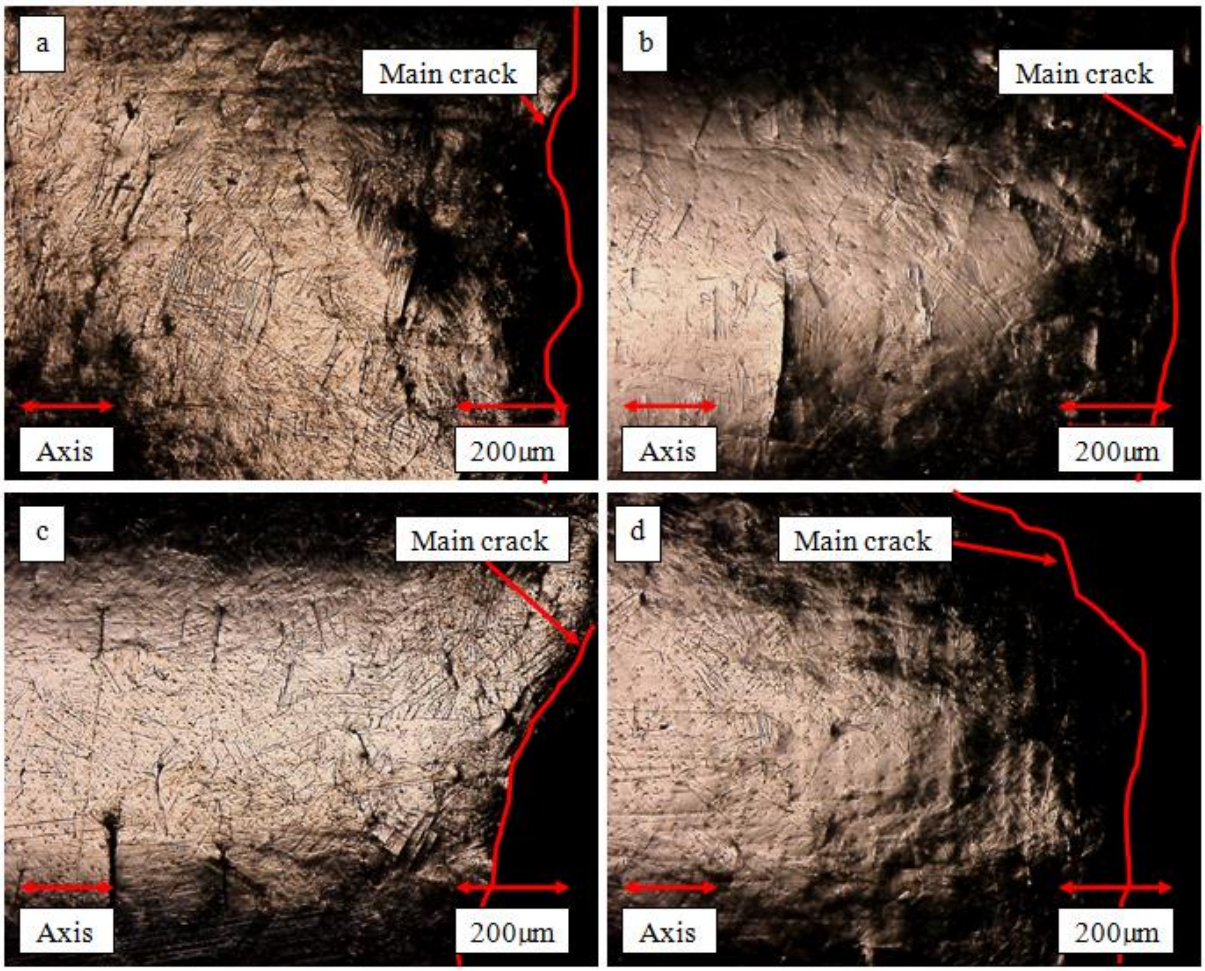

Fig. 4.15. Pictures of the main crack on (a) HTOP, (b) HNTOP, (c) VTOP and (d) VNTOP

Heat-treated specimens showed a higher number of microcracks compared with not heat-treated counterpart for both PP and OP. Furthermore, the fractured area was wider in case of heat-treated specimens. The micro-crack density was also depending on the specimen type: a higher micro-crack density was found in the heat-treated specimens. The strain path determined the orientation of the micro-cracks: cracks perpendicular to the load direction were find in case of PP, while cracks oriented in multiple direction were detected for OP due to the rotation of the principal stress direction. The main crack was found intersecting superficial voids in many samples.

4.4.2 Fracture surface

In order to detect the crack initiation site, the fracture surface of the specimens have been observed with a scanning electron microscope (SEM). Due to the friction damage occurred on the specimens tested with OP strain path, only the specimens tested with PP strain path could be observed. The pictures of the fracture surface are reported in Fig. 4.13

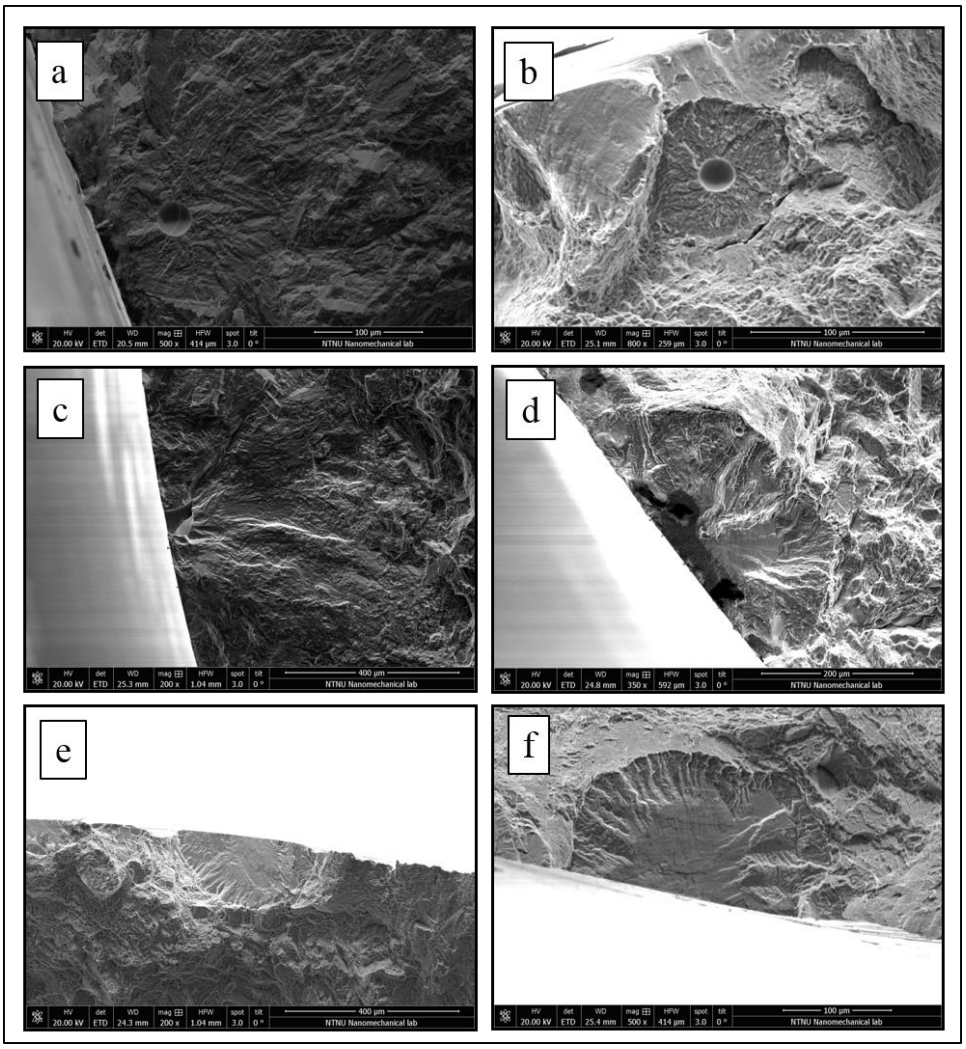

Fig. 4.17. SEM pictures of fracture surface of specimens tested with PP strain path: VT (a), VNT(b), HNT (c), HNT (d), VNT (e), HT (f) (Observation surface perpendicular to the specimen axis)

The first type of crack could be observed in Fig. 4.17 a and b, where the crack initiates from the void surface and propagates in a radial direction. An early crack initiation due to the high applied loading has been hypothesized. The crack confined circular area around the void is due to the stress decrease which inhibits a further propagation of the crack. This is possible due to strain-

controlled tests. Therefore, the early crack initiation might be the cause of the early softening which has not been observed in case of wrought titanium. The softening due the void growth has been extensively studied in the literature [8,9] and it is therefore possible that the same mechanism occurred in the tests conducted in this work. A schematic explanation of the hypothesized phenomenon is reported in Fig. 4.18.

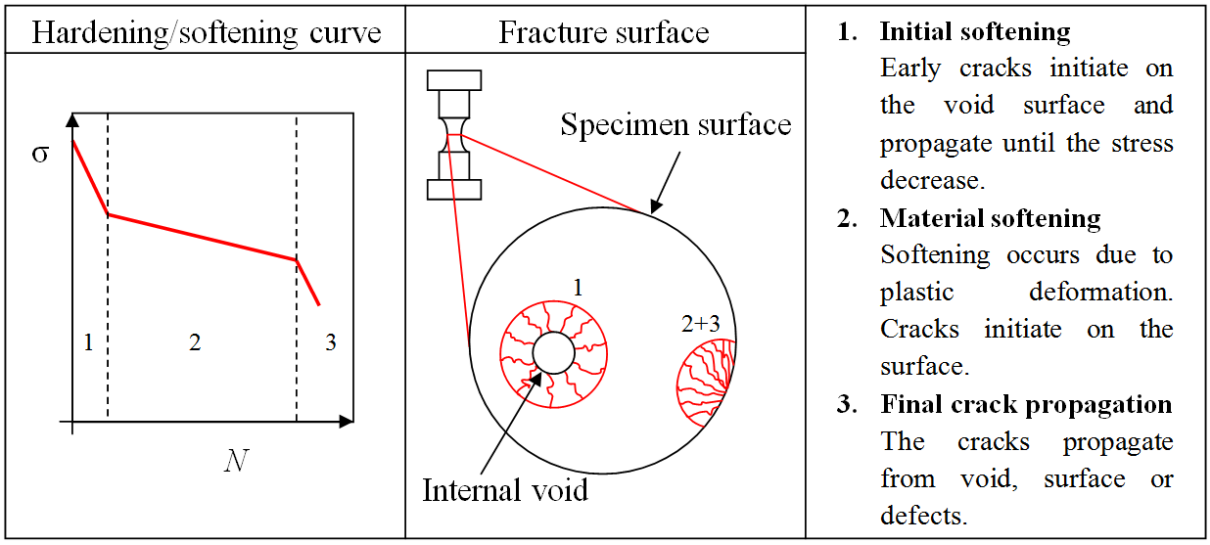

Fig 4.18. Schematic illustration of the cause of the initial drastic softening observed in the AM specimens

The second type of crack initiation site is represented in Fig. 4.17c and d, where the crack initiated from superficial defects. Crack initiating from the surface could be observed and are shown in Figs. 4.17e and f. No correlation between the cracking mechanism and heat treatment or layer orientation could be seen. Furthermore, the crack initiation process seems not having influence on the number of cycles to failure.

4.5. Discussion

The influence of layer orientation, heat treatment and voids on fatigue life and cyclic plastic deformation are discussed. The layer orientation has influence on the orientation on the prior β grains which axis was found perpendicular to the layer. The dark bands are correlated with the layer orientation but the influence of such sub-structures on the cyclic plastic deformation and failure is still unclear. The grain dimension, void number or size was not influenced by the layer orientation. Furthermore, the number of cycles to failure was not closely related to layer orientation. Although the layer orientation could not be correlated with the fatigue life, the last segment of the hardening and softening

curves corresponding to the final crack propagation was found to be depending on the layer orientation. In particular, the crack propagation speed of the H specimens was lower than the V specimens.

The heat-treatment influenced the fatigue life, the absorbed energy and the superficial microcracks number. The hysteresis loops showed that the heat-treated components absorb more energy than the not heat-treated counterparts. Although this may be the cause of the earlier failure of heat-treated specimens, further tests are necessary in order to take into account the scatter typical of fatigue. Additional hardening was found for the heat-treated samples subject to OP strain path and may be the cause of the early failure. Such behavior could not be detected in the plastic cyclic curves and the cause is still unclear. The incremental step method with an increasing step after 10 cycle might also be not suitable for the detection of the plastic cyclic hardening observed in the tests. However, such additional hardening was not found in works dealing with traditionally manufactured titanium [5,6].

The influence of voids was thought to be related to the initial drastic softening occurring in the majority of the specimens. As hypothesis, the elevated applied stress provokes the initiation of an early crack which propagates radially. Then, the stress decreases due strain control, and the crack propagation around the void interrupts (Fig. 4.18). This hypothesis was partially confirmed by testing wrought titanium, absent of voids, with high strain rates, which exhibited a constant softening due to the slip bands [5,6,10]. Although this phenomenon was thought to occur for both PP and OP, the friction between the fracture surfaces at the moment of rupture did not allow a clear visualization of the crack initiation sites in case of OP.

4.6. Conclusions

Multiaxial and multiaxial non-proportional tests have been conducted on 4 types AM Ti-6Al-4V. Layer orientation and heat treatment determined the variety of specimens. After the analysis of material mechanical properties and microstructure, the fatigue life has been discussed. Hysteresis loops and hardening softening curves have been analyzed to discuss the material plastic cyclic behavior and its dependence on the specimen types. The vicinity of the main crack and the fracture surface have been also observed to obtain information concerning the cracking mechanism. The conclusions can be summarized as follows:

1. Cyclic plastic deformation obtained from the step-up test is not dependent on the layer orientation or heat treatment. Cyclic plastic behavior of the AM material can be assumed similar with the wrought counterpart.

2. Fatigue life could be judged similar regardless of the specimen variety. However, not heat-treated samples showed a slightly higher fatigue compared to the heat-treated counterpart. This was related to the higher absorbed deformation energy by the heat-treated samples for both PP and OP strain path.

3. The final crack propagation velocity was found dependent on the layer orientation: crack propagation velocity on vertical layered components is higher than horizontal layered components.

4. The anomalous softening behavior observed in the hardening/softening curves could be attributed to the early cracks initiating from internal voids.

5. An anomalous additional hardening behavior could be observed in the horizontal layered samples subject to non-proportional loading. This was thought to be the cause of the lower fatigue life.

References

[1] Li, P., Warner, DH., Fatemi, A., Phan, N. (2016) Critical assessment of the fatigue performance of additively manufactured Ti–6Al–4V and perspective for future research. International Journal of Fatigue, 85, pp. 130–43. https://doi.org/10.1016/j.ijfatigue.2015.12.003.

[2] Bressan, S., Ogawa, F., Itoh, T., Berto, F. (2019) Cyclic plastic behavior of additively manufactured Ti-6Al-4V under uniaxial and multiaxial non-proportional loading, International Journal of Fatigue, 126, pp. 155-164.

[3] Bressan, S., Ogawa, F., Itoh, T., Berto, F. (2019) Low cycle fatigue behavior of additively manufactured Ti-6Al-4V under non-proportional and proportional loading, Frattura ed Integrità Strutturale, 48, pp. 18-25.

[4] Thijs, L., Verhaeghe, F., Craeghs, T., Van Humbeeck, J., Kruth, J-P. (2010). A study of the microstructural evolution during selective laser

melting of Ti–6Al–4V. Acta Materialia, 58, pp. 3303–3312. https://doi.org/10.1016/j.actamat.2010.02.004.

[5] Itoh, T., Yang, T. (2011). Material dependence of multiaxial low cycle fatigue lives under nonproportional loading. International Journal of Fatigue, 33, pp. 1025–1031. https://doi.org/10.1016/j. ijfatigue.2010.12.001.

[6] Nakamura, H., Takanashi, M., Itoh, T., Wu, M., Shimizu, Y. (2011) Fatigue crack initiation and growth behavior of Ti–6Al–4V under non-proportional multiaxial loading. International Journal of Fatigue, 33, pp. 842–848. https://doi.org/10.1016/j.ijfatigue.2010.12.013.

[7] Fatemi, A., Molaei, R., Sharifimehr, S., Shamsaei, N., Phan, N. (2017). Torsional fatigue behavior of wrought and additive manufactured Ti-6Al-4V by powder bed fusion including surface finish effect. International Journal of Fatigue, 99, pp. 187–201. https://doi.org/10.1016/j.ijfatigue.2017.03.002.

[8] Worswick, M. (1990) Void growth and constitutive softening in a periodically voided solid. Journal of the Mechanics and Physics of Solids, 38, pp. 601–625. https://doi.org/10.1016/0022-5096(90) 90025-Y.

[9] Hutchinson, J., Tvergaard, V. Softening due to void nucleation in metals. In: Fract mech perspect dir (Twentieth symp, 100 Barr Harbor Drive, PO Box C700, West Conshohocken, PA 19428-2959). ASTM International; n.d., p. 61–23. https://doi.org/10.1520/STP18820S.

[10] Nag, AK., Praveen, KVU., Singh, V. (2006). Low cycle fatigue behaviour of Ti–6Al–5Zr–0.5Mo–0.25Si alloy at room temperature. Bulletin of Material Science, 29, pp. 271–275.

5. Influence of layer orientation, heat-treatment and notch on low cycle uniaxial and multiaxial non-proportional fatigue life

5.1. Introduction

In this chapter, the results of low cycle uniaxial and multiaxial non-proportional strain-controlled fatigue tests are discussed. Four varieties of notched specimens made by additionally manufactured Ti-6Al-4V have been analyzed to verify the influence of layer orientation, heat treatment and geometry on fatigue life. The analysis was focused on the crack initiation position on the notched surface and the crack initiation site on the fracture surface.

5.2. Specimens and materials properties

5.2.1 Specimens

The employed specimens have been fabricated with the laser powder bed fusion (L-PBF) and the specimens varieties depended on layer orientation and heat treatment. The analyzed specimens' types are the same of chapter 4: horizontal heat-treated (HT), horizontal not heat-treated (HNT), vertical heat-treated (VT), vertical not-heat treated (VNT) (Fig. 4.2). The specimens have been successively machined to obtain a notch which provokes a stress concentration effect. The stress concentration factor referred to the net section is $K_{t,n}$ = 1.5. The geometry of the specimens is represented in Fig. 5.1.

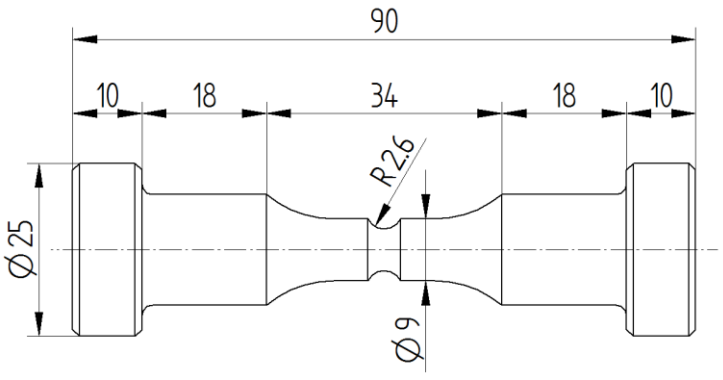

Fig. 5.1. Test specimen geometry (dimensions in mm).

5.2.2 Material properties

The specimens have been obtained with the same additive manufacture technique, machine and process parameter employed for the fabrication of the specimens tested in chapter 4. Therefore, the static mechanical properties (Table 4.3), microstructure (paragraph 4.2.3) and cyclic stress-strain curves (paragraph 4.3.1) which characterizes the specimens analyzed in chapter 4 are here assumed the same. Pictures of the specimens obtained from AM and after machining are represented in Fig. 5.2 and 5.3 respectively.

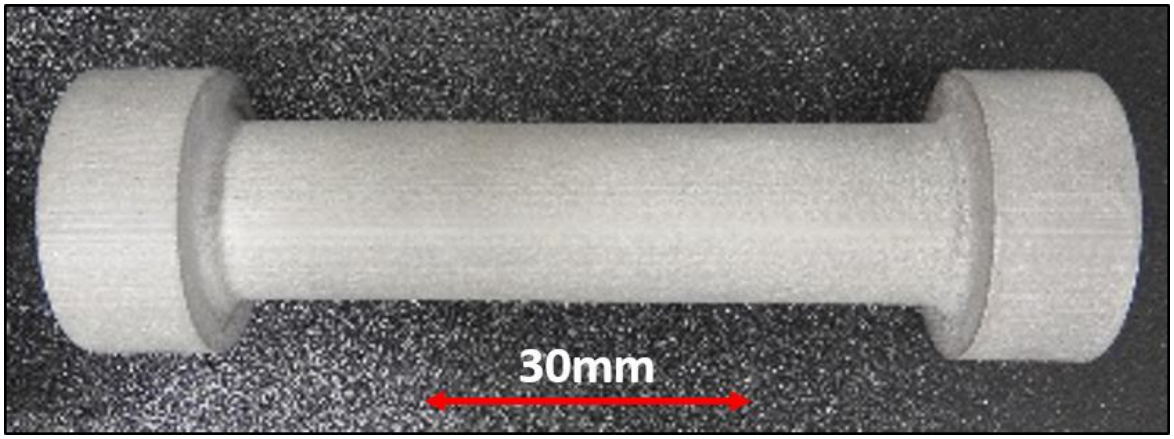

Fig. 5.2. Test specimen fabricated with L-PBF.

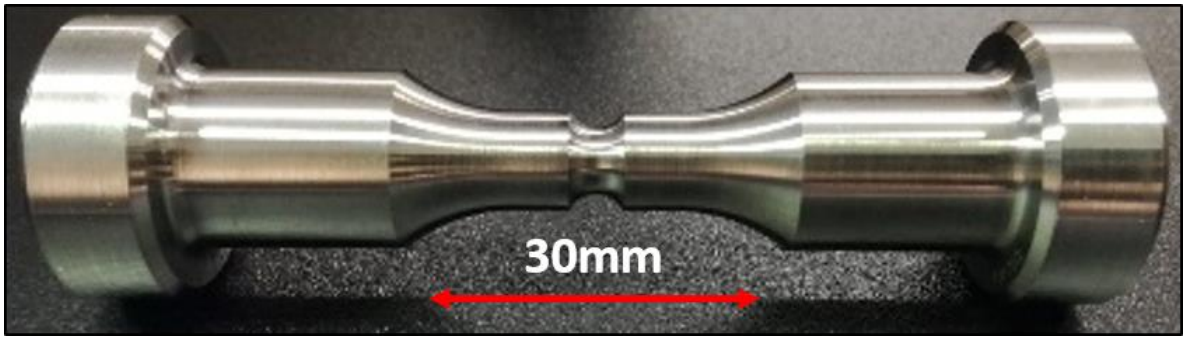

Fig. 5.3. Notched specimen after machining.

5.3. Fatigue tests

5.3.1 Fatigue tests conditions

The fatigue tests have been conducted with the servo-hydraulic test machine which can perform both axial and torsional test. The tests were strain-controlled with a gage length of 12 mm. The tests have been conducted by applying a von

Mises equivalent strain range of $\Delta\varepsilon_{eq}$ = 0.7% for both uniaxial and non-proportional loading.

5.3.2 Fatigue life results

The results of the fatigue tests are visualized in the graphic of Fig. 5.3.

Table 5.1 Fatigue test results

Strain path (-)	Specimen type (-)	N_f (Cycles)	$\Delta\sigma_{eq,n,max}/2$ (MPa)	$\Delta\tau/2$ (MPa)
PP	HT	12027	610	-
	HT	9705	658	-
	HNT	10022	600	-
	VT	7771	640	-
	VT	8017	640	-
	VNT	10297	637	-
	VNT	13105	630	-
OP	HT	1774	630	240
	HNT	1668	630	256
	HNT	463	650	269
	VT	1163	720	233
	VT	1221	750	248
	VNT	983	950	270
	VNT	694	950	250

Although there are differences in the number of cycles to failure among the specimen types, the fatigue life can be judged similar because of the intrinsic scatter of the data of fatigue. However, some considerations about the observed results can be made. In case of PP, the VT components exhibited the shortest fatigue life of approximately 8000 compared the other specimens which shown an average fatigue life of approximately 10000 cycles. In case of OP, the VT and VNT specimens fatigue life is about half of the HT and HNT specimens.

5.3.3 Hardening and softening curves

The hardening and softening curves have been obtained by plotting the nominal maximum axial stress amplitude over the cycles, similarly with the softening/hardening curves represented in chapter 4. The curves for uniaxial and multiaxial non-proportional strain path are represented in Fig. 5.4 a and b respectively. In case of PP, the stress remains constant with an average magnitude of 620 MPa upon failure. The same behavior on notched specimens

of the wrought material could be found in [1,2]. The stress at the notch tip becomes averagely 930 MPa due to a stress concentration factor of K_t = 1.5. Compared to the hardening/softening curves of chapter 4, no softening was detected in this case. This is probably due to the maximum stress 930 MPa being under the threshold of approximately 980 MPa where the plastic deformation becomes consistent (chapter 4, Table 4.4). The last segment of crack propagation seems dependent on the layer orientation as already described in chapter 4, Fig. 4.8. The crack propagation velocity in case of H specimens appears slower than the V specimens. In case of OP, the stress remains approximately constant until the final crack propagation in case of HT and HNT. In case of VT and VNT an anomalous additional hardening has been observed and the axial stress drastically increases.

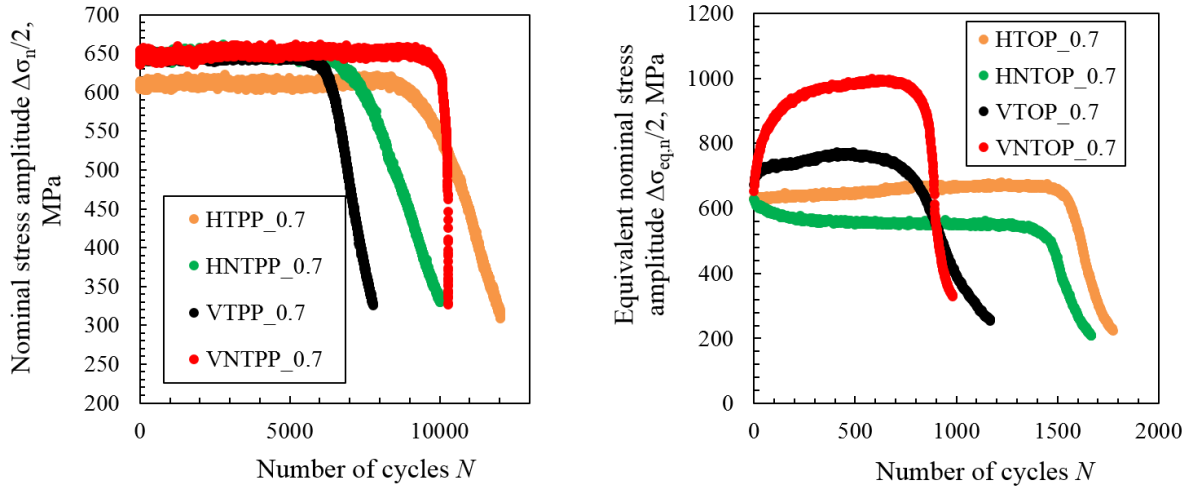

Fig. 5.4. Softening and hardening curves in case of PP (a) and OP (b) [3]

5.3.4 Fracture surface

The fracture surface of the tested specimens has been analyzed to verify the influence of the layer orientation, heat treatment and voids on the morphology of the fracture surface and the crack initiation site. The pictures of the fracture surface of tests specimens subject to PP and OP are reported in Fig 5.5 and 5.6 respectively. The main crack was located on the notch tip in every specimen. The crack initiation surface is located on the left side of the fracture surface in the figures. The bright portion of the fracture surface represents the fatigue crack. In case of PP the morphology of the main crack front part seems to depend on the layer orientation. Although the main crack initiation site was located in at the notch tip, secondary crack initiation sites could be observed in case of VT and

VNT. In case of OP strain path, the shape of the fracture surface area occupied by fatigue cracks seems not depending on the specimen variety.

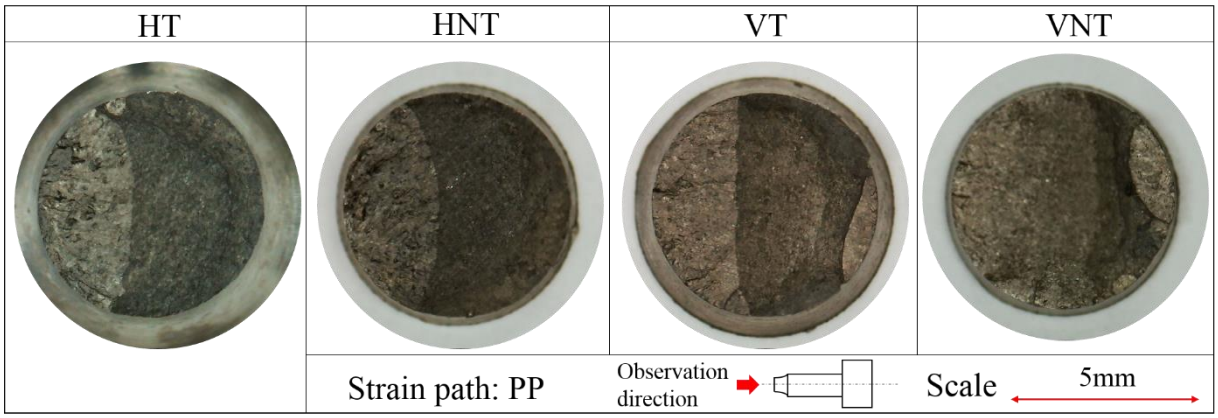

Fig. 5.5. Fracture surface of Ti-6Al-4V notched specimens subject to PP strain path.

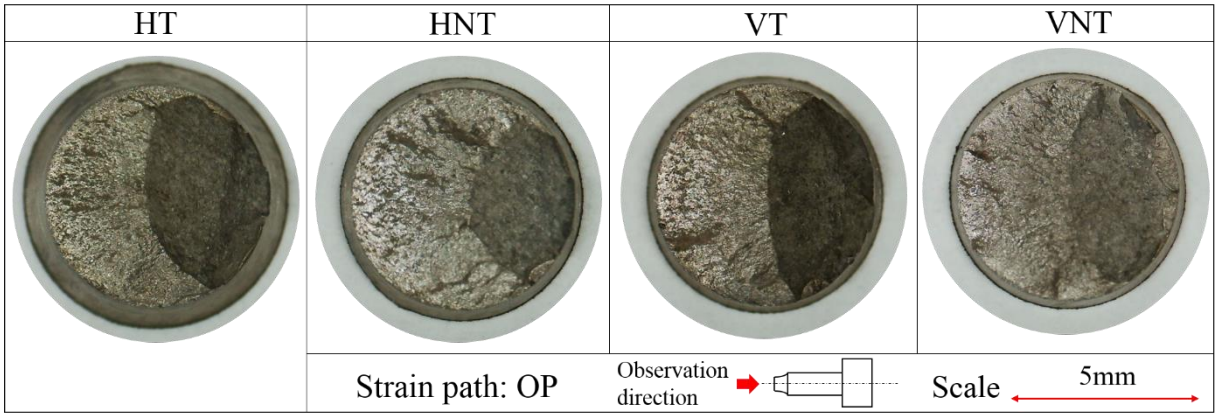

Fig. 5.6. Fracture surface of Ti-6Al-4V notched specimens subject to PP strain path.

In order to analyze the crack initiation site on the fracture surface, SEM observation have been conducted on the fracture surface. In each analyzed case the main crack initiated in the vicinity of the notched surface. The crack initiation site was located on lacks fusions, voids and surface defects. In Fig. 5.7a and b the picture of a crack initiating from an internal defect is represented. Cracks also initiated on internal voids located in the vicinity of the notched surface (Fig. 5.8). The majority of the main cracks observed in Fig. 5.5 and Fig. 5.6 initiated with the modality of Fig. 5.7 and Fig. 5.8 for both uniaxial and non-proportional loading. In case of non-proportional loading multiple crack initiation sites could be observed.

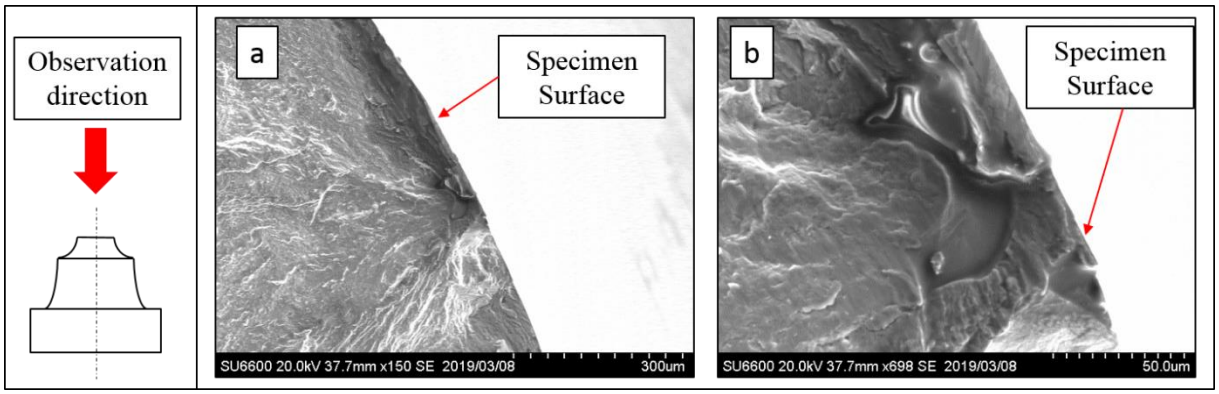

Fig. 5.7. Main crack initiation site on internal defect located on the vicinity of the notch surface (a) and magnification of the defect (b) (observation direction perpendicular to the axis)

The crack initiation site was also observed on superficial defects similar to the one depicted on Fig. 5.8.

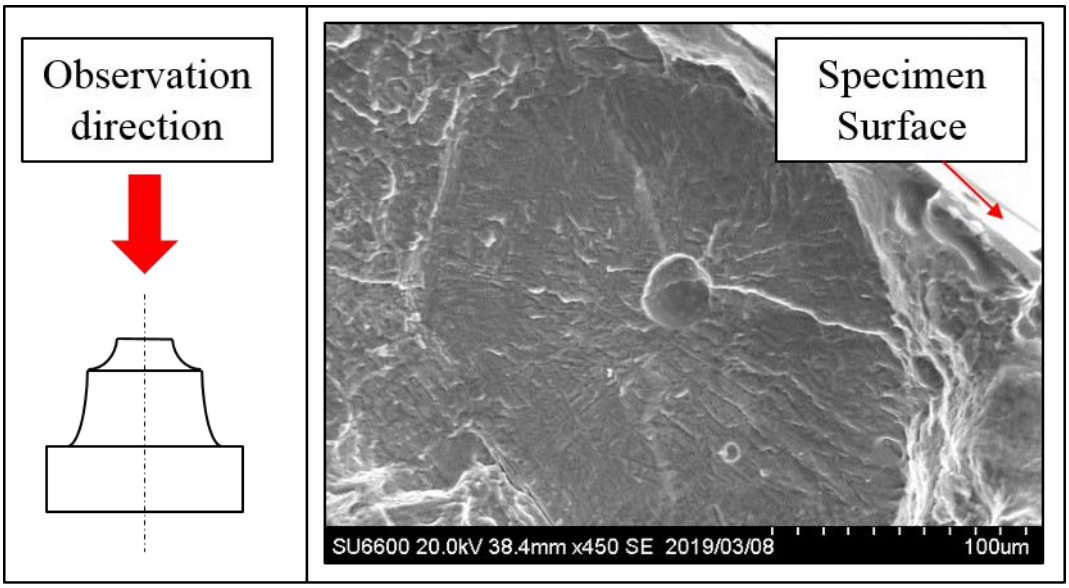

Fig. 5.8. Main crack initiation site on a void located in the vicinity of the notched surface

Crack initiation sites were also located on defects on the surface and internal voids, although they were not responsible for the initiation of the main crack. Crack initiation on internal intrusions due to the surface roughness and defects could be also find in reference [4].

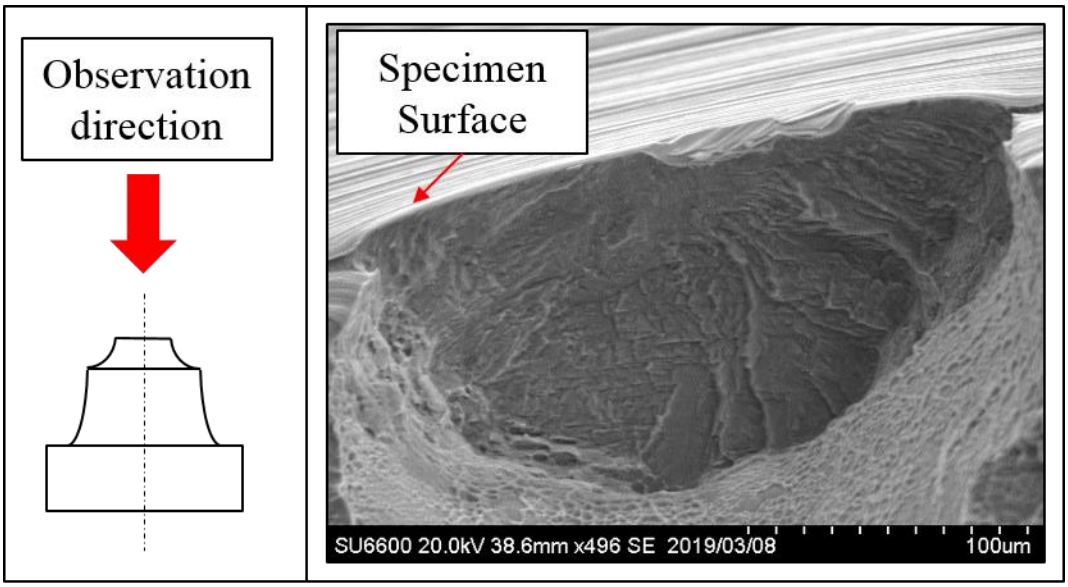

Fig. 5.9. Crack initiation site located on a defect located on the notched surface

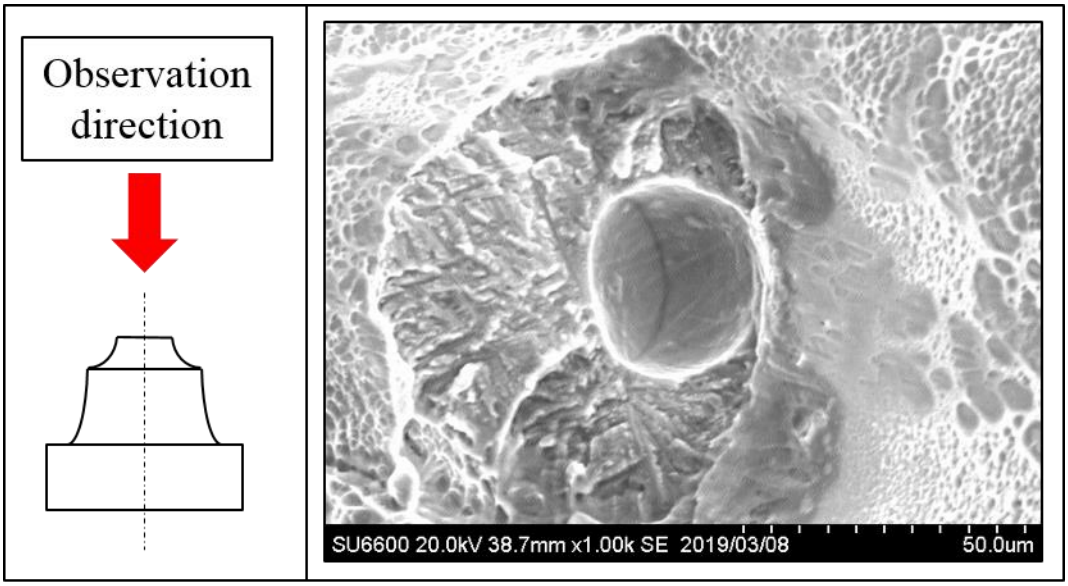

Fig. 5.10. Crack initiation site located on internal void

From the analysis of the fracture surface, a direct correlation between the crack initiation modality and heat treatment or layer orientation could not be verified, and further investigations are necessary.

5.4. Discussion

In this section, the influence of layer orientation, heat treatment, voids and notch on the low cycle fatigue life and crack initiation and propagation are discussed. The layer orientation does not exert influence on the fatigue life,

similarly to what observed in Chapter 4 for smooth specimens. However, the final crack propagation velocity in case of uniaxial loading could be correlated with the layer orientation. The final crack propagation in case of specimens with horizontal layer orientation was higher than their vertical counterpart (Fig. 5.4a and b). In case of non-proportional loading, the final crack propagation is not influenced by the layer orientation. This result could be also observed for the smooth specimens. Furthermore, the crack surface morphology in case of PP seems depending on layer orientation. An anomalous additional hardening was observed for vertical layer components but the caused could not be verified and further investigations are necessary to clarify this phenomenon. In case of notched specimens, the presence of the heat treatment does not influence the fatigue life contrarily to what observed in Chapter 4 for smooth specimens. From the hysteresis loops of chapter 4, the heat-treated components showed a higher absorbed energy compared to the not heat-treated counterpart and this was thought to be the cause of the lower fatigue life. Contrarily to the analyzed smooth specimens where the plastic deformation occurred in a wide volume of material, the notched components experience a localized plasticity in the vicinity of the notch. Therefore, the heat treatment influence can be neglected, although additional tests on notched specimens might be necessary to confirm this assumption. The higher influence on fatigue life is exerted by the stress concentration effect induced by the notch and the voids. The fatigue life results of the different varieties of specimens does not have a close correlation with the layer orientation or heat treatment. Fatigue life is in fact controlled by the defects or voids located on the notch tip. The synergic stress concentration effect induced by the notch and the defects are in fact determinant for the fatigue crack initiation process as the majority of the cracks initiate on internal defects such as the ones observed in Figs. 5.7, 5.8 and 5.9. The crack initiation site was located at the notch tip. This result is supported by the analyses and observations regarding the crack initiation site on the notch tip conducted in Chapter 2 and 3. The properties of additional hardening are similar with the properties of 6061Al analyzed in Chapter 3 and therefore the crack initiation site located on the notch tip was expected.

5.5. Conclusions

Four varieties additively manufactured notched specimens made by Ti-6Al-4V have been tested with uniaxial and multiaxial low cycle fatigue tests. The specimens' varieties depended on the layer orientation and the application of a

stress-relief heat treatment. A relationship between layer orientation, heat treatment, voids and fatigue life have been analyzed and discussed. The conclusions can be summarized as follows:

1) A relationship between fatigue life of the notched specimens and layer orientation or heat treatment could not be observed. However, layer orientation determines the final crack propagation velocity similarly to the smooth specimens analyzed in chapter 4.
2) Fatigue life depends on the crack initiation on internal defects or voids located in the vicinity of the notch tip. The main crack initiation site was in fact detected on voids and defects for the majority of the tested specimens.
3) The crack initiation site was located at the notch tip in case of non-proportional loading. The results are in accordance with the findings of previous works on notched specimens tested with non-proportional multiaxial low cycle fatigue.

5.6. Final conclusions and future developments

The cause of the shift of the crack initiation site on 316LSS notched specimens could be attributed to the additional hardening effect caused by non-proportional loading [5,6]. Such effect could not be detected on both 6061Al and AM Ti-6Al-4V specimens, as they don't exhibit additional hardening effect [7]. Although the consideration of this phenomenon improves the fatigue life evaluation, the definition of the field where the phenomenon has a drastic influence on the evaluation is still unknown. Giving that the crack initiation site shift increases with lower stress concentration factors, tests on materials with high additional hardening effects and stress concentration factors $1< K_{t,n} < 1.5$ are necessary to conduct for a more accurate evaluation of the phenomenon discussed in chapter Interrupting the tests after the crack initiation process is fundamental to analyze the fatigue damage contribution of the crack initiation phase.

The modified I-S model with the Bäumel-Seeger and accounting of notch sensitivity with the notch fatigue factor K_f returns satisfying results for materials with different characteristics in terms of plastic deformation, additional hardening and notch sensitivity [7]. Furthermore, the model is relatively simple to apply, as it requires the static mechanical properties of the material, the knowledge of the additional hardening parameter α (or α') and f_{NP}. However, giving the limited material varieties and strain paths for which this model has been verified, the model requires further verifications on materials with different

notch sensitivity and plastic behavior. The application of the modified model on AM materials requires a correct definition of the notch sensitivity. Therefore, the fatigue curves for smooth specimens and notched specimens must be obtained to apply the modified I-S model also for notched components. I-S model was modified with the K_f obtained analytically from the notch sensitivity of the material, and it has been employed for both uniaxial and multiaxial loading. A more precise evaluation could be obtained by evaluating empirically K_f as ratio between the fatigue life of smooth specimens and notched specimens. If this procedure is conducted for each loading path and material, the results of the fatigue life evaluation with I-S model might improve considerably.

AM Ti-6Al-4V have been widely investigated in this work, focusing on the influence of the material structure on fatigue life, plastic behavior, fracture initiation and propagation. The layer orientation influences the final crack propagation velocity in case of uniaxial loading. In case of multiaxial loading, such influence could not be observed. Such observations are valid for both smooth and notched specimens [3,8]. Heat treatment slightly influences fatigue life in case of smooth specimens and does not have influence on fatigue life on notched specimens. Voids have been found the factor which affects plastic behavior in case of smooth specimens and fatigue life in case of notched specimens. The initial softening mechanism described in Chapter 4 has been found depending on the voids, although more investigations are necessary to correctly address the phenomenon. Tests must be interrupted after the initial softening and the presence of cracks surrounding the voids must be verified. Crack initiation site was found at the notch tip in case of AM Ti-6Al-4V. Valuable data regarding the crack initiation site can be obtained by testing AM materials with a high degree of additional hardening such as AM 316LSS.

References

[1] Itoh, T., Yang, T. (2011). Material dependence of multiaxial low cycle fatigue lives under nonproportional loading. International Journal of Fatigue, 33, pp. 1025–1031. https://doi.org/10.1016/j. ijfatigue.2010.12.001

[2] Nakamura, H., Takanashi, M., Itoh, T., Wu, M., Shimizu, Y. (2011) Fatigue crack initiation and growth behavior of Ti–6Al–4V under non-proportional multiaxial loading. International Journal of Fatigue, 33, pp. 842–848. https://doi.org/10.1016/j.ijfatigue.2010.12.013.

[3] Bressan, S., Razavi, J., Ogawa, F., Itoh, T, Berto, F. (2019). Multiaxial fatigue strength under non-proportional loading of additively

manufactured notched components of Ti-6Al-4V. Proceedings of the 12th International Conference of Multiaxial Fatigue and Fracture, 24-26 June, Bordeaux, France.

[4] Razavi, J., Ferro, P., Berto, F., Torgersen, J. (2018) Fatigue strength of blunt V-notched specimens produced by selective laser melting of Ti-6l-4V. Theoretical and Applied Fracture Mechanics, 97, pp. 376-984.

[5] Bressan, S., Gallo, P., Morishita, T., Itoh, T. And Berto., F. (2017) Proceedings of the 14th International Conference on Fracture, June 18-23, Rhodes, Greece.

[6] Gallo, P., Bressan, S., Morishita, T., Itoh, T., Berto, F. (2017). Analysis of multiaxial low cycle fatigue of notched specimens for type 316L stainless steel under non-proportional loading, Theoretical and Applied Fracture Mechanics, 89, pp. 79-89. DOI: 10.1016/j.tafmec.2017.01.009.

[7] Bressan, S., Ogawa, F., Itoh, T., Berto, F. (2019) Influence of notch sensitivity and crack initiation site on low cycle fatigue life of notched components under multiaxial non-proportional loading, Frattura ed Integrità Strutturale, 47, pp. 126-140.DOI:10.1299/jmmp.5.230.

[8] Bressan, S., Ogawa, F., Itoh, T., Berto, F. (2019) Cyclic plastic behavior of additively manufactured Ti-6Al-4V under uniaxial and multiaxial non-proportional loading, International Journal of Fatigue, 126, pp. 155-164

6. Acknowledgements

This thesis is the results of three years of work begun three years ago at Ritsumeikan University. This long journey started in September 2016 has been filled with troubles and uncertainties that contributed to my growth as researcher and person. However, I wouldn't be able to reach this goal without the support of many people who I met and worked together with in this experience in Japan. Therefore, I want to express my gratitude to the persons who contributed to this achievement. First of all, I would like to thank my father and my mother who supported me for 28 years, allowing me to live the experience in Japan which totally changed my life. I also want to thank my brother who inspired me to pursue the scientific career. I would like to express my gratitude to prof. Filippo Berto and Pasquale Gallo who gave me the opportunity to discover Japan and helped me in my research activity. I also want to thank my supervisor, prof. Takamoto Itoh who made me discover the beauty of this country and taught me how to be a professional worker. He has been a life coach, and without him I wouldn't be able to face every day's challenges with serenity and positivity. I would like to thank also prof. Fumio Ogawa for his precious advices to develop and improve my research work. I would like also to express my gratitude to all my laboratory colleagues who always proven kind when I ask for advices. I also thank Máté, Peter, Rim and Jack for supporting me and spending a valuable time with me. There are also several people outside the university environment without whom I would have been impossible to grow and achieve this result. First of all, I would like to thank the Hirooka family and in particular Mutsuko, Yukio and Misaki. I lived together with them for two years and they had me as a guest without asking anything in exchange, allowing me to blend with the Japanese daily life and learn the local language. I would also like to thank the persons I met in Higashiosaka: Yoshito, Kayo, Yuki and the Mitsui family, who allowed me to explore the Japanese culture even deeper. I would like also to express my gratitude to the scout group of San Bonifacio. With 16 years of activity with them I learned the importance of begin new challenges and trying new experiences. Last but not least, I want to thank my wife Kazuki who supported me every day with her smile and reassuring words. Her determination inspired me for the achievement of this goal.

Il presente lavoro di tesi é frutto del lavoro di tre anni iniziato alla Ritsumeikan University. Il lungo viaggio cominciato a settembre del 2016 é stato colmo di difficoltà ed incertezze che tuttavia mi hanno aiutato a crescere come ricercatore e uomo. Tuttavia, da solo non sarei mai risucito a raggiungere tale risultato, ed é quindi doveroso ringraziare tutte le persone che hanno contribuito, in modo diretto o indiretto, alla realizzazione di questo lungo progetto di ricerca. Innanzitutto voglio ringraziare mio padre e mia madre, che mi hanno supportato per 28 lunghi anni, permettondomi di vivere questa esperienza in Giappone che mi ha totalmente cambiato la vita. Un grazie anche a mio fratello che mi ha sempre ispirato nel cammino di formazione scientifica. Vorrei inoltre ringraziare il Prof. Filippo Berto e Pasquale Gallo per avermi dato l'opportunità di scoprire il Giappone e avermi aiutato nell'attività di ricerca. Un grazie va al mio supervisore, professor Takamoto Itoh che mi ha fatto scoprire la bellezza di questo paese e mi ha insegnato molto sia dal punto di vista professionale sia dal punto di vista mentale. Un coach di vita, senza il quale non avrei la serenità nell' affrontare i problemi della vita di tutti i giorni. Un grazie anche al Prof. Ogawa che ha mi ha sempre fornito preziosi consigli per sviluppare e migliorare i miei lavori di ricerca. Vorrei oltrettutto ringraziare i miei compagni di laboratorio, che si sono sempre dimostrati gentili e pronti ad aiutarmi per qualsiasi problema. A Máté, Peter, Rim e Jack va un enorme grazie per essere stati dei punti di riferimento all'interno dell' università e con cui ho avuto il piacere di avere scambi di idee che mi hanno fatto crescere. Per quanto riguarda le attivita' fuori dall'università, ci sono persone senza le quali mi sarebbe stato impossibile crescere e conseguire questo risultato. Innanzitutto, devo ringraziare la famiglia Hirooka, in particolare Mutsuko, Yukio e Misaki. Ho vissuto questa famiglia per 2 anni e mi hanno ospitato senza mai chiedere nulla in cambio, facendomi integrare nella vita quotidiana nipponica e insegnandomi la lingua locale. Un grazie va alle persone di Higashiosaka: Yoshito, Kayo e la famiglia Mitsui grazie ai quali sono stato in grado di immergermi ancora di piú nella cultura giapponese. Vorrei ringraziare anche il gruppo scout di San Bonifacio 2 che con quasi 16 anni di attività insieme ho capito l'importanza di mettersi in gioco e provare esperienze sempre nuove e stimolanti. Un ultimo ed indispensabile grazie va a mia moglie Kazuki, che mi ha sempre supportato ogni giorno con il suo sorriso e la sua spensieratezza. La sua determinazione mi é stata di grande ispirazione per il raggiungimento di questo traguardo.

7. Works included in the thesis

7.1. Journal papers

[1] Bressan, S., Ogawa, F., Itoh, T., Berto, F. (2019) Influence of notch sensitivity and crack initiation site on low cycle fatigue life of notched components under multiaxial non-proportional loading, Frattura ed Integrità Strutturale, 47, pp. 126-140.DOI:10.1299/jmmp.5.230.

[2] Bressan, S., Ogawa, F., Itoh, T., Berto, F. (2019) Low cycle fatigue behavior of additively manufactured Ti-6Al-4V under non-proportional and proportional loading, Frattura ed Integrità Strutturale, 48, pp. 18-25

[3] Bressan, S., Ogawa, F., Itoh, T., Berto, F. (2019) Cyclic plastic behavior of additively manufactured Ti-6Al-4V under uniaxial and multiaxial non-proportional loading, International Journal of Fatigue, 126, pp. 155-164

7.2. Conference papers

[1] Bressan, S., Gallo, P., Morishita, T., Itoh, T. And Berto., F. (2017). Numerical analysis of multiaxial low cycle fatigue of notched specimens made by stainless steel 316 L under non-proportional loading Proceedings of the 14th International Conference on Fracture, June 18-23, Rhodes, Greece.

[2] Bressan, S., Razavi, J., Ogawa, F., Itoh, T, Berto, F. (2019). Multiaxial fatigue strength under non-proportional loading of additively manufactured notched components of Ti-6Al-4V. Proceedings of the 12th International Conference of Multiaxial Fatigue and Fracture, 24-26 June, Bordeaux, France.